

Extensional Tectonics in Western Anatolia, Turkey: Eastward continuation of the Aegean Extension

Elizabeth Catlos¹, Thomas Etzel², and Ibrahim Çemen³

¹The University of Texas at Austin

²ExxonMobil, 22777 Springwoods Village, Parkway Spring, TX 77389, USA

³University of Alabama, Dept. of Geological Sciences, Tuscaloosa, Alabama, 35487-0338, USA

November 22, 2022

Abstract

Western Anatolia is located at the boundary between the Aegean and Anatolian microplates. It is considered a type-location for marking a significant transition between compressional and extensional tectonics across the Alpine-Himalayan chain. The onset of lateral extrusion in Western Anatolia and the Aegean during the Eocene is only one of its transitional episodes. The region has a geological history marked by diverse tectonic events starting from the Paleoproterozoic through the Cambrian, Devonian, and Late Cretaceous, as recorded by its suture zones, metamorphic history, and intrusions of igneous assemblages. Extension in Western Anatolia initiated in a complex lithospheric tectonic collage of multiple sutured crustal fragments from ancient orogens. This history can be traced to the Aegean microplate, and today both regions are transitioning or have transitioned to a stress regime dominated by strike-slip tectonics. The control for extension in Western Anatolia is widely accepted as the rollback of the African (Nubian) slab along the Hellenic arc, and several outstanding questions remain regarding subduction dynamics. These include the timing and geometry of the Hellenic arc and its connections to other subduction systems along strike. Slab tear is proposed for many regions across the Anatolian and Aegean microplates, either trench-parallel or perpendicular, and varies in scale from regional to local. The role of magma in driving and facilitating extension in Western Anatolia and where and why switches in stress regimes occurred along the Anatolia and Aegean microplates are still under consideration. The correlation between Aegean and Anatolian tectonic events requires a better understanding of the detailed metamorphic history recorded in Western Anatolia rocks, possible now with advances in garnet-based thermobarometric approaches. Slab tear and ultimate delamination impact lithospheric dynamics, including generating economic and energy deposits, facilitating lithospheric thinning, and influencing the onset of transfer zones that accommodate deformation and provide conduits for magmatism.

1 **Extensional Tectonics in Western Anatolia, Turkey: Eastward continuation of** 2 **the Aegean Extension**

3
4 E. J. Catlos¹, T. M. Etzel^{1,2}, and I. Çemen³

5
6 ¹The University of Texas at Austin, Jackson School of Geosciences, Dept. of Geological
7 Sciences, Austin TX 78712-1722, USA

8 ²ExxonMobil, 22777 Springwoods Village, Parkway Spring, TX 77389, USA

9 ³University of Alabama, Dept. of Geological Sciences, Tuscaloosa, Alabama, 35487-0338, USA

10
11 Corresponding author: Elizabeth Catlos (ejcatlos@jsg.utexas.edu)

12 13 **Index terms**

14 8110 Continental tectonics: general (0905)

15 8109 Continental tectonics: extensional (0905)

16 3618 Magma chamber processes (1036)

17 3651 Thermobarometry

18 3652 Pressure-temperature-time paths

19 20 **Keywords**

21 Aegean, Anatolia, extension, Western Turkey, tectonics

22 23 **Abstract**

24 Western Anatolia is located at the boundary between the Aegean and Anatolian microplates. It is
25 considered a type-location for marking a significant transition between compressional and
26 extensional tectonics across the Alpine-Himalayan chain. The onset of lateral extrusion in
27 Western Anatolia and the Aegean during the Eocene is only one of its transitional episodes. The
28 region has a geological history marked by diverse tectonic events starting from the
29 Paleoproterozoic through the Cambrian, Devonian, and Late Cretaceous, as recorded by its
30 suture zones, metamorphic history, and intrusions of igneous assemblages. Extension in Western
31 Anatolia initiated in a complex lithospheric tectonic collage of multiple sutured crustal fragments
32 from ancient orogens. This history can be traced to the Aegean microplate, and today both
33 regions are transitioning or have transitioned to a stress regime dominated by strike-slip
34 tectonics. The control for extension in Western Anatolia is widely accepted as the rollback of the
35 African (Nubian) slab along the Hellenic arc, and several outstanding questions remain regarding
36 subduction dynamics. These include the timing and geometry of the Hellenic arc and its
37 connections to other subduction systems along strike. Slab tear is proposed for many regions
38 across the Anatolian and Aegean microplates, either trench-parallel or perpendicular, and varies
39 in scale from regional to local. The role of magma in driving and facilitating extension in
40 Western Anatolia and where and why switches in stress regimes occurred along the Anatolia and
41 Aegean microplates are still under consideration. The correlation between Aegean and Anatolian
42 tectonic events requires a better understanding of the detailed metamorphic history recorded in
43 Western Anatolia rocks, possible now with advances in garnet-based thermobarometric
44 approaches. Slab tear and ultimate delamination impact lithospheric dynamics, including
45 generating economic and energy deposits, facilitating lithospheric thinning, and influencing the
46 onset of transfer zones that accommodate deformation and provide conduits for magmatism.

47 **1 Introduction**

48 The Aegean and eastern Mediterranean are considered the most rapidly deforming
49 regions across the Alpine-Himalayan chain (Figure 1) (e.g., Papazachos & Delibasis 1969;
50 Papazachos & Comninakis, 1971; McKenzie, 1972; Şengör et al., 1985; Taymaz et al., 1991;
51 Jackson, 1994; Reilinger et al., 1997; Nyst & Thatcher, 2004; Le Pichon et al., 2019; Meng et al.,
52 2021). The Aegean and Anatolia microplates, sometimes classified as the single Aegean-
53 Anatolian microplate, are a complex amalgamation of a series of terranes that today experience
54 seismicity (e.g., Şengör & Yılmaz, 1981; Okay et al., 1996; Reilinger et al., 1997; Nyst &
55 Thatcher, 2004; Tan, 2013). The Anatolian microplate is a large peninsula that coincides with
56 over two-thirds of the country of Turkey (Figure 1) (Le Pichon et al., 1995; Oral et al., 1995;
57 Reilinger et al., 1997; Papazachos, 1999). It is the westernmost protrusion of the Asian continent,
58 with a pole of rotation located in the northern Sinai Peninsula (e.g., Reilinger et al., 2010). The
59 Black Sea bounds it to the north and the Mediterranean Sea to the south. The Aegean microplate
60 is largely comprised of continental crust and sediments obscured by the Aegean Sea (Le Pichon
61 & Angelier, 1981; Jolivet & Patriat, 1999; Makris et al., 2013). The Sea of Marmara connects the
62 Black and Aegean Seas through the Bosphorus and Dardanelles straits and separates a fragment
63 of Eurasia's microplate (Nyst & Thatcher, 2004).

64 Deciphering the assembly of the Aegean and Anatolian microplates and their past and
65 present-day deformation drivers impacts our understanding of continental tectonics, subduction
66 zone processes, lithospheric deformation, ore generation process, and hazards (e.g., Jackson,
67 1994; Meng et al., 2021; Rabayrol & Hart, 2021). The borders of the Aegean and Anatolian
68 microplates coincide with fault systems that played vital roles in triggering changes in their
69 tectonic nature (e.g., McKenzie, 1972; 1978). The microplates share some borders, including the
70 right-lateral strike-slip North Anatolian transform fault and the Western Anatolian Extensional
71 Province (WTEP) (Figure 1) (e.g., Ketin, 1948; Şengör et al., 1985; Barka, 1992; Armijo et al.,
72 1999; Çemen et al., 2006; Barka et al., 2000; McClusky et al., 2000; Chousianitis et al., 2015).
73 The subducting Hellenic and Cyprus arcs and the complex dynamics coinciding with the
74 Florence Rise make up their southern borders (e.g., Le Pichon & Angelier, 1979; Angelier et al.,
75 1982; Anastasakis & Kelling 1991; Papazachos et al., 2000; Ergün et al., 2005; Suckale et al.,
76 2009; Royden & Papanikolaou, 2011). Global Positioning System (GPS) constraints show that
77 the principal northern boundaries of the southwestern Aegean plate are the North Aegean Trough
78 (NAT) and Kephallonia (also Cephalonia and Kefalonia) Transform Zone (KTZ) (McKenzie
79 1972; Pichon et al. 1995; Kahle et al. 2000; Pearce et al., 2012; Chousianitis et al. 2015; Haddad
80 et al. 2020). The southern boundary is separated from the Anatolia plate by the WTEP., a zone of
81 N-S extension (Figure 1) (McClusky et al., 2000; Chousianitis et al., 2015). Although many of its
82 bounding fault systems are presently active, both the Anatolian and Aegean microplates contain
83 internal structures, including transfer zones (Figure 1 and Figure 2) (e.g., Nyst & Thatcher, 2004;
84 Çemen et al., 2006; Oner et al., 2010; Aktuğ et al., 2013; Özkaymak et al., 2013; Uzel et al.,
85 2013; Seghedi et al., 2015; Barbot & Weiss, 2021).

86 Several tectonic models applied to the Aegean and Anatolian microplates have
87 transformed our ideas about the lithosphere's response to extensional, strike-slip, and
88 compressional forces (see review in Aktuğ et al., 2013). Advances in tomography and GPS
89 technology have contributed to our understanding of its present-day dynamics (e.g., Barka &
90 Reilinger, 1997; McClusky et al., 2000; Ganas & Parsons, 2009; Komut et al., 2012; Aktuğ et al.,
91 2013; Jolivet et al., 2015; Ventouzi et al., 2018). The deformation, metamorphism, and igneous

92 activity exposed in the upper portions of the microplate's lithosphere provide constraints on
93 processes that operated in its lower lithosphere over long periods of geological time (e.g.,
94 Jackson, 1994; Komut et al., 2012).

95 This review paper is divided into two primary parts. The first section reviews some of the
96 chronology and tectonic history of the juncture between the Aegean and Anatolian microplates
97 from data available in Western Anatolia (Figure 1 and Figure 2). The goal is to outline how the
98 boundary results from an accumulation of a series of tectonic processes that record stress
99 transitions in the geological past. The second part of the paper aims to present outstanding
100 questions that remain in unraveling its complex dynamics. This particular area of the Anatolian
101 microplate has been the focus of attention for almost fifty years (e.g., McKenzie 1972) and has
102 become the type-locality for understanding subduction zone dynamics, a focus of diverse and
103 multi-disciplinary studies.

104 **2 Geological Background**

105 **2.1 Assembly of key components (Paleoproterozoic-Eocene)**

106 The Anatolian microplate is comprised of multiple continental fragments separated by
107 oceans that collided and ultimately combined by the Late Cretaceous-Eocene, with exposures of
108 ophiolitic and high-pressure/low-temperature rock assemblages that mark the suture zones
109 (Figure 2, Figure 3, Figure 4) (e.g., Şengör & Yılmaz, 1981; Okay, 2008; Moix et al., 2008;
110 Okay & Tuysuz, 1999; Pourteau et al., 2016; Okay et al., 2020). Western Anatolia is explicitly
111 defined by the amalgamation of two terranes: the Pontides to the north and the Anatolides-
112 Taurides to the south (e.g., Şengör & Yılmaz, 1981; Yılmaz et al., 1997; Okay & Tuysuz, 1999;
113 Pourteau et al., 2016). The Pontides extends across northern Turkey and is comprised mainly of
114 Pan-African basement blocks and Phanerozoic sedimentary cover units that may have originated
115 from the southern Eurasia margin before back-arc extension initiated and created the Black Sea
116 (Yılmaz et al., 1997; Moix et al., 2008; Pourteau et al., 2010; Okay et al., 2013).

117 The Intra-Pontide suture zone (IPS) is mapped within the Pontide zone between the
118 Sakarya continental zones and Istanbul-Zonguldak Unit (also Istanbul–Zonguldak Zone, Istanbul
119 Nappe, or Istanbul Zone, see Yiğitbaş et al., 2004) (Figure 2, Figure 3, Figure 4). The Istanbul
120 portion of the unit exists in the west (Istanbul, Gebze, south Camdağ regions) and the Zonguldak
121 to the east (north Camdağ, Zonguldak, Safranbolu regions), both being Gondwanan fragments
122 (e.g., Okay et al., 2006; Bozkaya et al., 2012). The IPS has varying interpretations, including an
123 accretionary complex, a suprasubduction zone, and a remnant of a former ocean basin that may
124 have extended into eastern Europe (e.g., Okay et al., 1996; Robertson & Ustaömer, 2004;
125 Göncüoğlu et al., 2012; 2014; Marroni et al., 2014; Akbayram et al., 2016; Sayit et al., 2016;
126 Frassi et al., 2018). Geological units within the IPS may also be from components from the
127 Istanbul-Zonguldak or Sakarya zones, which has led to a debate about its presence and utility of
128 the IPS in paleogeographic reconstructions (Moix et al., 2008).

129 Magmatic assemblages help us understand the tectonic processes involved in Western
130 Anatolia, so we present a summary of some available time constraints for several key granite
131 bodies dispersed throughout this region in Tables 1-8 and Figure 4. Zircon ages extracted from
132 metagranites and quartzite units indicate that the Istanbul-Zonguldak Unit has a Precambrian
133 basement with Gondwanan units (Chen et al., 2002; Yiğitbaş et al., 2004; Ustaömer et al., 2005;
134 2011) and stratigraphic similarities with Paleozoic rocks from the southern margin of Laurasia
135 (Görür et al., 1997; Kaldova et al., 2003). Some of the oldest Neoproterozoic granites in Western

136 Anatolia are found in the Istanbul Zone (Table 1, Karadere or Karabuk metagranite, Figure 4;
137 Chen et al., 2002; Ustaömer et al., 2016; Di Rosa et al. 2019), although zircons from the
138 Karacabey (Tamsali) and Karaburun plutons in the Western Sakarya Zone and the Çine Massif in
139 the southern portion of the Menderes Massif also yield Paleoproterozoic and Neoproterozoic
140 ages (Tables 5 and 8; Loos & Reischmann 1999; Aysal et al., 2012; Ustaömer et al., 2012). The
141 Triassic ages from granites that intrude the Istanbul-Zonguldak Unit are thought to time partial
142 closure of the Paleotethyan Ocean (Table 1, e.g., Ustaömer et al., 2016). Some of the youngest
143 mineral ages from Istanbul-Zonguldak granites are Late Cretaceous ($^{40}\text{Ar}/^{39}\text{Ar}$ ages, 93.3 ± 2.0
144 Ma, 86.1 ± 2.0 Ma, Delaloye & Bingöl, 2000), which are similar to estimates for the activity
145 within the subduction-accretion complex associated with the Izmir-Ankara-Erzincan Suture Zone
146 (IAESZ) (Figure 2, Figure 3, Figure 4) (Okay et al., 2020).

147 The IAESZ separates the Pontide's Sakarya Composite Terrane in the north from the
148 Anatolide-Tauride block to the south (Figure 2 and Figure 4) (Şengör & Yılmaz, 1981; Okay &
149 Tüysüz, 1999; Tekin et al., 2002; Göncüoğlu, 2010). Both the IPS and IAESZ mark late
150 Cretaceous–earliest Tertiary closure of Neo-Tethyan ocean basins (e.g., Pourceau et al., 2010;
151 Akbayram et al., 2016). In the Aegean microplate, the IAESZ is thought to record the closure of
152 the Vardar ocean and link with the Vardar ophiolite (or Axios-Vardar suture zone) (Channell &
153 Kozur, 1997; Okay & Tuysuz, 1999; Tekin et al., 2002; Moix et al., 2008), but its exposure
154 beneath the Aegean Sea is masked (e.g., Burtman, 1994; Stampfli, 2000; Yılmaz et al., 2001;
155 Burchfiel et al., 2008). The Vardar suture may also connect to the IPS that separates the Sakarya
156 Zone from the Istanbul Zone (Şengör & Yılmaz, 1981; Okay & Satir, 2000; Okay et al., 2001;
157 Beccalotto & Jenny, 2004; Okay et al., 2010; d'Atri et al., 2012; Di Rosa et al. 2019), and may
158 connect to the Meliata-Balkan suture of Greece (Stampfli, 2000). The IPS and Vardar connection
159 may be evidenced in the Biga Peninsula by an isolated ophiolite-bearing accretionary complex
160 that was active until the Late Cretaceous (Figure 2 and Figure 4) (e.g., Okay et al., 1991). Some
161 disagree and do not map any major suture within the Biga Peninsula (Altunkaynak & Genc,
162 2008; Burchfiel et al., 2008; Sengun et al., 2011). Because of the uncertain link between the
163 sutures, the relationship of the basement of the Biga Peninsula to that in the Rhodope-Thrace
164 Massif is debated (Bonev & Beccalotto, 2007; Elmas, 2012). In Western Anatolia, the
165 Pamphylian Suture (Figure 2) may connect to the Alanya and Bitlis suture zones further to the
166 east (Centikapan et al., 2016) and beneath the Lycian nappes to the Cycladic domain to the west
167 (Stampfli & Kozur, 2006).

168 In Western Anatolia, blueschist assemblages exposed along the IAESZ are intruded by
169 Suture Zone Granitoids (SZGs) [Topuk, Orhaneli, Tepeldag (Gürgenyayla and Gürgenyayla),
170 Table 2; Figure 4]. These granitoids have Paleocene (63.5 ± 2.8 Ma) to Oligocene (31.4 ± 0.6 Ma)
171 ages but are largely thought to have crystallized in the early Eocene (~ 45 - 47 Ma, Okay & Satir,
172 2006; Altunkaynak, 2007). The SZGs intrude the western portion of the Tavşanlı Zone, a
173 blueschist sequence overlain by a Cretaceous accretionary complex and ophiolitic sheet. The
174 zone formed as a result of northward-dipping subduction and represents the Mesozoic to Eocene
175 closing of the northern branch of the Neo-Tethyan Ocean (Okay, 1986; 2008; Okay & Kelley,
176 1994; Sherlock et al., 1999; Moix et al., 2008, Shin et al., 2013; Plunder et al., 2013; Fornash &
177 Whitney, 2020). The Tavşanlı Zone is narrow (~ 50 km) and trends E-W for approximately 250-
178 350 km (Okay & Whitney, 2010; Plunder et al., 2013). The western and central portions contain
179 blueschist facies metavolcanic and metasedimentary rocks with rare metabasalts (Okay, 1980a,
180 1980b, 1982; Okay & Kelley, 1994, see Seaton et al., 2009).

181 The Sivrihisar Massif further to the east is the only portion of the Tavşanlı Zone to
182 contain eclogite and blueschist and Barrovian sequences (Figure 4 and Figure 5) (Gautier, 1984;
183 Seaton et al., 2009). Rb-Sr and $^{40}\text{Ar}/^{39}\text{Ar}$ phengite ages from the Sivrihisar Massif constrain
184 high-pressure/low-temperature (HP/LT) metamorphism to ~88–80 Ma (Sherlock et al., 1999;
185 Seaton et al., 2009; Whitney et al., 2011; Pourteau et al., 2013; Shin et al., 2013). Older ages
186 from the HP/LT assemblages reported from the western portion of the Tavşanlı Zone may suffer
187 from excess argon (see review in Shin et al., 2013). Barrovian-metamorphosed marble from the
188 Sivrihisar massif contains ~59 Ma muscovite ($^{40}\text{Ar}/^{39}\text{Ar}$), timing their exhumation (Seaton et al.,
189 2009). Late Cretaceous and early Paleocene ages are also reported from eastern Tavşanlı Zone
190 granitoids, which are medium to high K., calc-alkaline, metaluminous, I-type, and post-
191 collisional [Kaymaz, Sivrihisar, Sarıkavak (Topkaya), Günyüzü (Karacaören, Tekoren, Dinek,
192 Kadinicik bodies) Figure 4 and Figure 5, Table 2] (e.g., Shin et al., 2013; Demirbilek et al.,
193 2018). However, these results are interpreted as inheritance (Shin et al., 2013; Demirbilek et al.,
194 2018). The Sivrihisar granite's age is often cited to be 53 ± 3 Ma, based on a hornblende $^{40}\text{Ar}/^{39}\text{Ar}$
195 age clearly affected by excess argon (Sherlock et al., 1999) (Figure 5B and C). However, the
196 Sivrihisar granite contains zircon that is 78.4 ± 8.5 Ma (likely inherited) to 41.9 ± 2.3 Ma (U-Pb,
197 $\pm 1\sigma$, Shin et al., 2013). Figure 5B and C show the K-feldspar $^{40}\text{Ar}/^{39}\text{Ar}$ age from the same
198 sample, which yields a plateau age of 46.02 ± 0.21 Ma (MSWD 4.21), similar to those reported
199 for the Sivrihisar and nearby Kaymaz granite and SZGs (Table 2). The flat $^{40}\text{Ar}/^{39}\text{Ar}$ age
200 spectrum is consistent with rapid cooling during exhumation (Figure 5D). Paleocene-Eocene
201 ages from the Tavşanlı Zone granites mark the timing of the closure of the IAESZ (e.g., Okay et
202 al., 2020).

203 The Tavşanlı zone is one component of the larger Anatolide-Tauride block, a
204 microcontinent that rifted away from the northern margin of Gondwana beginning in the early
205 Permian (Figure 2, Figure 3, and Figure 4) (Stampfli & Kozur, 2006) or Triassic (e.g., Şengör &
206 Yılmaz, 1981; Şengör et al., 1984; Okay & Tuysuz, 1999; Robertson & Ustaömer, 2009a,
207 2009b). The Taurides comprise the southern portion of the Anatolide-Tauride block and is
208 Neoproterozoic-Early Cambrian (Infracambrian) basement overlain by Cambrian to Eocene
209 marine sediments (e.g., Gutnic et al., 1979; Özgül, 1997; Candan et al., 2016). The Anatolide
210 terrane is the metamorphic equivalent of the Taurides and is subdivided into zones based on
211 lithologies and the type and age of metamorphism (see review in Bozkurt & Oberhansli, 2001;
212 Candan et al., 2016; Moix et al., 2008). These include the Tavşanlı Zone, Afyon Zone, Menderes
213 Massif, and Lycian nappes (Figure 2, Figure 3, and Figure 4). The Tavşanlı and Afyon zones are
214 sometimes considered as part of a single Kütahya–Bolkardağ Belt (Özcan et al., 1988;
215 Gönçüoğlu et al., 1997; 2012).

216 Note that a series of granite bodies intrude the IPS between the Sakarya and Istanbul
217 Zones also ages that resemble the SZGs and eastern portions of the Tavşanlı Zone. These Middle
218 Eocene Magmatic Rocks (MEMR), also known as the South Marmara Granitoids [Şevketiye,
219 İlyasdağ tonalite (Marmara Island), Karabiga (Lapeski), Fistikli (Armutlu–Yalova), Kapıdağ,
220 and Avsa Island; Figure 4, Table 3] are located in close association with the IPS and range in age
221 from the Late Cretaceous (71.9 ± 1.8 Ma) to Late Eocene (34.3 ± 0.9 Ma). The MEMR are unique
222 in these ages, as further east, along strike of the IPS and into the central portion of the Sakarya
223 Zone, some of the oldest plutons in Western Anatolia are exposed (Pamukova, Gemlik, Inhisar,
224 Gevyke, Bilecik, Söğüt, Figure 4, Table 4). Some of these intrusions are associated with
225 economically important kaolinite deposits (e.g., Kadir & Kart, 2009). The Cambrian Gemlik
226 granite body is located in the vicinity of the MEMR granites (Figure 4). Its age is more

227 consistent with Cadomian Orogeny (650–550 Ma) granites further north in the Istanbul-
228 Zonguldak and Strandja zones (e.g., Şahin et al., 2014) and similar-age rocks from the basement
229 or core of the Afyon Zone and Menderes Massif (e.g., Dannat, 1997; Loos & Reichmann, 1999;
230 Şahin et al., 2014; Hetzel & Reischmann, 1996). Western Anatolian granites with Cambrian ages
231 are termed the Late Pan-African Granitoids or Cadomian Granitoids and are associated with
232 tectonic events along the northern margin of Gondwana (Gürsu & Göncüoğlu, 2006; Şahin et al.,
233 2014). We identify some of these granites in their particular zones in Figure 4 and distinct
234 sections of Tables 1, 4, and 8. Note that the entire core of the Menderes Massif is considered
235 Pan-African (primarily late Neoproterozoic to Cambrian) basement (see review in Oberhänsli et
236 al., 2010).

237 Proterozoic zircon ages are found in the Pontides zone, but some of its central and
238 western granite assemblages also record Silurian-Devonian ages [Saricakaya, Table 4;
239 Karaburun, Güveylərbası (Çamlık-related), Karacabey (Tamsalı), Eybek (Çamlık),
240 Güveylərbası, Table 5; Figure 4]. These ages are linked to the amalgamation of a fragment of
241 Avalonia terrane in a subduction-zone type setting (Aysal et al., 2012; Sunal, 2012; Topuz et al.,
242 2020). Variscan-age (Carboniferous) granites are also reported for granites in the Central and
243 Western Sakarya Zone and Afyon Zone (Tables 4 and 6; Figure 4). Some of these results could
244 represent inherited cores or xenocrystic grains from the surrounding metamorphic assemblages.
245 For example, the Miocene-age Alaçam granite in the Afyon Zone has reported Carboniferous
246 ages, but the older ages were likely entrained from its basement units (Hasözbeke et al. 2010;
247 Candan et al. 2016).

248 The Afyon zone is considered the southward palaeogeographic extension of the Tavşanlı
249 zone (Candan et al., 2005; Pourteau et al., 2010; Akal, 2013; Özdamar et al., 2013). Although it
250 is often mapped as closely and narrowly paralleling the Tavşanlı Zone, the southern extent of the
251 Afyon Zone is unclear, and a portion may also be exposed between the southern Menderes
252 Massif and Lycian Nappes (Okay, 1986; Candan et al., 2005; Pourteau et al., 2013; Ustaömer et
253 al., 2020). The zone has also been termed the Afyon–Bolkardag Zone (Okay, 1986; Özdamar et
254 al., 2013) and Ören–Afyon Zone (Pourteau et al., 2013). The zone consists of Pan-African-
255 related basement underlying shelf-type Palaeozoic-Mesozoic sequence of the Taurides and
256 metasedimentary and metavolcanic rocks, portions of which have undergone regional greenschist
257 to blueschist facies (Fe–Mg carpholite and glaucophane) metamorphism (Figure 3) (Okay, 1984;
258 Candan et al., 2005, Pourteau et al., 2010; Özdamar et al., 2013). In this sense, its stratigraphy
259 resembles that of the Tavşanlı Zone (Candan et al., 2005). Rhyolitic volcanic assemblages
260 contain zircon that crystallized in the Late Triassic time extension along the northern margin of
261 Gondwana as the Neo-Tethyan Ocean developed (230 ± 2 Ma and 229 ± 2 Ma; Özdamar et al.,
262 2013). Triassic ages reported for granitic assemblages found within the Istanbul-Zonguldak zone,
263 central and western Sarkarya, and Menderes Massif are also attributed to this event (Figure 4;
264 Okay et al., 2020). LT/HP metamorphism in the Afyon Zone is thought to have occurred at 70-
265 65 Ma coincident with the closure of the Neo-Tethyan Ocean (Pourteau et al., 2010, 2013;
266 Özdamar et al., 2013; Plunder et al., 2013). Based on zircon ages from granites intruding
267 Tavşanlı Zone blueschist and altered ophiolitic assemblages, portions of the Afyon Zone may
268 have subducted beneath the Tavşanlı Zone during the Late Cretaceous (Speciale et al., 2012;
269 Shin et al., 2013). Upper Palaeocene-Lower Eocene sedimentary rocks overly the metamorphic
270 rocks of the Afyon Zone (Candan et al., 2005).

271 The Menderes Massif is considered the metamorphic basement on which the rocks of the
272 Afyon Zone were deposited before regional metamorphism (Okay, 1984). The Menderes Massif
273 exposes ~40,000 km² of metamorphic and igneous rocks, and its stratigraphy was originally
274 described as a gneiss ‘core’ and Paleozoic schist envelope with overlying Mesozoic-Cenozoic
275 marble ‘cover’ (e.g., Schuilings, 1962; Durr, 1975; Şengör et al., 1984). The massif has also been
276 mapped as a large-scale recumbent fold (Okay, 2001; Gessner et al., 2002), a series of nappes
277 stacked during south-directed thrusting (Ring et al., 1999; 2001; Gessner et al., 2001), or north-
278 directed thrusting (Hetzel et al., 1995a,b) (see Gessner et al., 2013). In the nappe model, the core
279 is represented by the Çine and Bozdağ nappes, whereas the cover would be the Bayındır and
280 Selimiye nappes (Ring et al., 2001), although all nappes may be part of the Menderes Massif
281 core series stacked during Eocene out-of-sequence thrusting (Régnier et al., 2007). Timeframes
282 recorded by the massif begin in the Archean and Neoproterozoic based on zircons extracted from
283 metagranites and orthogneisses with geochemical signatures dominated by reworking of old
284 crust (Oberhansli et al., 2010; Zlatkin et al., 2013). During this time, the Menderes Massif was
285 part of a collage of terranes associated with NE Africa and Arabia (Şengör et al., 1984; von
286 Raumer et al., 2015). Some Neoproterozoic zircons (ca. 570 Ma) have an older crust signature,
287 but others suggest a proximal juvenile source resembling the Arabian-Nubian shield (Zlatkin et
288 al., 2013).

289 Cambrian metagranites, orthogneisses, granulites, and eclogites, mica schists are
290 exposed throughout the massif (Hetzel & Reischmann, 1996; Dannat, 1997; Loos & Reichmann,
291 1999; Neubauer, 2002; Oberhansli et al., 2010; Zlatkin et al., 2013; Koralay, 2015). Cambrian-
292 Ordovician monazite and zircon inclusions are found in Menderes Massif garnets (Catlos &
293 Çemen, 2005; Etzel et al., 2019). During this time, the Menderes Massif was affected by events
294 related to the Cadomian Orogeny, and its core units were intruded by Pan African S- and I-type
295 granites followed by metamorphism (Neubauer, 2002). Note that other terranes within Western
296 Anatolia likewise have a Cadomian signature (Figure 4, e.g., Kozur & Göncüoğlu, 1998).
297 Granulite-facies metamorphism in the Menderes Massif was suggested to have occurred at
298 580.0 ± 5.7 Ma to 660 ± 61 Ma by (U-Pb monazite ages, Oelsner et al., 1997; U-Pb zircon ages,
299 Koralay et al., 2006). Middle-Triassic zircons in metagranites are found in its central portions
300 (Figure 4; Dannat, 1997; Koralay et al., 2001).

301 The timing of Menderes Massif nappe stacking is largely thought to have occurred during
302 the Eocene-Oligocene, or sometime after the Late Cretaceous (Main Menderes Metamorphism,
303 MMM., e.g., Satir & Friedrichsen, 1986; Konak et al., 1987; Dora et al., 1995; Bozkurt & Park,
304 1999; Bozkurt & Satir, 2000; Bozkurt & Oberhansli, 2001; Candan et al., 2001; Lips et al., 2001;
305 Gessner et al., 2011). Gessner et al. (2001) report that the Bayındır nappe deformed once during
306 the Eocene related to MMM., whereas the Bozdağ, Çine, and Selimiye nappes record pre-MMM
307 and MMM events. Figure 6 shows a paleogeographic reconstruction of the possible setting of the
308 fragments comprising Western Anatolia during the closure of the IAESZ during the Eocene. This
309 paleogeographic timeframe is critical for understanding the complex tectonic scenario that set the
310 scene before the onset of extension.

311 The Aegean Orogeny (Searle & Lamont, 2020a) is proposed for the tectonic history
312 further to the west of the Menderes Massif, including the Cycladic Metamorphic Core
313 Complexes but may mirror its development. In this scenario, subduction and a continent-
314 continent collision occur between the Eurasian and Adria-Apulia/Cyclades plates as marked by
315 ophiolite obduction at 74 Ma (Lamont et al., 2020a) and HP eclogite and blueschist facies

316 metamorphism at 57 Ma–46.5 Ma (Tomaschek et al., 2003; Lagos et al., 2007; Bulle et al., 2010;
317 Dragovic et al., 2012). The HP metamorphism ($P = 11\text{--}12$ kbar) is documented by ophiolitic
318 melanges that may record a cycle of Alpine collisional thickening followed by extension and
319 overprinting via extension (Papanikolaou, 1987, Okrusch & Bröcker, 1990; Avigad & Garfunkel,
320 1991; Katzir et al., 2000; Parra et al., 2002; Laurent et al., 2018; Lamont et al., 2020b). HP
321 metamorphism is recognized as part of a NE-trending subduction-exhumation channel (e.g.,
322 Xypolias & Alsop, 2014; Laurent et al., 2018; Gerogiannis et al., 2019). Crustal thickening and
323 regional kyanite – sillimanite grade Barrovian-type metamorphism occur from 22–14 Ma,
324 followed by orogenic collapse. The island of Naxos exemplifies the process with structural data
325 that suggest it is the result of the gravitational collapse of the Aegean orogenic wedge
326 (Vanderhaeghe, 2004). This model emphasizes the role of compression in forming Aegean
327 metamorphic core complexes (e.g., Coney and Harms, 1984; Searle and Lamont, 2020a,b),
328 which is an alternative to the perspective of solely extensionally-driven core complexes
329 discussed in the next section.

330 **2.2 Extensional history (Oligocene-Miocene)**

331 Following the final amalgamation of the various terranes as described in the previous
332 section, Western Anatolia experienced a switch from the dynamics of collision to extension and
333 extrusion (e.g., Berckhemer, 1977; Le Pichon & Angelier, 1979; 1981; Şengör & Yılmaz, 1981;
334 Şengör et al., 1985; Meulenkamp et al., 1988; Buick, 1991; Jolivet et al., 1994; Seyitoğlu &
335 Scott, 1996; Okay & Satir, 2000; Bozkurt, 2001; Çemen et al., 2006). A sequence of partial
336 melting, Barrovian metamorphism, and granitoid emplacement has been cited for providing
337 evidence of a change from crustal shortening to extensional tectonism (e.g., Keay et al., 2001;
338 Altunkaynak, 2007; Dilek & Altunkaynak, 2007; Altunkaynak et al., 2012; Rossetti et al., 2017).
339 The process may be recorded by numerous Oligocene to Miocene-age granites (Figure 4, Tables
340 5-8) and linked to the development of metamorphic core complexes located from northeastern
341 Greece and southern Bulgaria through the Aegean Sea and western Turkey.

342 In continental orogenic domains, metamorphic core complexes are deep crustal domes
343 exhumed and deformed during extension and are commonly surrounded by sedimentary and
344 volcanic rocks, which may be partly deposited during their exhumation (Tirel et al., 2008). Core
345 complexes in western Turkey and the Aegean region include the Rhodope, Kazdağ, Uludağ,
346 Cyclades, Menderes, and Crete massifs (Figure 1, Figure 2, and Figure 4) (Sokoutis et al., 1993;
347 Hetzel et al., 1995a,b; Burg et al., 1996; Lips et al., 1999; Bozkurt & Oberhänsli, 2001; Candan
348 et al., 2001; Lips et al., 2001; Ring et al., 2003; Bozkurt & Sözbilir, 2004; Duru et al., 2004;
349 Vanderhaeghe, 2004; Catlos & Çemen, 2005; Brun & Sokoutis, 2007; Okay et al., 2008;
350 Cavazza et al., 2009; Kruckenberg et al., 2011; Gessner et al., 2013; Baran et al., 2017).

351 In Western Anatolia specifically, the Menderes, Kazdağ, and Uludağ massifs are central
352 locations for studying post-collision extensional tectonics (Figures 1, Figure 2, and Figure 4)
353 (e.g., Şengör et al., 1984, Bozkurt & Park, 1994; Hetzel et al., 1995a,b; Yılmaz et al., 2001; Işık
354 & Tekeli, 2001; Çemen et al., 2006; Topuz & Okay, 2017). The Menderes Massif has global
355 importance due to its role as the largest zone of active continental extension (e.g., Jolivet &
356 Faccenna, 2000; Çemen et al., 2006). The region has long attracted the attention of those seeking
357 to understand the driving forces of extension from a variety of perspectives (e.g., Lister et al.,
358 1984, Thomson & Ring, 2006; Régnier et al., 2007; Gessner et al., 2013; Uzel et al., 2015). Both
359 low-angle detachment faults and high-angle normal faults bound sedimentary basins and separate
360 the Menderes Massif into northern (Gördes), central (Ödemiş), and southern (Çine) submassifs

361 (Figure 2). In the central Menderes Massif, Miocene-age granites are cut by the low-angle
362 Alasehir detachment, helping to constrain the timing of extension (Alasehir, Salihli, Turgutlu,
363 Table 8). The Kazdağ Massif is smaller in scale compared to the Menderes Massif and is a NE-
364 SW oriented structural dome or tectonic window flanked by detachment structures (Figure 2 and
365 Figure 4) (Okay et al., 1991; Okay & Satir, 2000; Duru et al., 2004; Bonev et al., 2009; Cavazza
366 et al., 2009). This massif's Evciler (Kazdağ) pluton routinely yields Oligo-Miocene
367 crystallization ages from a range of chronometers (Table 5). The Uludağ Massif is NW-SE
368 trending and has high-grade metamorphic and intrusive Eocene-Miocene age granitic rocks
369 (Figure 4, Table 5, Okay et al., 2008). Large Neogene basins bind the northern and southern
370 sections of the Uludağ Massif, and late-stage exhumation is largely thought to have occurred
371 during the Early Miocene (e.g., Topuz & Okay, 2017).

372 Besides these localities, Miocene ages have been reported for granites in the eastern
373 Tavşanlı zone (Table 2) [Kaymaz and Tekoren granodiorite (Günyüzü); Shin et al., 2013;
374 Demirbilek et al., 2018]. These ages likely represent metamorphism and subsequent alteration
375 associated with the large-scale extension/exhumation affecting Western Anatolia during this
376 time. Early Miocene ages also characterize granites closely associated with the Menderes,
377 Kazdağ, and Uludağ metamorphic core complexes. For example, Miocene ages are reported for a
378 group of granites near the Kazdağ Massif, extensively exposed in the Biga Peninsula and western
379 Pontides [Kozak, Eybek, Katrandag, Cataldag (Bozenkoy, Cataltepe, Turfaldag, Balicikhisar),
380 Kuscayir, and Kestanbol (Ezine), Figure 4, Table 5] and from a series of plutons grouped as the
381 Younger South Marmara Granitoids (Yenice, Ilica, Kizildam, Danisment, Sarioluk, Davutlar,
382 and Yeniköy; Figure 4, Table 5; Karacık et al. 2008). North of the Menderes Massif, Miocene-
383 age plutons also intrude the Afyon Zone, in close association with the Simav fault system, which
384 includes the lower angle Simav Detachment Fault (SDF) and higher-angle Simav Fault further
385 south (Koyunoba, Alaçam, and Egrigöz, Figure 2, Figure 4 and Figure 7, Table 7; Isik et al.,
386 2003).

387 The Simav structures are at the boundary between two dynamically distinct regions in
388 western Turkey: a northern component dominated by the NAFZ that accommodates the lateral
389 extrusion of the Anatolian block and a southern zone of large-scale crustal extension (Seyitoğlu,
390 1997; Ersoy et al., 2010). The Simav Fault is a distinct, a high-angle (~45-60°) system that
391 extends ~150 km between the towns of Banaz in the east and Sındırgı in the west (Figure 7)
392 (Ambraseys & Tchalenko, 1972; Seyitoğlu, 1997; Ersoy et al., 2010; Hetzel et al., 2013). The
393 structure near the town of Simav has >200 m of relief between the top of the hanging-wall and
394 footwall, and dips steeply to the north, roughly perpendicular to the current extension direction
395 (Tekeli et al., 2001; Işık et al., 2003). This fault is thought to have formed during the Pliocene
396 and is currently active (Seyitoğlu, 1997; Ring & Collins, 2005). Deciphering the sense of motion
397 of the Simav Fault has implications for the understanding of the neotectonic regime of Turkey
398 and is discussed further in the section regarding outstanding questions in Aegean tectonics.

399 Estimates of timing core complex exhumation and extension in Western Anatolia have
400 relied on calc-alkaline magmatism, widespread continental sedimentation, and mineral
401 chronometers (Sokoutis et al., 1993; Gautier et al., 1999; Catlos & Çemen, 2005; Altunkaynak &
402 Genç, 2008; Brun & Sokoutis 2010; Brun et al., 2016). In some locations, the complexes record
403 progression of magmatism from earlier Eocene-age mantle melts and input from asthenosphere
404 upwelling to later Oligocene to Late Miocene crustal contamination and subduction signatures,
405 with emplacement ages that young to the south (e.g., Delaloye & Bingöl, 2000; Altunkaynak &

406 Dilek, 2006; Dilek & Altunkaynak, 2007; Altunkaynak, 2007; Altunkaynak & Genç, 2008; Dilek
407 & Altunkaynak, 2009; Altunkaynak et al., 2012; Karaoğlu & Helvacı, 2014). However, this
408 simple scenario of melt origin and emplacement can be complicated, as the melts are influenced
409 by varied protoliths of varying sources, ages, and degrees of crustal anatexis (Pe-piper, 2000;
410 Stouraiti et al., 2010; 2018).

411 Late Cenozoic (since ~32 Ma) plutonic rocks are also widespread in the Aegean (e.g.,
412 Altherr et al., 1982; Henjes-Kunst et al. 1988; Pe-piper, 2000; Keay et al., 2001; Brichau et al.,
413 2007; 2008). The origin of the granites is linked to subduction migration along the Hellenic arc
414 (e.g., Fytikas et al., 1984; Schaarschmidt et al., 2021) or regional, widespread extensional
415 deformation (e.g., Boztuğ et al., 2009). Barrovian metamorphism on Naxos is thought to have
416 influenced the development of fluid-fluxed melts at ca. 8–10 kbar between 18.5 Ma and 17 Ma
417 (Lamont et al., 2019; Searle and Lamont, 2020b). Peak metamorphism is thought to have
418 occurred at 20.7–16.7 Ma (Keay et al., 2001). In some locations, coeval mafic and felsic melts
419 were emplaced (Seyitoğlu & Scott, 1996; Aldanmaz et al., 2000; Okay & Satir, 2000; Pe-Piper &
420 Piper 2001; Ozgenç & Ilbeyli, 2008). Magma compositions were influenced by a range of
421 factors, including inflowing mantle at the site of melting, the nature of the subduction component
422 and the degree of interaction between mantle and subduction components, as well as the melting
423 of fluid-rich mantle and the assimilation/crystallization history of the resulting hydrous magma
424 (e.g., Pearce & Stern, 2006). Extensive geochemical and isotopic studies of Miocene I-type
425 granitoid plutons of the central Aegean Sea show little evidence for a significant contribution of
426 mantle-derived magmas (Altherr & Siebel, 2002).

427 Cenozoic magmatism in the Anatolian microplate consists of three distinct, continuous
428 geochemical phases (Innocenti et al., 2005; Dilek & Altunkaynak, 2007; Altunkaynak & Genc,
429 2008; Akay, 2009; Altunkaynak et al., 2012). Magmatic rocks represent a Late Eocene-Middle
430 Miocene phase with orogenic character and a petrological affinity ranging from calc-alkaline to
431 dominant high-K calc-alkaline to shoshonites. During the Late Miocene–Early Pliocene, alkaline
432 volcanic rocks appear. The third phase is characterized by Pliocene–Quaternary Na-enriched
433 alkali basalts with an oceanic island basalt (OIB) signature (Aldanmaz, 2012). The first volcanic
434 activity in the South Aegean Active Volcanic Arc occurred between 5 and 2 Ma (e.g., Müller et
435 al., 1979; Fytikas et al., 1984; Matsuda et al., 1999; Elburg & Smet, 2020). The driver of
436 extension is widely thought to be the rollback of a subducting African slab (Figure 8, Figure 9,
437 and Figure 10) (e.g., Jolivet & Faccenna, 2000; Çemen et al., 2006; van Hinsbergen, 2010;
438 Royden 1993; Faccenna et al. 2003, 2014; Brun & Faccenna 2008). We discuss the slab and arc
439 dynamics, geometry, and age in the section regarding outstanding questions in Aegean tectonics.

440 **2.3 Strike-slip History (Late Miocene, Pliocene-present)**

441 The Aegean and Anatolian microplates have emerged to be type-localities for the model
442 of tectonic escape based on GPS vectors (Reilinger et al., 2006). In this scenario, the Anatolian
443 plate moves westward in response to the collision of Arabia and Eurasia (e.g., Şengör & Yılmaz,
444 1981; Şengör et al., 1985; Bozkurt, 2001). The North and East Anatolian transform fault systems
445 accommodate extrusion, and rollback along the Hellenic arc is suggested to provide space to
446 accommodate the escaping plate (McKenzie, 1972; Dewey & Şengör, 1979; Le Pichon &
447 Angelier, 1979; Jackson & McKenzie, 1984; Barka & Kadinsky-Cade, 1988; Taymaz et al.,
448 1991; Reilinger et al., 1997; McClusky et al., 2000; Tatar et al., 2013). Philippon et al. (2014)
449 suggest a two-stage evolution of the arc. At 30 Ma, extension was only driven by the southward
450 retreat of the Hellenic trench at a rate lower than 1 cm/yr, but since the last 13 Ma, the

451 interaction of trench retreat with Anatolia escape accelerated the rate of trench retreat in the
452 southwest direction at a rate of up to 3 cm/yr.

453 In western Turkey, extrusion tectonics is dominated by the active right-lateral North
454 Anatolian strike-slip fault (NAF) and North Anatolian Shear Zone (NASZ), which extends for
455 ~1200 from the Karlıova triple junction through the Sea of Marmara and Biga Peninsula (Figure
456 1) (Ketin, 1948; Barka, 1992; Armijo et al., 1999; Şengör & Zabcı, 2019). The NASZ contains
457 the NAF and is speculated to have accommodated from 25 to 110 km of displacement,
458 depending on location since the late Miocene (Westaway 1994; Yoshioka 1996; Armijo et al.,
459 1999; Hubert-Ferrari et al. 2002; Şengör & Zabcı, 2019). The structure accommodates ~24
460 mm/year of slip along northern Turkey (McClusky et al., 2000; Bulut et al., 2018). The
461 geometries of its western and eastern terminations are poorly defined (Barbot & Weiss, 2021).

462 The NAF splits into three strands as it trends westward into Western Anatolia and the
463 Aegean Sea (Figure 1) (e.g., Emre et al., 1998; Kürçer et al., 2008; Beniest et al., 2016; Şengör
464 & Zabcı, 2019). Each segment is comprised of several en échelon fragments (Emre et al., 1998;
465 Kürçer et al., 2008). The northernmost E-W striking segments within the Sea of Marmara change
466 strike in the Northern Aegean Sea towards a NE-SW orientation in the North Aegean Trough,
467 maintaining its right-lateral strike-slip character but splits across three basins and two
468 transpressional ridges (Bulut et al., 2018). A branch between the northern and central segments
469 originates southeast of Sapanca Lake (Kürçer et al., 2008) and terminates at the western end of
470 the North Aegean Trough (Ferentinos et al., 2018). This structure enters the Aegean Sea and
471 trends into the Northern Skyros Basin. Strands of the NAF have also been linked to the KTZ
472 through the transtensional Central Hellenic Shear Zone (Royden & Papanikolaou, 2011;
473 Evangelidis, 2017). In the Western Anatolia -Marmara region, the NAF may have been active
474 since the Pliocene (e.g., Ünay et al., 2001).

475 Sakellariou et al. (2013) suggest that the southwestward expansion and stretching of the
476 Aegean microplate during Plio-Quaternary is accommodated by a northern right lateral tectonic
477 boundary marked by the KTZ and NASZ, and a southern left-lateral tectonic boundary, marked
478 by the Pliny and Strabo trenches (Figure 9). Papanikolaou and Royden (2007) note that regional
479 extension has a much-reduced role in the dynamics of the Aegean microplate and that, in fact, no
480 active extensional strain is present, except for a small southeastern domain (Figure 1) (Corinth
481 rift, south Viotia, south of Evia, and across the Sperchios-Kammena Vourla rift; Brooks &
482 Ferentinos 1980; Chousianitis et al., 2013, 2015). Maggini & Caputo (2020) report that
483 seismogenic faults in the internal Aegean domain associated with the Hellenic subduction arc are
484 characterized by pure normal and strike-slip kinematics or by a combination and that active
485 thrusting is limited to the central and western sectors of the Hellenic subduction zone and the
486 offshore regions external to it.

487 Figure 11 shows the focal mechanisms for some recent earthquakes (2010-2020) that
488 appear along the Aegean-Anatolian microplate boundary. Recent earthquakes with focal
489 mechanisms consistent with reverse faulting have occurred south of Crete, including those
490 associated with an Mw 6.4 earthquake on 5/2/2020. These earthquakes occurred at relatively
491 shallow depths (6.5-9.6 km, Table 10) and may be associated with a plate interface zone defined
492 by the upper plate and splay-thrust faults (Saltogianni et al., 2020). Observations and modeling
493 of historical and recent earthquakes have shown that uplift along the Hellenic arc margin
494 offshore of Crete is controlled by reverse fault motion with little contribution from plate-
495 interface slip (e.g., Mouslopoulou et al., 2015).

496 Extrusion and deformation in Western Anatolia are also accommodated by transfer zones,
497 where strain is transferred from one structural element to another and displacement changes
498 between individual fault and basin segments (e.g., Gawthorpe & Hurst, 1993; Barbot & Weiss,
499 2021). Some examples of these zones include the NE-SW trending strike-slip dominated Izmir–
500 Balıkesir transfer zone (İBTZ), Uşak-Mugla Transfer Zone (UMTZ), and Southwestern
501 Anatolian Shear Zone (SWASZ) (Figure 1 and Figure 2) (Çemen et al., 2006; Oner et al., 2010;
502 Sözbilir et al., 2011; Gessner et al., 2013; Özkaymak et al., 2013; Uzel et al., 2013; Karaoğlu &
503 Helvacı, 2014; Seghedi et al., 2015). These transfer zones have been considered as significant
504 portions of the larger Western Anatolian Shear Zone (WASZ) or Western Anatolian Extensional
505 Province (Figure 1) and may have developed due to mantle processes related to the subduction of
506 the Aegean slab (e.g., Gessner et al., 2013; Uzel et al. 2020). Some transfer zones trend into
507 other fault systems. For example, the İBTZ is speculated to connect to the Mid-Cycladic
508 Lineament (MCL) in central Greece and the NASZ in northern Turkey (Figure 1, Figure 11)
509 (Uzel et al., 2013; Seghedi et al., 2015; Westerweel et al., 2020). The MCL is a strike-slip
510 structure that may be the result of the reactivation of the Vardar suture zone, evidenced by the
511 North Cycladic Detachment (Figure 11), to accommodate westward extrusion of Anatolia in the
512 Late Miocene (e.g., Philippon et al., 2014). These transfer zones have been used to illustrate that
513 the Aegean and Anatolian microplates experienced or are currently transitioning from a stress
514 regime dominated by extension to transform tectonics (Papanikolaou & Royden, 2007; Cavazza
515 et al., 2009).

516 Presently, normal fault motion exists within the İBTZ as illustrated by focal mechanisms
517 from a 2020 Mw 6.6 earthquake and 2018 Mw 4.5 earthquake within the zone. An Mw 4.4
518 earthquake with normal motion occurred off the coast of Amorgos near the 1956 Mw 7.7 (or 7.8)
519 earthquake, one of the strongest earthquakes of the 20th century in the area of the South Aegean
520 (Okal et al., 2009; Alatza et al., 2020). The 1956 event has debated focal mechanisms, as either
521 strike-slip or normal faulting geometries (see Okal et al., 2009). A normal sense of motion also is
522 found with some recent earthquakes near the NASZ, including 2017 Mw 6.2 and 2017 Mw 5.3
523 earthquakes (Figure 11, Table 10). These events are likely associated with transtensional motion.

524 **3. Outstanding Questions in Aegean Tectonics**

525 As outlined in the previous section, significant contributions have been made regarding
526 the fundamental tectonics and geological history recorded by rocks throughout the Western
527 Anatolian microplate. However, outstanding questions remain to be addressed regarding the
528 boundary between the Aegean and Anatolian microplates that affect our understanding of the
529 mechanisms that drive extension in the Earth's lithosphere. Most of these questions center on
530 how upper lithospheric and crustal deformation are linked and are related to lower lithosphere
531 and mantle processes.

532 **3.1. Slab dynamics**

533 **3.1.1 African slab geometry and connections to other subduction systems**

534 Based on several geophysical, tectonic, and geochemical developments, the subducting
535 African (Nubian or Aegean) slab has emerged as the primary driver for extension in the Aegean
536 and Anatolian microplates and the development of their metamorphic core complexes (Figure 1,
537 Figure 2, Figure 8, Figure 9, and Figure 10) (e.g., Jolivet et al. 2013; Jolivet & Faccenna, 2000;
538 Çemen et al., 2006; Dilek & Sandvol, 2009; van Hinsbergen et al., 2010; van Hinsbergen &
539 Schmid 2012; Salaün et al., 2012; Faccenna et al., 2014; El-Sharkawy et al., 2020; Barbot &

540 Weiss, 2021). The Hellenic and Cyprus arcs are the surface expression of the subducting African
541 plate and eastern Mediterranean lithosphere beneath the Anatolian and Aegean microplates (e.g.,
542 Le Pichon & Angelier, 1979; Angelier et al., 1982; Anastasakis & Kelling, 1991; Papazachos et
543 al., 2000; Ergün et al., 2005; Ganas & Parsons, 2009; Hall et al., 2009; Royden & Papanikolaou,
544 2011; Hall et al., 2014; Symeou et al., 2018; Ventouzi et al. 2018).

545 Although it has a well-developed Wadati-Benioff zone dipping $\sim 30^\circ$ from 20-100 km
546 depth and $\sim 45^\circ$ from 100-150 km depths (Figure 10B) (e.g., Papazachos & Comninakis, 1971;
547 Papazachos et al., 2000; Sukale et al., 2009; Hayes, 2018), it has a debated slab geometry at
548 intermediate depths (150-250 km, Suckale et al., 2009; Agostini et al., 2010; see review in
549 Hansen et al., 2019; El-Sharkawy et al., 2020). Seismic body wave tomography shows it extends
550 into the upper and lower mantle to 1400 ± 100 km depth (Figure 10A) (e.g., Spakman et al., 1988;
551 Bijwaard et al., 1998; van der Meer et al., 2018; see review in Bocchini et al., 2018). However,
552 the slab may be a single folded body that overturned in the lower mantle (Faccenna et al., 2003),
553 or two slabs, located between 2000-1500 km and from 1500 km to the surface (van Hinsbergen
554 et al., 2005; van der Meer et al., 2018). Mantle tomography has shown multiple subducted slabs
555 beneath the Aegean and Anatolian microplates (e.g., Spakman et al., 1988; Spakman, 1990;
556 1991; Wortel & Spakman, 2000; Govers & Fichtner, 2016; van der Meer et al., 2018; Wei et al.,
557 2019). Blom et al. (2019) show the Hellenic slab, visible in both S and P velocity, extending
558 from the surface to the transition zone in a bent, arcuate shape. A high-velocity structure exists
559 beneath the Hellenic arc and the Aegean Sea that flattens from the 410 km discontinuity and is
560 not seen at deeper levels. Wei et al. (2020) show a gap in the subducting slab at depths of 60-100
561 km just west of the south Hellenides. In the South Hellenides, slab tear may be visible at the 660
562 km discontinuity, whereas four slabs are imaged beneath the North Hellenides.

563 Interpretations of these tomographic images have indicated that more slab is imaged than
564 is reflected by seismicity (e.g., Spakman et al., 1988; Papadopoulos, 1997; Bijwaard et al.,
565 1998), and that a variation of slab exists thickness across the Aegean Sea (e.g., Karagianni et al.,
566 2002). Mantle tomography has also shown that not all slabs in the Mediterranean region are
567 connected to the lithosphere at the surface, consistent with past delamination (e.g., Spakman et
568 al., 1988; Dilek & Sandvol, 2009; Wortel & Spakman, 2000). Challenges in imaging the
569 subduction zone include its small size, its spatially highly variable nature, and the uneven
570 distribution of its seismic stations (El-Sharkawy et al., 2020).

571 The Hellenic subduction system is comprised of three regions: an outer compressional
572 non-volcanic arc, a volcanic arc, and an extensional back-arc region that makes up the broader
573 Aegean Sea region (Figure 8) (McKenzie 1972; Papazachos, 2019). Although the Western
574 Hellenic Arc (also termed the North and Southern Hellenic arc, Royden & Papanikolaou, 2011)
575 has a well-defined topography, trench, sedimentation, and strain pattern (Stanley et al., 1978;
576 Papadopoulos et al., 1988; Hatzfeld et al., 1990; Cocard et al., 1999), the central and eastern
577 portions of the Hellenic arc are more difficult to characterize as the boundary becomes diffuse
578 (Beißer et al., 1990; Shaw & Jackson, 2010; Özbakır et al., 2013). The Hellenic arc's connection
579 with the Cyprus arc and even the nature of plate motion along strike of the Cyprus arc has been
580 debated (Anastasakis & Kelling, 1991; Woodside et al., 2002; Ergün et al., 2005; Hall et al.,
581 2009; Harrison et al., 2012; Kinnaird & Robertson, 2012; Symeou et al., 2018). The surface
582 morphology of the southern and eastern portions of the Hellenic arc and its connection to the
583 Cyprus arc is obstructed by up to 300-km wide, 6-10 km-thick section of sediments that
584 comprise the Mediterranean Ridge (Figure 8 and Figure 9; Heezen & Ewing, 1963; Emery et al.,

1966; Le Pichon et al., 1982; Kenyon et al. 1982; Kastens et al., 1992; Foucher et al., 1993; Westbrook & Reston, 2002; Kopf et al., 2003). The ridge is a giant accretionary complex, extending ~2000 km from the Calabrian Rise east of Greece to the Florence Rise, and is the largest structural unit of the Eastern Mediterranean Sea (Liminov et al., 1996; Cita et al., 1996). The front of subduction of the Hellenic arc is located south of the Mediterranean Ridge (e.g., Jost et al., 2002; Westbrook & Reston, 2002; Jolivet et al., 2013). The majority of the subducting African plate beneath the ridge is oceanic, except along the central sector of its southern margin, where the accretionary complex collides with the African continental margin (Chaumillon & Mascle, 1997; Westbrook & Reston, 2002). The ridge may be the fastest outward growing wedge in most recent Earth history, with a rate of up to 10 km/Myr (Kastens, 1991; Kopf et al., 2003). It has been speculated to grow by off scraping against a backstop formed by the Alpine nappes of the Hellenic Arc (Kastens, 1991).

The intensively folded and faulted rocks of the Mediterranean Ridge vary in geometry along strike (Cita et al., 1996; Chaumillon & Mascle, 1997; Westbrook & Reston, 2002; Kopf et al., 2003). In its western and eastern portions, the wedge accumulates sediments, but in its central portion between Libya and Crete, the ridge behaves unlike a typical accretionary complex. In this area, a trench system (the Hellenic trenches; Ptolemy, Pliny, and Strabo; Figure 9) developed in between the accretionary complex and volcanic arc, likely as a result of back-thrusting beneath the northern edge of the complex (Galindo-Zaldivar et al., 1996; Westbrook & Reston, 2002). The accretionary complex is unusual compared to others worldwide, not only because of these back thrusts but also because it appears to have formed in a continent-continent collisional setting and contains shallow, Messinian-age evaporites (e.g., Cita et al., 1996; Chaumillon & Mascle, 1997). These evaporites influence its deformation and fast growth rate due to their mechanical properties and effect upon fluid flow and pressure (Kastens, 1991; Westbrook & Reston, 2002; Kopf et al., 2003). Understanding the development of the Mediterranean Ridge is critical to determining the initiation age of the Hellenic arc, as described in the next section.

3.1.2 The age of subduction of the African slab

The Subduction Zone Initiation (SZI) age is defined as the onset of downward plate motion forming a new slab, which later evolves into a self-sustaining subduction zone (Crameri et al., 2020). Constraints regarding SZI age of the present-day expression of the Hellenic arc developed from several independent approaches, including timing sedimentation within the Mediterranean Ridge (Kastens, 1991; Kopf et al., 2003), analysis of topography combined with estimates of slab age and depth (McKenzie, 1978; Le Pichon et al., 2019), reconstructions of subducted slabs using tomography (e.g., Spakman et al., 1988), paleomagnetism (Savostin et al., 1986; Marsellos et al., 2010), and the timing of metamorphism and volcanic activity (e.g., Fytikas et al., 1984). Early estimates for the initiation of Hellenic arc subduction are 13 ± 3 -5 Ma (Le Pichon & Angelier, 1979) to 5-10 Ma (McKenzie, 1978; Mercier, 1981) based on interpretations of seismic activity coupled with assumptions regarding the age of subducted lithosphere and subduction depths. These ages are similar to the onset of the KTZ based on geodynamic modeling and GPS data (Figure 1) (6-8 Ma, Royden & Papanikolaou, 2011) and the timing of the earliest volcanic activity in the South Aegean arc (Pliocene, Pe-Piper & Piper, 2005). Reconstructions of fault systems in the northern margin of the eastern Mediterranean Sea are consistent with estimates of 15 Ma (Le Pichon et al., 2019).

However, interpretations of the Aegean seismic velocity structure, tomography, and seismicity data in the Aegean area suggest older estimates (26-40 Ma; Meulenkamp et al., 1988;

630 Spakman et al., 1988; Papadopoulos, 1997; Brun & Sokoutis, 2010). These ages are more
631 consistent with the ages of granitic intrusions found throughout Western Anatolia (Figure 4,
632 Tables 5-8) and the timing of the onset of sedimentation associated with the Mediterranean
633 Ridge at 23.6-33 Ma (Fytikas et al., 1984; Kastens, 1991). Younger estimates from the ridge are
634 also reported (~19 Ma, Kopf et al., 2003). Plate reconstructions suggest that the Northern
635 Hellenic trench experienced the onset of subduction from 27-34 Ma, whereas the southern
636 Hellenic segment was active at 34 Ma (Royden & Papanikolaou, 2011).

637 If the incoming lithosphere is heterogeneous in terms of thickness and compositions,
638 subduction zones may behave chaotically, in that they may, over time, retreat, advance, or
639 remain stationary at different stages (e.g., Royden & Husson 2009; Husson et al., 2009). The
640 progressive deceleration in motion of Africa with respect to Europe in the Mediterranean region
641 is observed to have occurred since 35 Ma, and in the eastern Mediterranean from 35 Ma to 10
642 Ma to a convergence rate of a few mm/yr (Savostin et al., 1986; Marsellos et al., 2010). The rate
643 of trench retreat is estimated to have accelerated from ~0.6 cm/y during the first 30 M.y. of
644 subduction to 3.2 cm/yr during the past 15 m.y., perhaps due to Middle Miocene-Pliocene slab
645 tear (Brun et al., 2017). Differences in the timing of initiation and rate of subduction exist
646 between segments along the Western Hellenic Arc and should also be expected to occur along
647 other portions of the Hellenic and Cyprus arcs (Royden & Papanikolaou, 2011; Pearce et al.,
648 2012). The timing of interpreted ductile ‘extensional’ shear fabrics in metamorphic rocks can
649 also be complicated as these may record extrusion instead of processes associated with slab
650 rollback (see Searle and Lamont, 2020b).

651 These Late Cenozoic estimates are difficult to reconcile with the model in which the
652 Hellenic arc is a single, evolving subduction zone system that initiated in the Mesozoic (Jurassic)
653 (Faccenna et al., 2003; van Hinsbergen, 2005; Royden & Papanikolaou, 2011; Jolivet et al.,
654 2013; Malandri et al., 2017). In this scenario, the Vardar suture in Greece, equivalent to the
655 IAESZ (Channell & Kozur, 1997; Okay & Tuysuz, 1999; Moix et al., 2008), and Pindos suture
656 zone, equivalent to units within the Antalya domain and Dilek peninsula (Stampfli & Kozur,
657 2006) had buoyant microcontinents that entered and locked subduction, triggering southward
658 slab rollback and migration of the volcanic arc (van Hinsbergen et al. 2005; Brun & Faccenna
659 2008; Jolivet & Brun 2010; Jolivet et al., 2013; Cornée et al., 2018). The model eliminates the
660 need for multiple sutures and subducted slabs to be present beneath western Turkey and the
661 Aegean and simplifies the evolution of the Aegean microplate to a single evolving, long-lived
662 subduction system. The present-day curvature of the Hellenic forearc thus represents oblique
663 subduction and a plate-boundary expression that grew systematically over long periods of
664 geological time (Huchon et al., 1982; Le Pichon et al., 1995; ten Veen & Kleinspehn, 2003;
665 Gautier et al. 1999; Le Pichon et al., 2002; Wallace et al., 2005, 2008; van Hinsbergen &
666 Schmid, 2012; Philippon et al., 2014; Cornée et al., 2018).

667 The single subduction system requires all the lower plate continental crust to be accreted
668 into the upper plate while subducting continental lithosphere and requires the entire Aegean
669 Crust from the Vardar suture to the Mediterranean ridge was derived from the lower plate (e.g.,
670 Figure 2 in van Hinsbergen et al. 2005). Oceans between the accreted domains were of
671 significant size (500 km in some cases), and the process would lead to significant elevation
672 changes, crustal thicknesses, and critical changes in the zone of subduction transitions occurred
673 from oceanic to continental shear zones (see discussion in Le Pichon et al., 2019). Not all units

674 record blueschist facies conditions, and some experienced Barrovian prograde (burial) P-T paths,
675 such as on the island of Naxos (e.g., Lamont et al., 2019).

676 Currently, the Hellenic arc is migrating SW faster than the counterclockwise rotation of
677 Anatolia (ten Veen & Kleinspehn, 2003), and the rate of convergence between Africa and
678 Eurasia is 4 cm/yr (Reilinger et al., 1997; Kahle et al., 2000; McClusky et al., 2000; Hollenstein
679 et al., 2008). Timing constraints on Aegean forearc curvature, due to opposite rotations,
680 clockwise in the west and counterclockwise in the east, are Eocene and Middle Miocene (Morris
681 & Robertson 1993; Cornée et al., 2018). Trench bending and rollback increased subduction
682 obliquity over time, which has been accommodated by strain partitioning within the upper
683 Eurasian plate (Philippon et al. 2014; Brun et al. 2016; Cornée et al., 2018). Subduction zones
684 with limited trench-parallel lengths on the order of the Hellenic arc (600-800 km) and narrow
685 slabs (<1,500 km) typically have rapid retreat rates (Schellart et al., 2007; Bolhar et al., 2010).

686 **3.1.3 The number, location, and impacts of slab detachments and tears**

687 An additional key focus of study has been identifying the location, depth, and
688 relationship of ancient and present-day active subducting slabs and their detachment mechanisms
689 beneath the Aegean and Anatolian microplates (see review in Hansen et al., 2019; El-Sharkawy
690 et al., 2020). Several locations across the Aegean and Anatolian microplates have been suggested
691 to be affected by slab tear, either trench parallel or perpendicular (Figure 1). The tearing process
692 in the near term can lead to intermediate-depth seismicity (e.g., Meighan et al., 2013) and explain
693 earthquakes that appear inconsistent with a coherent subducting slab (e.g., Clark et al., 2008).
694 Tears can lead to large volume magmatism (e.g., Cocchi et al., 2017), changes in igneous
695 geochemistry, and facilitate the ore-forming process and mineral deposits (e.g., de Boorder et al.,
696 1998; Rabayrol et al., 2019; Rabayrol and Hart, 2021). The process leads to asthenosphere
697 upwelling and changes in thermal and fluid regimes (e.g., Roche et al., 2018; Gessner et al.,
698 2018). Slab tear has been related to present and past geothermal activity in Western Anatolia and
699 the generation of a late Eocene-Miocene metallogenic period (Pb-Zn- followed by Au-rich)
700 (Menant et al., 2018; Gessner et al., 2018; Rabayrol & Hart, 2021). Their presence significantly
701 affects plate dynamics, including subduction rates, plate motion, and mantle dynamics (e.g.,
702 Gianni et al., 2019).

703 These sites vary in scale from regional to local and include the boundary between the
704 Hellenic and Cyprus arcs (Wortel & Spakman, 1992; Biryol et al., 2011), at the Anaximander
705 Mountains (Woodside et al., 1992), south of Crete at the Pliny–Strabo Shear Zone (Özbaşır
706 et al., 2013), the İBTZ transfer zone (e.g., Kaya, 1981; Gessner et al., 2013), and beneath the
707 Menderes Massif itself (Biryol et al., 2011; Rabayrol & Hart, 2021). A tear is speculated to
708 generate a ~200 km-depth low-velocity anomaly below western Turkey (Roche et al., 2019).
709 Slab tear has been used to interpret the deep Rhodes Basin (Faccenna et al., 2014; Woodside et
710 al., 2000) and tectonic activity within southwest Anatolia (Biryol et al., 2011; Roche et al.,
711 2019).

712 Trench-parallel tear affects the subducting African lithosphere between northern Greece
713 and the Gulf of Corinth along the Western Hellenic Arc (Hansen et al., 2019). Trench-
714 perpendicular tear may accommodate the region between the Hellenic and Cyprian arcs, which
715 differ in subduction steepness and material subducted (Dilek & Sandvol, 2009). The Cyprian arc
716 involves shallower subduction dynamics with the Eratosthenes seamount and Anixamander
717 Mountains (mud volcanoes; Lykousis et al., 2009) impinging on the trench (Figure 9) (Kempler

718 & Ben-Avraham 1987; Zitter et al. 2003). The back thrusts and tectonic geometry of the
719 Mediterranean Ridge has led to speculation that the African slab detached in the region between
720 Libya and Crete (Kopf et al., 2003). Alternatively, a Subduction Transform Edge Propagator
721 (STEP, a tear fault or a hinge fault, Govers & Wortel, 2005) may exist in this region (Özbakır et
722 al., 2013). Nine of these structures have been proposed to exist beneath southern Greece,
723 segmenting the subducting African slab and contributing to seismicity and deformation
724 (Sachpazi et al., 2016). A STEP is also proposed for the transition between the Cyprus and
725 Hellenic arcs (e.g., Salaün et al., 2012; Elitez et al., 2016; Portner et al., 2018).

726 The KTZ (Figure 1 and Figure 9) has been a particular subject of the debate regarding
727 slab tear (see Bocchini et al., 2018; Hansen et al., 2019). The structure is part of the Western
728 Hellenic Subduction Zone, considered one of the most seismically active areas in Europe (Pearce
729 et al., 2012; Halpaap et al., 2018). The KTZ may represent a vertical tear along oceanic and
730 continental lithosphere (Suckale et al., 2009), forming the KTZ as a STEP-fault (Govers &
731 Wortel, 2005). The STEP fault may be in its initial stages of forming (Evangelidis, 2017;
732 Özbakır et al., 2020), or the slab may have entirely detached (Wortel & Spakman, 2000). A
733 smooth transition has also been proposed between two segments, without the presence of a tear
734 between, at least at depths shallower than 100 km (Pearce et al., 2012; Halpaap et al., 2018).

735 Despite the fragmentation of the subducting African lithosphere, the thickness of the
736 Aegean and Anatolian crust is remarkably similar (Zhu et al., 2005; Sodoudi et al., 2006;
737 Karabulut et al., 2019). Estimates from the central Menderes Massif are 28–30 km (Zhu et al.,
738 2005), whereas the thickness beneath the Aegean Sea averages ~25 km (Zhu et al., 2005; Tirel et
739 al., 2004; Kind et al., 2015). The crustal thickness in the southern and central parts of the Aegean
740 is reported to be thinner (20–22 km), whereas the northern Aegean Sea shows a relatively thicker
741 crust (25–28 km) (Karagianni et al., 2005; Sodoudi et al., 2006). Depending on the model used,
742 the crustal thickness beneath western Crete could be 32.5–35 km or up to 45 km (Snopek et al.,
743 2007). Karabulut et al. (2019) demonstrates large crustal thickness variations (20–47 km) from
744 western Greece to eastern Anatolia but shows that these are fairly uniform within specific
745 regions. In Western Anatolia, the crustal thicknesses are 25–30 km, increasing slightly to the
746 north, whereas in southern Anatolia, crustal thicknesses decrease from 35 to 25 km in the
747 Mediterranean Sea, except north of Antalya Bay, where the thickness locally reaches 40 km. A
748 thickness of 40 km is in line with estimates of Eastern Anatolia (Kind et al., 2015), western
749 Greece (Karagianni et al., 2005), and the Anatolian plateau (Saunders et al., 1998).

750 These thickness estimates seem at odds with large-scale back-arc thinning typically seen
751 in subduction zone settings (e.g., Saunders & Tarney 1984). The Aegean is not a typical back-arc
752 basin (Agostini et al., 2010; Doglioni et al., 2002) because it is underlain by a thick layer of
753 continental crust and lacks an ocean floor (e.g., Makris, 1978), is disrupted by the active North
754 Anatolian Shear Zone (NASZ) in its northern portion (e.g., Brooks & Ferentinos, 1980; Gürer et
755 al., 2006; Kokkalas et al., 2006; Kreemer et al., 2004; Lyberis, 1984). The region displays a
756 complex tensional regime where crustal stretching is inconsistent with the geometry and
757 direction of the subducting Hellenic slab (e.g., Mantovani et al., 1997; Agostini et al., 2010). The
758 premise of extrusion tectonics driven by convergence in the west requires a free lateral boundary
759 in the east. However, the Aegean plate is constructed mainly of continental lithosphere and has a
760 similar thickness as the Anatolian plate, as seen in both bathymetry (Figure 9) and seismic
761 reflection (e.g., Zhu et al., 2005; Sodoudi et al., 2006). However, slab ruptures associated with
762 the differential retreat, inherited lower plate lithospheric heterogeneities, and mantle upwelling

763 would provide accommodation for the microplates to extrude (Agostini et al., 2010; Govers &
764 Fichtner et al., 2016; Karabulut et al., 2019). The onset of the NASZ may be the result of slab
765 deformation and detachment beneath the Bitlis–Hellenic subduction zone, which accelerated slab
766 retreat in the west and indentation of the continent along the Bitlis–Zagros suture zone (Figure 1)
767 (Faccenna et al., 2006; Schildgen et al., 2014)

768 **3.2 Timing, number, and geometry of transfer zones**

769 Transfer zones play a significant role in accommodating tectonic escape (Barbot &
770 Weiss, 2021), and despite their importance in accommodating the present-day subduction
771 dynamics, when, how, and why specific transfer zones occur across Western Anatolia is debated.
772 For example, the İBTZ is a deep crustal transform fault zone consisting of NE-trending active
773 strike-slip dominated faults and accommodates differential deformation between the Cycladic
774 and Menderes core complexes (Uzel et al., 2013; 2020). The İBTZ is also mapped as the
775 Western Anatolian Transfer Zone (WATZ, Gessner et al., 2013; 2017). The zone may be the
776 surface expression of a tear in the subducting African slab (Gessner et al., 2013; Uzel et al.,
777 2015; Sümer et al., 2018) or a transition between extensional and strike-slip dynamics due to the
778 southward rotation rollback of the subduction zone (Ersoy & Palmer, 2013; Özkaymak et al.,
779 2013; Ersoy et al., 2014; Ersoy et al., 2017; Uzel et al., 2020). Based on a compilation of data
780 from igneous rocks throughout Western Anatolia, Uzel et al. (2020) suggest that volcanic
781 activity in the region is always associated with the İBTZ as recorded by the positions of the
782 eruption centers that follow the trend of the transfer zone. A lack of $^{40}\text{Ar}/^{39}\text{Ar}$ ages from igneous
783 assemblages between 15.97 and 13.82 Ma is attributed to a pulse of core complex exhumation
784 and a change in partitioning extension between the Cyclades and Menderes Massif. Geochemical
785 compositions of Miocene-age (17.48–14.94 Ma) volcanoes within the transfer zone indicate their
786 origins are decompression melting of the upper mantle/lower crust, consistent with the outcome
787 of regional transtensional movements in a post-collisional setting (Seghedi et al., 2015). Slab-
788 tear typically results in asthenosphere-derived (Ocean-Island Basalt, OIB-like) Na-alkaline
789 basalts, which are only exposed in the region within the northern Menderes Massif (Kula
790 volcanics) (Holness & Bunbry, 2006; Ersoy et al., 2017).

791 The İBTZ may trend further south into the MCL, an extensional fault exposed near or on
792 the island of Paros that records orogen-parallel extension or transform fault motion (Figure 11)
793 (Morris & Anderson, 1996; Avigad et al., 1998; Walcott & White, 1998; Pe-Piper et al., 2002;
794 Tirel et al., 2009; Gessner et al., 2013; Philippon et al., 2014; Beniest et al., 2016; Malandri et
795 al., 2017). Besides the İBTZ, the SWASZ and UMTZ are located near each other on the border
796 of the Menderes Massif, but their influence on each other is presently unclear (Figure 2).

797 **3.3 Magmatic influence in driving extension**

798 Throughout Western Anatolia, magmatic pulses are exposed as geochemically variable
799 extrusive and intrusive igneous rocks (Tables 1-9; Figure 4; e.g., Rossetti et al., 2017).
800 Metamorphic core complexes with their associated post-collisional magmatic suites offer
801 insights into the tectonic processes controlling crustal extension (e.g., Perkins et al., 2018).
802 Extensional systems cut igneous intrusions in Western Anatolia metamorphic core complexes,
803 and their ages are critical for timing events that facilitated their emplacement. Geochemical data
804 regarding the depths of granite formation lends additional insight into how the mantle processes
805 operated in the past. The picture, however, is complicated by the influence of the collisional
806 dynamics that characterized the earlier assembly of the microplate (see Assembly section).

807 Granite crystallization ages provide information regarding how extension during the Eocene to
808 Miocene migrated through Western Anatolia and the Aegean region in the past (e.g., Delaloye &
809 Bingöl, 2000; Pe-Piper, 2000; Altunkaynak & Dilek, 2006; Altunkaynak et al., 2012).

810 Magma bodies can drive extension through the conductive transfer of heat from
811 upwelling of hot, asthenospheric mantle beneath significantly extended crust, and small volume
812 partial melts can exploit crustal pathways developed during extensional deformation (e.g.,
813 McKenzie & Bickle 1988; von Blanckenburg & Davies 1995; Perkins et al., 2018). Volatiles
814 facilitate additional crustal deformation and metamorphism, resulting in feedbacks between
815 decompression and mantle upwelling and driving additional lithospheric melting (Teyssier &
816 Whitney, 2002; Kendall et al., 2005; Whitney et al., 2013; Platt et al., 2015; Perkins et al., 2018).
817 The Menderes Massif of western Turkey is suggested to be a key area to study feedback
818 relationships between magma generation/emplacement, rheological weakening, activation of
819 extensional detachment tectonics (Rossetti et al., 2017). The island of Naxos likewise illustrates
820 the interplays between lower crustal flow and upper crustal extension and between buoyancy-
821 and isostasy-driven controls in developing migmatite domes (Kruckenberg et al., 2011). The
822 connections between detachment faulting and magma emplacement have also been explored in
823 the Cyclades (e.g., Rabillard et al., 2018).

824 To determine the role between magma generation and extension requires understanding
825 intrusive rock relationships to fault structures. In Western Anatolia, maps of the same pluton are
826 commonly inconsistent in terms of the locations of structures that may have affected or result
827 from exhumation. For example, the northern boundary of the Kozak pluton (Figure 4) is shown
828 by some as an intrusive contact (Akal & Helvacı, 1999) but by others as fault-bounded
829 (Altunkaynak & Yilmaz, 1998; 1999; Yilmaz et al., 2001). The Eğrigöz, Koyunoba, and Alaçam
830 plutons (Figure 4) have been the focus of many field-based, geochemical and geochronological
831 studies, but conflicting ideas exist regarding their relationship to the SDF (Figure 7) (see Catlos
832 et al., 2012). For example, Işık and Tekeli (2001) map the SDF only along the northern portion
833 of the Eğrigöz pluton, whereas Ring and Collins (2005) and Işık et al. (2004) indicate the SDF is
834 exposed along the western edge of both the northern Eğrigöz and Koyunoba plutons. Seyitoğlu et
835 al. (2004) place the SDF within the central portion of the Eğrigöz pluton, whereas Ersoy et al.
836 (2010) mark the structure as following the outer boundaries of the Eğrigöz and Koyunoba
837 bodies. Thomson and Ring (2006) place the detachment prominently along the northern edge and
838 central portion of the Eğrigöz granite and along the eastern edge of the Koyunoba body. Recent
839 gravity measurements suggest an igneous intrusion at depth near the Simav Fault (Toker et al.,
840 2018, 2019). The 12-15 km-thick intrusion is located in the NE margin of the Simav graben at
841 2.5-3 km below the surface and has been suggested to be a primary driver of recent-day
842 seismicity. Developing links between magmatism and extensional dynamics requires a critical
843 structural understanding of the granite petrology, structures, and clear delineation between how it
844 appears affected by fault systems (e.g., Kruckenberg et al., 2011; Rabillard et al., 2018).

845 In Western Anatolia, many published maps also do not distinguish different granite types
846 or textural orientations (Karacik & Yilmaz, 1998; Akal & Helvacı, 1999; Şahin et al., 2010).
847 Mineral lineations and solid-state or magmatic fabrics associated with faulting or shearing are
848 rarely reported. Besides the standard structural and petrographic analyses, cathodoluminescence
849 (CL) images of extensional-related Western Anatolia granites (Salihli and Turgutlu, Catlos et al.,
850 2010; Eğrigöz, Koyunoba, and Alaçam, Catlos et al., 2012; Figure 4) help document mineral
851 zoning, deformation, and fluid alteration (e.g., Ramseyer et al., 1992; Catlos et al., 2016).

852 Western Anatolia granites share many similar microtextural characteristics in CL.,
853 including evidence for fluid interactions and multiple generations of microcracks. The samples
854 show secondary alteration textures, mineral growth generations, and evidence for fluid
855 migration. The generations of microfractures, microcracks, and microfaults seen in CL document
856 that these granites experienced brittle deformation multiple times, both at depth and at lower
857 temperatures near the surface (Catlos et al., 2010; 2012). CL imagery is a powerful tool for
858 identifying mineral textural relationships, growth histories, and deformation structures of
859 Western Anatolia granite assemblages.

860 **3.4 Timing the switches in the stress regimes in Western Anatolia**

861 The Simav Fault system illustrates another outstanding question regarding deciphering
862 stress regimes within Western Anatolia (Figure 7). On 19 May 2011, a magnitude 5.7 (M_{ww},
863 USGS and Turkish Ministry of the Interior, Disaster and Emergency Management Presidency,
864 Earthquake Department, AFAD) earthquake occurred near the town of Simav. The epicenter was
865 located ~53 km NNW of Uşak and ~82 km WSW from Kütahya in western Turkey at 20:15:23.4
866 GMT. The estimated depth of the earthquake varies (Doğangün et al., 2013). Table 9 reports the
867 24.46 km result from AFAD, although the USGS Earthquake Catalog suggests a shallower 7.0
868 km depth. Görgün (2014) estimated a best-fit hypocenter depth of 10 km and 6.0 magnitude
869 (M_w). Karasözen et al. (2016) indicate that the centroid depth was 7–9 km, but the hypocenters
870 of the mainshock and largest aftershocks were located systematically deeper at depths of 10–22
871 km. In approximately the same location, an M_w ~5.1 event preceded the mainshock on 17
872 February 2009, and an M_w 4.4 foreshock occurred 15 min before the mainshock (e.g., Karasözen
873 et al., 2016).

874 The Simav region is considered to be one of the most seismically active portions of
875 Western Anatolia (Inel et al., 2013; Görgün, 2014), and the 19 May 2011 Simav (Kütahya)
876 earthquake was the largest felt in the region since the destructive 1969 Demirci and 1970 Gediz
877 earthquake sequences (e.g., İlhan, 1971; Ambraseys & Tchalenko, 1972; Eyidoğan & Jackson,
878 1985). All of these earthquakes involved dominant normal faulting with nucleation zones from 6-
879 10 km depth and dips of 30-50° (Eyidoğan & Jackson, 1985; Emre & Duman, 2011; Görgün,
880 2014; Karasözen et al., 2016). However, a strike-slip component is recorded by some of the
881 aftershocks of the 1969 and 1970 earthquakes and the 2011 Simav event (Figure 7B) (Ambraseys
882 & Tchalenko, 1972; Eyidoğan & Jackson, 1985; Emre & Duman, 2011). In addition, Figure 7B
883 shows that some earthquakes in the Simav region after the 2011 event also yield fault plane
884 solutions that include some or a significant strike-slip component.

885 The epicenters of these earthquakes occurred near the Simav Fault (Figure 7) (Seyitoğlu,
886 1997; Ersoy et al., 2010). The fault extends ~150 km between the towns of Banaz in the east and
887 Sındırgı in the west (Ambraseys & Tchalenko, 1972; Seyitoğlu, 1997; Ersoy et al., 2010). It may
888 be part of a larger extensional Akşehir-Simav Fault System (Koçyiğit & Deveci, 2007), which
889 extends >250 km from the town of Akşehir in south-central Turkey and includes the Sultandağ
890 Fault in the east (Aksarı et al., 2010). Or, it may be part of the Sındırgı-Sincanlı Fault Zone
891 (SSFZ) between the towns of Soma and Afyon (Doğan & Emre, 2006). The Simav Fault may
892 also connect to the Muratdağ Fault near the town of Gediz in an en echelon pattern, which lends
893 support for a right-lateral system (Ambraseys & Tchalenko, 1972). Where the Akşehir-Simav
894 Fault System is located between the cities of Uşak and Afyon is unclear (e.g., Karasözen et al.
895 2016).

896 The Simav Fault is assigned as an active right-lateral strike-slip fault in active tectonic
897 maps of Turkey (Şaroğlu et al., 1992; Emre et al., 2011). This sense of motion is based on offsets
898 of metamorphic zones east of Simav (Konak, 1982; Seyitoğlu, 1997) and its relationship to the
899 formation of the NAFZ (Konak, 1982; Doğan & Emre, 2006; Emre & Duman, 2011). The strike-
900 slip motion is also consistent with uniform (magnitude and orientation) GPS plate velocity
901 vectors that show the region is extruding through an SW motion from 30–40 mm/yr (McClusky
902 et al., 2000; Reilinger et al., 2006, 2010). However, the detailed analysis of the Simav fault
903 mechanisms consistently indicates a normal mechanism (Görgün, 2014; Yolsal-Çevikbilen et al.,
904 2014; Demirci et al., 2015; Karasözen et al., 2016; Bello et al., 2017; Mutlu, 2020). This origin is
905 linked to subduction-related extension along the Hellenic and Cyprus arcs (e.g., Seyitoğlu, 1997;
906 Işık et al., 2003; Ersoy et al., 2010; Görgün, 2014; Yolsal-Çevikbilen et al., 2014; Demirci et al.,
907 2015; Karasözen et al. 2016; Bello et al., 2017).

908 If the Simav Fault was initiated as a strike-slip system but switched to extension
909 sometime after the Late Miocene is possible (Oygür & Erler, 2000). Strike-slip motion has also
910 been speculated to predate subsidence currently experienced by Western Anatolia and may be
911 related to Eocene to Oligocene compression (Oygür & Erler, 2000). Based on an analysis of the
912 available data from the 19 May 2011 event, Görgün (2014) indicate that the hypocenter
913 distribution is consistent with the activation of two nearly parallel faults: one northern one with a
914 fault plane trending mainly E–W and dipping towards SE and a southern fault plane trending
915 NW–SE and dipping towards SE. The strike-slip mechanisms are delegated to smaller fault
916 segments that experience a stress change after the mainshock and more minor secondary faults in
917 the region with different mechanisms. Karasözen et al. (2016) suggest the potential involvement
918 of structures inherited from earlier deformation phases of shortening and extension in evaluating
919 the nature of motion along the structure.

920 The Simav E-W trending-graben hosts one of Turkey’s most important geothermal
921 systems (Bello et al., 2017). Based on a study of geothermal activity, soil radon gas release, and
922 regional seismicity patterns, İnan et al. (2012) suggests that the epicentral area of the 19 May
923 2011 Simav earthquake is located within a block that is tectonically separated from Aegean
924 Extensional Province and the Marmara Region. The observation is also supported by geodetic
925 data that show a region surrounding the event behaves distinctly from the Aegean Extensional
926 Province (Tiryakioğlu, 2011). Yolsal-Çevikbilen et al. (2014) suggest the magnitude of the stress
927 drop associated with the 19 May 2011 event (62 bars) is more consistent with an intraplate
928 earthquake compared to those associated with Aegean plate boundaries (3-11 bars).

929 **3.5 Relating geological units and events across boundaries**

930 As noted in the Geological Background section, several units and structures can be
931 correlated from Western Anatolia to the Aegean region. For example, the Cyclades Blueschist
932 Unit (CBU) from the southern portion of the Menderes Massif (Figure 12A) is often matched to
933 outcrops exposed in the Cyclades (Ring et al., 1999; Roche et al., 2018; Çetinkaplan et al., 2020;
934 Barbot and Weiss, 2021), but distinguishing structures developed during subduction-related
935 burial and prograde metamorphism from those that formed due to decompression and
936 retrogression is problematic (e.g., Rosenbaum et al., 2002; Xypolias et al., 2012; Çetinkaplan et
937 al., 2020). The CBU experienced multiple phases of deformation and mineralogical
938 transformations (e.g., Seman et al., 2017; Gerogiannis et al., 2019). Identifying local internal
939 structures from those that would correlate as significant deformation zone poses a challenge.

940 Çetinkaplan et al. (2020) suggest that the contact between the Menderes Massif and the CBU,
941 now defined by a ductile thrust fault, was originally a lithosphere-scale transform fault zone.

942 The timing of detachment systems in the Menderes Massif are similar to those estimated
943 in the Cyclades. Three major Aegean microplate detachment systems include the North Cycladic
944 Detachment on Andros, Tinos, and Mykonos (Figure 11) (e.g., Jolivet et al., 2010), the Naxos-
945 Paros Detachment on Naxos and Paros (Buick, 1991; John & Howard, 1995; Cao et al., 2013),
946 and the West Cycladic Detachment on Serifos (Grasemann et al., 2012). The North Cycladic
947 Detachment may have initiated activity in the Oligocene until the Late Miocene (e.g., Jolivet et
948 al., 2010). The Naxos-Paros Detachment records retrogression associated with its latest activity
949 in the Late Miocene (e.g., Cao et al., 2017). These time frames are similar to constraints
950 estimated for the activity of detachment faulting in the central Menderes Massif (Hetzl et al.,
951 1995a, Hetzel et al., 1995b, Işık et al., 2003, Glodny & Hetzel, 2007; Catlos et al., 2010). The
952 Cyclades Detachments cross-cut blueschist-amphibolite facies fabrics and post-date HP
953 metamorphism and peak Barrovian metamorphism (Searle and Lamont, 2020a).

954 Another correlation links the lithologies, conditions, and metamorphic history of
955 Menderes Massif nappes to those in the Cyclades (e.g., Robertson et al., 1991; Ring et al., 1999;
956 Stampfli, 2000; Çetinkaplan et al., 2020). Menderes Massif nappes have zoned garnets useful for
957 generating P-T conditions and paths (e.g., Figure 12B and Figure 13). These paths are often
958 developed by connecting peak metamorphic conditions of individual rocks, inferences from
959 mineral assemblages, pseudosections, or Gibbs method thermodynamic modeling (e.g.,
960 Ashworth & Evirgen, 1984; 1985a,b; Ring et al., 2001; Whitney & Bozkurt, 2002; Cenk-Tok et
961 al., 2016; Etzel et al., 2019; 2020). Despite these studies, the number and timing of garnet-
962 growth events recorded in the rocks remain unclear. Some Çine nappe rocks experienced two
963 stages of garnet growth (Ring et al., 2001), whereas other samples are consistent with one
964 episode (Régnier et al., 2007). Pan-African garnet growth is recorded in the Menderes Massif,
965 and conditions could reflect events unrelated to MMM (Ring et al., 2004; Catlos & Çemen,
966 2005). Gessner et al. (2001) report that the Bayındır nappe deformed once during the Eocene
967 related to MMM., whereas the Bozdağ, Çine, and Selimiye nappes record pre-MMM and MMM
968 events. This contradicts Oberhaensli et al. (1997), who suggest the cover sequence records
969 deformation during the Eocene, but structurally lower units record pre-MMM events. Studies of
970 Bozdağ nappe rocks show prograde burial, but conditions decrease downward by ~40°C/kbar per
971 km of structural section (inverted metamorphism, Ring et al., 2001). Selimiye nappe rocks record
972 exhumation and retrogression (Régnier et al., 2007). Paths in Figure 12B were generated by
973 connecting peak metamorphic conditions of individual rocks, inferring from mineral
974 assemblages, pseudosections, or Gibbs method thermodynamic modeling. P-T paths that
975 decrease in pressure or temperature suggest the potential for tectonic switching as unloading and
976 refrigeration occur when the thrust reverses and experiences extension.

977 Challenges for generating P-T conditions and paths include a prior garnet-producing
978 history and retrograde fluid-induced alteration and overprinting as the core complex formed
979 (e.g., Satir & Taubald, 2001; Régnier et al., 2003; Catlos & Çemen, 2005; Baker et al., 2008;
980 Candan et al., 2011). Menderes Massif rocks are known to yield problematic P-T estimates based
981 on evidence of disequilibrium among phases and the application of barometers to inappropriate
982 (uncalibrated) mineral compositions (Ashworth & Evirgen, 1984; 1985a,b). In some cases,
983 calculated conditions appear at odds with observed mineral assemblages and structural data
984 (Ring et al., 2001; Whitney & Bozkurt, 2002). Pressure estimates using conventional approaches

985 are challenging to obtain due to the lack of appropriate mineral assemblages (Iredale et al.,
986 2013). Problems may arise if the chosen mineral compositions for thermobarometric calculations
987 are associated with retrogression instead of the desired prograde conditions. P-T paths that only
988 rely on core and rim measurements are also limited in their ability to test models developed
989 regarding lithospheric response to perturbations, including motion within fault zones.

990 One promising avenue to address this issue is the application of isochemical phase
991 equilibria modeling. Figure 13 shows this approach applied to garnets from the Menderes
992 Massif's Çine, Selimiye, and Bayindir nappe from Etzel et al. (2019) and Etzel et al. (2020) and
993 a sample from the Northern Menderes Massif from Cenki-Tok et al. (2016). The researchers
994 report petrological details, X-ray element maps, and geochemical data from the rocks. They
995 compositionally analyzed micaschists with a mineral assemblage of garnet + biotite +
996 plagioclase + muscovite + quartz + rutile ± ilmenite ± apatite ± pyrite ± zircon ± monazite. The
997 sample from the Northern Menderes Massif contains kyanite and small porphyroblasts of
998 staurolite. Using data reported in the papers, isochemical phase diagrams were created using rock
999 bulk compositions, the software package Theriak-Domino (de Capitani & Brown, 1987; de
1000 Capitani & Petrakakis, 2010) with the Holland and Powell (1998; 2010) thermodynamic data set,
1001 and appropriate mixing models in the system $\text{MnO-Na}_2\text{O-CaO-K}_2\text{O-FeO-MgO-Al}_2\text{O}_3\text{-}$
1002 $\text{SiO}_2\text{-H}_2\text{O-TiO}_2$. Isopleths of ± 0.01 mole fraction spessartine, almandine, pyrope, and grossular
1003 corresponding with the garnet core composition, are plotted on the phase diagram. This portion
1004 of the diagram with intersecting isopleths approximates the chemical system at the time garnet
1005 began growth. This diagram also tests if the thermodynamic data set and mixing models used in
1006 the modeling are appropriate for these particular samples, as expected mineral assemblages
1007 appeared in the phase diagrams with intersecting isopleths.

1008 After the garnet core conditions are estimated, a Matlab script was applied to each step
1009 along a garnet compositional traverse from core to rim to yield both an estimate of the P-T
1010 conditions of incremental growth and a new effective bulk rock composition, ultimately
1011 culminating in a high-resolution P-T path. High-resolution P-T paths are defined as those derived
1012 from fractionated equilibrium phase diagram modeling and the resolution is an outcome of the
1013 number of garnet fractionated steps. Garnets with complex zoning profiles, modified by
1014 diffusion, or rocks that experienced major changes in bulk composition over their growth history
1015 are not candidates (e.g., Catlos et al., 2018). However, even these types of samples may provide
1016 clues by exploring the reason for their failure (e.g., Catlos et al., 2018; Etzel et al., 2020). Ideal
1017 samples are those with garnets that preserve prograde, gradational core-to-rim zoning profiles.
1018 Garnets from the Selimiye and Bayindir nappes of the Southern and Central Menderes Massif,
1019 respectively, show similar trajectories. However, the Çine nappe garnet yields an N-shape path
1020 and a significantly different metamorphic history.

1021 Either tectonically-driven extension may have created the N-shaped P-T path during
1022 orogenesis or the result of erosional exhumation during pulses of thrust motion (Etzel et al.,
1023 2019). Etzel et al. (2019) developed two thermal models: erosional denudation followed by fault
1024 reactivation (Figure 14A) and tectonic switching (Figure 14B), which are briefly summarized
1025 here. Figure 14A and Figure 14B show an upper equilibrium thermal grid (depth vs. horizontal
1026 distance) before faulting with the position of fault (grey line) arbitrarily selected at 30° . Fault
1027 displacement varies linearly across shear zones. The grid includes reflecting side boundaries and
1028 top and bottom maintained at 25°C and 700°C and an initial geothermal gradient at $25^\circ\text{C}/\text{km}$
1029 indicated by shaded zones. A hatched area shows the position of the Selimiye samples, and the

1030 grey bar represents the approximate initial location of the Çine nappe garnet with the N-shaped
1031 P-T path. This position is also represented by point 1 in the P-T path insets. In Figure 14C and
1032 Figure 14D, the fault is active. A finite-difference solution to the diffusion-advection equation is
1033 used to examine the P-T variations in the hanging wall and footwall due to its motion. The rock
1034 sample experiences the point 1 to 2 in the P-T path insets. Fault motion stops and denudation
1035 occurs in Figure 14E and, whereas extension occurs in Figure 14F. This process is based on the
1036 mid-rim lower pressure portion of the garnet P-T path and is represented by points 2 to 3 on the
1037 P-T path insets. Although the end, the surface geometry in the denudation phase (Figure 13E)
1038 and extensional phase (Figure 14F) are similar, the shape of the isotherms is different and leads
1039 to the development of a decrease in temperature in the P-T loop observed in the tectonic
1040 switching model. Finally, the fault is reactivated, represented by Figure 14G to Figure 14H. The
1041 decrease in pressure with increasing temperature is related to an episode of denudation (model 1)
1042 rather than a tectonic switch from compression to extension (Etzel et al., 2019).

1043 The P-T paths reported in Figure 13 approximate how a garnet with specific
1044 compositional zoning would behave in a closed system of a known bulk composition as it
1045 evolves during increasing T. A critical assumption is that the minerals in a sample experienced
1046 equilibrium, which can never be proven for any rock system (e.g., Spear & Peacock, 1989;
1047 Lanari & Duesterhoeft, 2019). Closed system behavior also requires the original compositions of
1048 the mineral phases, and the bulk rock has not changed significantly since metamorphism (e.g.,
1049 Lanari and Engi, 2017). Multiple sources of error are inherent, including uncertainty in the
1050 accuracy of end-member reactions, electron microprobe analyses, calibration errors, variations in
1051 activity models, compositional heterogeneity, and uncertainty associated with the
1052 thermodynamic properties inherent in the choice of internally consistent database (e.g., Kohn &
1053 Spear, 1991; White et al., 2014; Palin et al., 2016; Lanari & Duesterhoeft, 2019). Garnets with
1054 significant changes in composition over short distances from core to the rim and those affected
1055 by diffusion cannot be modeled. Garnets in samples that experienced significant changes in bulk
1056 composition or multiple deformation episodes resulting in modification of composition are also
1057 unsuitable.

1058 A significant value of the high-resolution P-T path and isopleth approaches is that a user
1059 can detect when systems stray from the equilibrium and closed system assumptions. Confidence
1060 in paths and conditions increases when minerals assemblages agree with rock observations and if
1061 the P-T paths reproduce trends in garnet zoning. Samples collected from the same outcrop or
1062 nearby should yield similar P-T conditions and paths. In addition, a user can gauge the extent of
1063 overlapping mineral isopleths in P-T space, including if matrix mineral compositions overlap the
1064 garnet rim conditions. These paths are the first steps in developing critical insights into the
1065 metamorphic history of the assembly of the Menderes Massif and, combined with age
1066 information from the garnet itself or matrix or mineral inclusions, can be used to test models for
1067 the development of Western Anatolia.

1068 **4. Conclusions**

1069 This paper is divided into two major sections. The first outlines, as much as is possible,
1070 our present-day understanding of the geological history of Western Anatolia from its assembly
1071 through its extensional and strike-slip history. We aim to illustrate the complex tectonic scenario
1072 before the onset of large-scale extension and emphasize the present-day change in stress regime
1073 towards strike-slip tectonics. The transitions are also comparable in duration and timing to those
1074 experienced by the Aegean microplate.

1075 The second part highlights some outstanding questions that remain to be addressed.
1076 These include issues regarding the dynamics of the African slab along the Hellenic arc, the arc's
1077 geometry and connections to other subduction systems, and reconciling the Jurassic initiation age
1078 of subduction with Late Cenozoic sedimentation, magmatic, and paleogeographic data that are
1079 consistent with younger initiation. In addition, a large number of regions of slab tear are
1080 proposed throughout the African slab, and their influence on accommodating extrusion, creating
1081 economic resources, and driving lithospheric thinning and magmatism should be explored. Other
1082 questions include investigating the influence of transfer zones in accommodating deformation
1083 and the role of magma in driving extension in Western Anatolia.

1084 The interface between Western Anatolia and the Aegean region exemplifies tectonic
1085 transitions and how the interplay between large-scale tectonics influences smaller-scale
1086 processes. The Aegean and western Turkey contain helpful assemblages that can be exploited to
1087 time these processes that shape the lithosphere and are critical in understanding the region's
1088 hazards and mineralizations. Extracting high-resolution P-T paths from Western Anatolia garnet-
1089 bearing rocks is a promising approach to evaluate tectonic models and correlate and compare
1090 metamorphic histories of nearby assemblages and from those across long distances.

1091 **Data Availability Statement**

1092 Data supporting the conclusions of this paper and color figures are publically available from
1093 Texas Data Repository Dataverse (<https://doi.org/10.18738/T8/ER3WQV>).

1094 **Acknowledgements**

1095 We appreciate constructive reviews of the original manuscript from Spyros Pavlides (Aristotle
1096 University of Thessaloniki, Greece), Thomas Lamont (University of Bristol) and three
1097 anonymous reviewers. We appreciate analytical assistance with the $^{40}\text{Ar}/^{39}\text{Ar}$ analysis from the
1098 Australia National University Argon Facility.

1099 **References**

- 1100 Agostini, S., Doglioni, C., Innocenti, F., Manetti, P., & Tonarini, S. (2010). On the geodynamics
1101 of the Aegean Rift. In I. Çemen (Ed.), *Extensional tectonics in the Basin and Range, the*
1102 *Aegean, and western Anatolia*. *Tectonophysics*, 488, 7-21.
1103 <https://doi.org/10.1016/j.tecto.2009.07.025>
- 1104 Akal, C. (2013). Coeval shoshonitic–ultrapotassic dyke emplacements within the Kestanol
1105 Pluton, Ezine-Biga Peninsula (NW Anatolia). *Turkish Journal of Earth Sciences*, 21, 1–20.
- 1106 Akal, C., & Helvacı, C. (1999). Mafic microgranular enclaves in the Kozak granodiorite, western
1107 Anatolia. *Turkish Journal of Earth Sciences*, 8, 1–17.
- 1108 Akay, E. (2009). Geology and petrology of the Simav Magmatic Complex (NW Anatolia) and its
1109 comparison with the Oligo-Miocene granitoids in NW Anatolia: implications on Tertiary
1110 tectonic evolution of the region. *International Journal of Earth Sciences*, 98, 1655–1675.
- 1111 Akbayram, K., Şengör, A. M. C., & Özcan, E. (2016). The evolution of the intra-Pontide suture;
1112 implications of the discovery of late Cretaceous-early Tertiary melanges. In R. Sorkhabi
1113 (Ed.), *Tectonic evolution, collision, and seismicity of southwest Asia; in honor of Manuel*
1114 *Berberian's forty-five years of research contributions*. *Special Paper - Geological Society of*
1115 *America* (Vol. 525). [https://doi.org/10.1130/2016.2525\(18\)](https://doi.org/10.1130/2016.2525(18))
- 1116 Aksari, D., Karabulut, H., Ozalaybey, S. (2010). Stress interactions of three moderate size
1117 earthquakes in Afyon, southwestern Turkey. *Tectonophysics*, 485, 141-153.
1118 <https://doi.org/10.1016/j.tecto.2009.12.010>

- 1119 Aktuğ, B., Parmaksız, E., Kurt, M., Lenk, O., Kılıçoğlu, A., Ali, M., & Soner Özdemir, G.
1120 (2013). Deformation of Central Anatolia: GPS implications. *Journal of Geodynamics*, 67, 78-
1121 96. <https://doi.org/10.1016/j.jog.2012.05.008>
- 1122 Aldanmaz, E. (2012). Osmium isotope and highly siderophile element geochemistry of mantle
1123 xenoliths from NW Turkey: implications for melt depletion and metasomatic history of the
1124 sub-continental lithospheric mantle. *International Geology Review*, 54(7), 799-815.
1125 <https://doi.org/10.1080/00206814.2011.581799>
- 1126 Aldanmaz, E., Pearce, J. A., Thirlwall, M. F., & Mitchell, J. G. (2000). Petrogenetic evolution of
1127 Late Cenozoic, post-collision volcanism in Western Anatolia, Turkey. *Journal of*
1128 *Volcanology and Geothermal Research*, 102, 67–95.
- 1129 Alatza, S., Papoutsis, I., Paradissis, D., Kontoes, C., & Papadopoulos, G.A. (2020). Multi-
1130 Temporal InSAR Analysis for Monitoring Ground Deformation in Amorgos Island, Greece.
1131 *Sensors*, 20(2), 338. <https://doi.org/10.3390/s20020338>
- 1132 Altherr R., Henjeskunt, F., Matthews, A., Friedrichsen, H., Hansen, & B.T. (1988). O-Sr
1133 isotopic variations in Miocene granitoids from the Aegean—evidence for an origin by
1134 combined assimilation and fractional crystallization. *Contributions to Mineralogy and*
1135 *Petrology*, 100(4), 528–541
- 1136 Altherr, R., & Siebel, W. (2002). I-type plutonism in a continental back-arc setting: Miocene
1137 granitoids and monzonites from the central Aegean Sea, Greece. *Contribution to Mineralogy*
1138 *and Petrology*, 143, 397–415. <https://doi.org/10.1007/s00410-002-0352-y>
- 1139 Altunkaynak, Ş. (2007). Collision-driven slab breakoff magmatism in northwestern Anatolia,
1140 Turkey. *Journal of Geology*, 115, 63–82
- 1141 Altunkaynak, Ş., & Dilek, Y. (2006). Timing and nature of postcollisional volcanism in western
1142 Anatolia and geodynamic implications. In Y. Dilek, S. Pavlides (Eds.), *Postcollisional*
1143 *tectonics and magmatism in the Mediterranean region and Asia*. Special Paper - Geological
1144 Society of America, 409, 321-351.
- 1145 Altunkaynak, Ş., & Genç, S. (2008). Petrogenesis and time-progressive evolution of the
1146 Cenozoic continental volcanism in the Biga Peninsula, NW Anatolia (Turkey). In: Xu, Y.,
1147 Farmer, L., Menzies, M., Rudnick, R., Zhou Meifu, Z. *Continental volcanism and chemistry*
1148 *of the Earth's interior*. *Lithos*, 102, 316-340.
- 1149 Altunkaynak, Ş., & Yılmaz, Y. (1998). The mount Kozak magmatic complex, western Anatolia.
1150 *Journal of Volcanology and Geothermal Research*, 85, 211–231.
- 1151 Altunkaynak, Ş., Dilek, Y., Genç, C. Ş., Sunal, G., Gertisser, R., Furnes, H., Foland, K.A., &
1152 Yang, J. (2012). Spatial, temporal and geochemical evolution of Oligo–Miocene granitoid
1153 magmatism in western Anatolia, Turkey. *Gondwana Research*, 21(4), 961-986.
1154 <https://doi.org/10.1016/j.gr.2011.10.010>
- 1155 Amaru, M.L. (2007). Global travel time tomography with 3-D reference models. PhD Thesis
1156 Utrecht University.
1157 [http://dspace.library.uu.nl/bitstream/handle/1874/19338/index.htm;jsessionid=88B6AA4941](http://dspace.library.uu.nl/bitstream/handle/1874/19338/index.htm;jsessionid=88B6AA4941C5E76FD65034D89D4065E0?sequence=17)
1158 [C5E76FD65034D89D4065E0?sequence=17](http://dspace.library.uu.nl/bitstream/handle/1874/19338/index.htm;jsessionid=88B6AA4941C5E76FD65034D89D4065E0?sequence=17)
- 1159 Ambraseys, N.N., & Tchalenko, J.S. (1972). Seismotectonic aspects of the Gediz, Turkey,
1160 Earthquake of March 1970. *Geophysical Journal of the Royal Astronomical Society*, 30(3),
1161 229-52,
- 1162 Anastasakis, G., & Keling, G. (1991). Tectonic connection of the Hellenic & Cyprus arcs &
1163 related geotectonic elements. *Marine Geology*, 97(3-4), 261-277.
1164 [https://doi.org/10.1016/0025-3227\(91\).90120-S](https://doi.org/10.1016/0025-3227(91).90120-S)

- 1165 Angelier, J., Lyb eris, N., Le Pichon, X., Barrier, E., & Huchon, P. (1982). The tectonic
1166 development of the hellenic arc & the sea of crete: A synthesis. *Tectonophysics*, 86(1-3),
1167 159-196. [https://doi.org/10.1016/0040-1951\(82\).90066-X](https://doi.org/10.1016/0040-1951(82).90066-X)
- 1168 Armijo, R., Meyer, B., Hubert, A., & Barka, A. (1999). Westward propagation of the North
1169 Anatolian fault into the northern Aegean: Timing and kinematics. *Geology*, 27, 267-270. ,
1170 [https://doi.org/10.1130/0091-7613\(1999\)027<0267:WPOTNA>2.3.CO;2](https://doi.org/10.1130/0091-7613(1999)027<0267:WPOTNA>2.3.CO;2)
- 1171 Ashworth, J. R., & Evirgen, M. M. (1984). Garnet and associated minerals in the southern
1172 margin of the Menderes Massif, Southwest Turkey. *Geological Magazine*, 121(4), 323-337.
- 1173 Ashworth, J. R., & Evirgen, M. M. (1985a). Plagioclase relations in pelites, central Menderes,
1174 Massif, Turkey; II., Perturbation of garnet-plagioclase geobarometers. *Journal of*
1175 *Metamorphic Geology*, 3(3), 219-229.
- 1176 Ashworth, J. R., & Evirgen, M. M. (1985b). Plagioclase relations in pelites, central Menderes
1177 Massif, Turkey; I., The peristerite gap with coexisting kyanite. *Journal of Metamorphic*
1178 *Geology*, 3(3), 207-218.
- 1179 Avigad, D., Baer, G., & Heimann, A. (1998). Block rotations and continental extension in the
1180 central Aegean Sea: Palaeomagnetic and structural evidence from Tinos and Mykonos
1181 (Cyclades, Greece). *Earth and Planetary Science Letters*, 157, 23–40.
1182 [https://doi.org/10.1016/S0012-821X\(98\)00024-7](https://doi.org/10.1016/S0012-821X(98)00024-7)
- 1183 Avigad, D. & Garfunkel, Z. (1991). Uplift and exhumation of high-pressure metamorphic
1184 terrains: the example of the Cycladic blueschist belt (Aegean Sea). *Tectonophysics*, 188,
1185 357–372.
- 1186 Aydođan, M.S., Coban, H., Bozcu, M., & Akinci, O. (2008). Geochemical and mantle-like
1187 isotopic (Nd, Sr). composition of the Baklan Granite from the Muratdagi region (Banaz,
1188 Usak), western Turkey; implications for input of juvenile magmas in the source domains of
1189 western Anatolia Eocene-Miocene granites. *Journal of Asian Earth Sciences*, 33, 155-176.
1190 <https://doi.org/10.1016/j.jseaes.2006.10.007>
- 1191 Aysal, N., Ongen, S., Peytcheva, I., & Keskin, M. (2012). Origin and evolution of the Havran
1192 Unit, western Sakarya basement (NW Turkey); new LA-ICP- MS U-Pb dating of the
1193 metasedimentary-metagranitic rocks and possible affiliation to Avalonian microcontinent. In
1194 E. Bozkurt (Ed.), *Tectonics of the Eastern Mediterranean-Black Sea region; Part A.*,
1195 *Dedicated in honor of Aral Okay's 60th birthday. Geodinamica Acta (Vol. 25, pp. 226-247).*
1196 <https://doi.org/10.1080/09853111.2014.882536>
- 1197 Aysal, N., Şahin, S.Y., G ng r, Y., Peytcheva, I., &  ngen, S. (2018). Middle Permian-early
1198 Triassic magmatism in the Western Pontides, NW Turkey: Geodynamic significance for the
1199 evolution of the Paleo-Tethys. *Journal of Asian Earth Sciences*, 164, 83-103.
1200 <https://doi.org/10.1016/j.jseaes.2018.06.026>
- 1201 Bađcı, M., Ilbeyli, N., Yildiz, A., Kibici, Y., & Demirbilek, M. (2012). Geochemical and
1202 geochronological (Rb/Sr) properties of the G ny z  granitoids (Sivrihisar, Eskişehir). 12th
1203 International Multidisciplinary Scientific GeoConference, www.sgem.org, SGEM2012
1204 Conference Proceedings, 1, 47-56. <https://doi.org/10.5593/SGEM2012/S01.V1007>
- 1205 Baker, C.B., Catlos, E.J., Sorensen, S.S.,  emen, I., & Hancer, M. (2008). Evidence for
1206 polymetamorphic garnet growth in the Cine (southern Menderes). Massif, Western Turkey.
1207 IOP Conference Series, *Earth & Environmental Sciences*, 2, 012020.
1208 <https://doi.org/10.1088/1755-1307/2/1/012020>

- 1209 Baran, Z.O., Dilek, Y., & Stockli, D. (2017). Diachronous uplift & cooling history of the
1210 Menderes core complex, western Anatolia (Turkey), based on new zircon (U-Th)/He ages.
1211 *Tectonophysics*, 694, 181-196. <https://doi.org/10.1016/j.tecto.2016.12.005>
- 1212 Barbot, S., & Weiss, J.R. (2021). Connecting subduction, extension and shear localization across
1213 the Aegean Sea and Anatolia. *Geophysical Journal International*, 226(1), 422–445.
1214 <https://doi.org/10.1093/gji/ggab078>
- 1215 Barka, A.A. (1992). The north Anatolian fault zone. *Annales Tectonicae*, 6, 64-195.
- 1216 Barka, A.A., & Kadinsky-Cade, K. (1988). Strike-slip fault geometry in Turkey and its influence
1217 on earthquake activity, *Tectonics*, 7(3), 663– 684. <https://doi.org/10.1029/TC007i003p00663>
- 1218 Barka, A.A., & Reilinger, R. (1997). Active tectonics of the Eastern Mediterranean Region:
1219 deduced from GPS., neotectonic and seismicity data. *Annelis de Geofisica*, 40(3), 587–610.
- 1220 Beccaletto, L., Bonev, N., Bosch, D., Bruguier, O. (2007). Record of a Palaeogene syn-
1221 collisional extension in the north Aegean region: evidence from the Kemer micaschists (NW
1222 Turkey). *Geological Magazine*, 144(2), 393–400.
1223 <https://doi.org/10.1017/S001675680700310X>
- 1224 Beccaletto, L., & Jenny, C. (2004). Geology and Correlation of the Ezine Zone: A Rhodope
1225 Fragment in NW Turkey? *Turkish Journal of Earth Sciences*, 13, 45-176.
- 1226 Beißer, M., Wyss, M., & R. Kind, R. (1990). Inversion of source parameters for subcrustal
1227 earthquakes in the Hellenic Arc. *Geophysics Journal International*, 103, 439-450.
- 1228 Bello, O.A., Özgür, N., & Çalışkan, T.A. (2017). Hydrogeological, Hydrogeochemical and
1229 Isotope Geochemical Features of Geothermal Waters in Simav and Environs, Western
1230 Anatolia, Turkey. *Procedia Earth and Planetary Science*, 17, 29-32.
1231 <https://doi.org/10.1016/j.proeps.2016.12.014>.
- 1232 Beniést, A., Brun, J.P., Gorini, C., Crombez, V., Deschamps, R., Hamon, Y., & Smit, J. (2016).
1233 Interaction between trench retreat and Anatolian escape as recorded by neogene basins in the
1234 northern Aegean Sea. *Marine and Petroleum Geology*, 77, 30-42.
1235 <https://doi.org/10.1016/j.marpetgeo.2016.05.011>
- 1236 Berckhemer H (1977). Some aspects of the evolution of marginal seas deduced from
1237 observations in the Aegean region. In B. Biju-Duval, L. Montadert (Eds.), *Structural History*
1238 *of the Mediterranean Basins*. Ed. Technip: Paris France, p. 303-314.
- 1239 Bijwaard, H., W. Spakman, & E. R. Engdahl (1998). Closing the gap between regional and
1240 global travel time tomography, *Journal of Geophysical Research*, 103, 30,055 – 30,078.
- 1241 Birkle, P. (1992). *Petrologie-Geochemie und Geochronologie des miozänen Magmatismus auf*
1242 *der Biga-Halbinsel (Ezine, NW-Türkie)*. Diplomarbeit an der Geowissenschaftlichen Fakultät
1243 der Eberhard-Karls-Universität Tübingen, 1992.
- 1244 Biryol, C.B., Beck, S.L., Zandt, G., & Ozacar, A.A. (2011). Segmented African lithosphere
1245 beneath the Anatolian region inferred from teleseismic P-wave tomography. *Geophysics*
1246 *Journal International*, 184, 1037–1057. <https://doi.org/10.1111/j.1365-246X.2010.04910.x>
- 1247 Black, K.N., Catlos, E.J., & Oyman, T. (2013). Timing Aegean extension: Evidence from in situ
1248 U–Pb geochronology and cathodoluminescence imaging of granitoids from NW Turkey
1249 (Special Issue: Geodynamics and Magmatism). *Lithos*, 180-181, 92-108.
1250 <https://doi.org/10.1016/j.lithos.2013.09.001>
- 1251 Blom, N., Gokhberg, A., Fichtner, A. (2019). Seismic waveform tomography of the central and
1252 eastern Mediterranean upper mantle. *Solid Earth*, 11, 669-690. [https://doi.org/10.5194/se-11-](https://doi.org/10.5194/se-11-669-2020)
1253 [669-2020](https://doi.org/10.5194/se-11-669-2020).

- 1254 Bocchini, G.M., Brüstle, A., Becker, D., Meier, T., van Keken, P.E., Ruscic, M., Papadopoulos,
 1255 G.A., Rische, M., & Friederich, W. (2018). Tearing, segmentation, and backstepping of
 1256 subduction in the Aegean: New insights from seismicity. *Tectonophysics*, 734–735, 96-118.
 1257 <https://doi.org/10.1016/j.tecto.2018.04.002>.
- 1258 Bolhar, R., Ring, U., & Allen, C.M. (2010). An integrated zircon geochronological and
 1259 geochemical investigation into the Miocene plutonic evolution of the Cyclades, Aegean Sea,
 1260 Greece: Part 1: Geochronology. *Contributions to Mineralogy and Petrology*, 160, 719–742.
 1261 <https://doi.org/10.1007/s00410-010-0504-4>
- 1262 Bonev, N., & Beccaletto, L. (2007). From syn- to post-orogenic Tertiary extension in the north
 1263 Aegean region: constraints on the kinematics in the eastern Rhodope–Thrace, Bulgaria–
 1264 Greece and the Biga Peninsula, NW Turkey. *Geological Society, London, Special
 1265 Publications*, 291, 113-142. <https://doi.org/10.1144/SP291.6>
- 1266 Bonev, N., Beccaletto, L., Robyr, M., & Monié, P. (2009). Metamorphic and age constraints on
 1267 the Alakeçi shear zone: Implications for the extensional exhumation history of the northern
 1268 Kazdağ Massif, NW Turkey, *Lithos*, 113(1-2), 331-345.
 1269 <https://doi.org/10.1016/j.lithos.2009.02.010>
- 1270 Bozkaya, Ö, Yağın, H., & Göncüoğlu, M.C. (2012). Diagenetic and very low-grade
 1271 metamorphic characteristics of the Paleozoic series of the Istanbul Terrane (NW Turkey).
 1272 *Swiss Journal of Geoscience*, 105, 183–201. <https://doi.org/10.1007/s00015-012-0108-2>
- 1273 Bozkurt, E. (2001). Neotectonics of Turkey - a synthesis. *Geodinamica Acta*, 14, 3-30.
- 1274 Bozkurt, E., & Oberhänsli, R. (2001). Menderes Massif (western Turkey).; structural,
 1275 metamorphic and magmatic evolution; a synthesis. *Geologische Rundschau = International
 1276 Journal of Earth Science* [1999], 89(4), 679-708.
- 1277 Bozkurt, E., & Park, R. G. (1994). Southern Menderes Massif; an incipient metamorphic core
 1278 complex in western Anatolia, Turkey. *Journal of the Geological Society of London*, 151(22),
 1279 213-216.
- 1280 Bozkurt, E., & Park, R.G. (1999). The structure of the Palaeozoic schists in the Southern
 1281 Menderes Massif, western Turkey: A new approach to the origin of the Main menderes
 1282 metamorphism and its relation to the Lycian Nappes. *Geologische Rundschau = International
 1283 Journal of Earth Sciences*, 12(1), 25-42. [https://doi.org/10.1016/S0985-3111\(99\).80021-7](https://doi.org/10.1016/S0985-3111(99).80021-7)
- 1284 Bozkurt, E., & Satir, M. (2000). The southern Menderes Massif (western Turkey).;
 1285 geochronology and exhumation history. *Geological Journal*, 35(3-4), 285-296.
- 1286 Bozkurt, E., & Sözbilir, H. (2004). Tectonic evolution of the Gediz Graben: Field evidence for
 1287 an episodic, two-stage extension in western Turkey. *Geological Magazine*, 141(1), 63-79.
 1288 <https://doi.org/10.1017/S0016756803008379>
- 1289 Boztuğ, D., Harlavan, Y., Jonckheere, R., Can, İ, & Sari, R. (2009). Geochemistry and K-Ar
 1290 cooling ages of the Ilica, Çataldağ (Balıkesir) and Kozak (İzmir) granitoids, west Anatolia,
 1291 Turkey. *Geological Journal*, 44, 79-103. <https://doi.org/10.1002/gj.1132>
- 1292 Brichau, S., Ring, U., Carter, A., Monié, P., Bolhar, R., Stockli, D., & Brunel, M. (2007).
 1293 Extensional faulting on Tinos Isl&, Aegean Sea, Greece: How many detachments? *Tectonics*,
 1294 26, TC4009. <https://doi.org/10.1029/2006TC001969>
- 1295 Brichau, S., Ring, U., Carter, A., Bolhar, R., Monie, P., Stockli, D., & Brunel, M. (2008).
 1296 Timing, slip rate, displacement and cooling history of the Mykonos detachment footwall,
 1297 Cyclades, Greece, and implications for the opening of the Aegean Sea basin. *Journal of the
 1298 Geological Society*, 165, 263–277.

- 1299 Brooks, M., & Ferentinos, G. (1984). Tectonics and sedimentation in the Gulf of Corinth and the
1300 Zakynthos and Kefallinia channels, Western Greece. *Tectonophysics*, 101(1-2). 25-54.
1301 [https://doi.org/10.1016/0040-1951\(84\)90040-4](https://doi.org/10.1016/0040-1951(84)90040-4)
- 1302 Brun, J.-P., & Faccenna, C. (2008). Exhumation of high-pressure rocks driven by slab rollback,
1303 *Earth and Planetary Science Letters*, 272, 1-7. <https://doi.org/10.1016/j.epsl.2008.02.038>
- 1304 Brun, J.-P., Faccenna, C., Gueydan, F., Sokoutis, D., Philippon, M., Kydonakis, K., Gorini, C.
1305 (2016). The two-stage aegean extension, from localized to distributed, a result of slab
1306 rollback acceleration. *Canadian Journal of Earth Sciences*, National Research Council
1307 Canada, 53(11), 1142-1157. <https://doi.org/10.1139/cjes-2015-0203ff>. fffinsu-01271296f
- 1308 Brun, J.-P., Faccenna, C., Gueydan, F., Sokoutis, D., Philippon, M., Kydonakis, K., & Gorini, C.
1309 (2017). Effects of slab rollback acceleration on Aegean extension. *Bulletin of the Geological*
1310 *Society of Greece*, 50(1), 5-23. <https://doi.org/10.12681/bgsg.11697>
- 1311 Brun, J.-P., Sokoutis, D. (2007). Kinematics of the Southern Rhodope Core Complex (North
1312 Greece). *International Journal of Earth Sciences*, 96(6), 1079-1099.
1313 <https://doi.org/10.1007/s00531-007-0174-2>
- 1314 Brun, J.-P., & Sokoutis, D. (2010). 45 m.y. of Aegean crust and mantle flow driven by trench
1315 retreat. *Geology*, 38(9), 815–818. <https://doi.org/10.1130/G30950.1>
- 1316 Buick I.S. (1991). The late Alpine evolution of an extensional shear zone, Naxos, Greece.
1317 *Journal of the Geological Society of London*, 148, 93-103.
- 1318 Bulle, F., Bröcker, M., Gärtner, C., & Keasling, A. (2010). Geochemistry and geochronology of
1319 HP mélanges from Tinos and Andros, cycladic blueschist belt, Greece. *Lithos*, 117(1–4), 61-
1320 81. <https://doi.org/10.1016/j.lithos.2010.02.004>
- 1321 Bulut, F., Özener, H., Doğru, A., Aktuğ, B., & Yaltrak, C. (2018). Structural setting along the
1322 Western North Anatolian Fault and its influence on the 2014 North Aegean Earthquake (Mw
1323 6.9). *Tectonophysics*, 745, 382-394. <https://doi.org/10.1016/j.tecto.2018.07.006>
- 1324 Burchfiel, B.C., Nakov, R., Dumurdzanov, N., Papanikolaou, D., Tzankov, T., Serafimovski, T.,
1325 King, R.W., Kotzev, V., Todosov, A., & Nurce, B. (2008). Evolution and dynamics of the
1326 Cenozoic tectonics of the South Balkan extensional system. *Geosphere*, 4, 918–938.
- 1327 Burg, J.-P., Ricou, L.-E., Ivano, Z., Godfriaux, I., Dimov, D., & Klain, L. (1996). Syn-
1328 metamorphic nappe complex in the Rhodope Massif. Structure and kinematics. *Terra Nova*,
1329 8, 6-15. <https://doi.org/10.1111/j.1365-3121.1996.tb00720.x>
- 1330 Burtman, V.S. (1994). Meso-Tethyan oceanic sutures and their deformation. *Tectonophysics*,
1331 234, 305–327.
- 1332 Candan, O., Akal, C., Koralay, O.E., Okay, A.I., Oberhänsli, R., Prelević, D., & Mertz-Kraus, R.
1333 (2016). Carboniferous granites on the northern margin of Gondwana, Anatolide-Tauride
1334 Block, Turkey - Evidence for southward subduction of Paleotethys. *Tectonophysics*, 683,
1335 349-366.
- 1336 Candan, O., Çetinkaplan, M., Oberhänsli, R., Rimmelé, G., & Akal, C. (2005). Alpine high-
1337 P/low-T metamorphism of the Afyon zone and implications for the metamorphic evolution of
1338 Western Anatolia, Turkey. *Lithos*, 84, 102–124.
- 1339 Candan, O., Dora, O.O., Oberhänsli, R., Çetinkaplan, M., Partzsch, J.H., Warkus, F.C., & Durr,
1340 S. (2001). Pan-African high-pressure metamorphism in the Precambrian basement of the
1341 Menderes Massif, western Anatolia, Turkey. *International Journal of Earth Science*, 89, 793-
1342 811.
- 1343 Candan, O., Oberhänsli, R., Dora, O. O., Çetinkaplan, M., Koralay, E., Rimmelé, G., & ... Akal,
1344 C. (2011). Polymetamorphic evolution of the Pan-African basement and Palaeozoic-early

- 1345 Tertiary cover series of the Menderes Massif. *Bulletin of Mineral Resources and Exploration*
1346 *Turkey*, 142, 121163.
- 1347 Cao, S., Neubauer, F., Bernroider, M., Genser, J., Liu, J., & Friedl, G. (2017). Low-grade
1348 retrogression of a high-temperature metamorphic core complex: Naxos, Cyclades, Greece.
1349 *Geological Society of America Bulletin*, 129 (1-2), 93–117. <https://doi.org/10.1130/B31502.1>
- 1350 Cao, S., Neubauer, F., Bernroider, M., & Liu, J. (2013). The lateral boundary of a metamorphic
1351 core complex: The Moutsounas shear zone on Naxos, Cyclades, Greece. *Journal of Structural*
1352 *Geology*, 54, 103–128. <https://doi.org/10.1016/j.jsg.2013.07.002>
- 1353 Catlos, E.J., & Çemen, I. (2005). Monazite ages and the evolution of the Menderes Massif,
1354 western Turkey. *Geologische Rundschau = International Journal of Earth Science* [1999], 94,
1355 204 -217.
- 1356 Catlos, E.J., Baker, C., Sorensen, S.S., Çemen, I., & Hancer, M. (2010). Geochemistry,
1357 geochronology, and cathodoluminescence imagery of the Salihli and Turgutlu granites
1358 (central Menderes Massif, western Turkey): Implications for Aegean tectonics.
1359 *Tectonophysics*, 488, 110-130. <https://doi.org/10.1016/j.tecto.2009.06.001>
- 1360 Catlos, E.J., Jacob, Lg, Oyman, T., & Sorensen S.S. (2012). Long-term exhumation of an
1361 Aegean metamorphic core complex granitoids in the northern Menderes Massif, western
1362 Turkey. *American Journal of Science*, 312, 534-571. <https://doi.org/10.2475/05.2012.03>
- 1363 Catlos, E.J., Lovera, O.M., Kelly, E.D., Ashley, K.T., Harrison, T.M., & Etzel, T. (2018).
1364 Modeling High-resolution Pressure-Temperature Paths across the Himalayan Main Central
1365 Thrust (central Nepal): Implications for the Dynamics of Collision. *Tectonics*, 37, 2363-
1366 2388. <https://doi.org/10.1029/2018TC005144>
- 1367 Catlos, E.J., Reyes, E., Brookfield, M., & Stockli, D.F. (2016). Age and Emplacement of the
1368 Permian- Jurassic Menghai Batholith, Western Yunnan, China. *International Geology*
1369 *Review*, 59(8), 919-945. <https://doi.org/10.1080/00206814.2016.1237312>
- 1370 Cavazza, W., Okay, A.I., & Zattin, M. (2009). Rapid early-middle Miocene exhumation of the
1371 Kazdağ Massif (western Anatolia). *Geologische Rundschau = International Journal of Earth*
1372 *Science* [1999], 98, 1935–1947. <https://doi.org/10.1007/s00531-008-0353-9>
- 1373 Çemen, I., Catlos, E. J., Gogus, O., & Ozerdem, C. (2006). Postcollisional extensional tectonics
1374 and exhumation of the Menderes Massif in the western Anatolia extended terrane, Turkey.
1375 *Special Paper - Geological Society of America*, 409, 353-379.
- 1376 Cenko-Tok, B., Expert, M., Işık, V., Candan, O., Monié, P., & Bruguier, O. (2016). Complete
1377 Alpine reworking of the northern Menderes Massif, western Turkey. *Geologische Rundschau*
1378 *= International Journal of Earth Science* [1999], 105, 1507. [http://dx.doi.org/10.1007/s00531-](http://dx.doi.org/10.1007/s00531-015-1271-2)
1379 [015-1271-2](http://dx.doi.org/10.1007/s00531-015-1271-2).
- 1380 Çetinkaplan, M., Pourteau, A., Candan, O., Koralay, O., Oberhänsli, R., Okay, A., Chen, F.,
1381 Kozlu, H., & Sengün, F. (2016). P–T–t evolution of eclogite/blueschist facies metamorphism
1382 in Alanya Massif: time and space relations with HP event in Bitlis Massif, Turkey.
1383 *Geologische Rundschau = International Journal of Earth Science* [1999], 105(1), 247-281.
1384 <https://doi.org/10.1007/s00531-014-1092-8>
- 1385 Çetinkaplan, M., Candan, O., Oberhänsli, R., Sudo, M., & Cenko-Tok, B. (2020). P–T–t
1386 evolution of the Cycladic Blueschist Unit in Western Anatolia/Turkey: Geodynamic
1387 implications for the Aegean region. *Journal of Metamorphic Geology*, 38, 379– 419.
1388 <https://doi.org/10.1111/jmg.12526>

- 1389 Channell, J.E.T., & Kozur H.W. (1997). How many oceans? Meliata, Vardar and Pindos oceans
1390 in Mesozoic Alpine paleogeography. *Geology* 25(2), 183–186. [https://doi.org/10.1130/0091-](https://doi.org/10.1130/0091-7613(1997)025<0183:HMOMVA>2.3.CO;2)
1391 [7613\(1997\)025<0183:HMOMVA>2.3.CO;2](https://doi.org/10.1130/0091-7613(1997)025<0183:HMOMVA>2.3.CO;2)
- 1392 Chaumillon, E., & Mascle, J. (1997). From foreland to forearc domains: New multichannel
1393 seismic reflection survey of the Mediterranean ridge accretionary complex (Eastern
1394 Mediterranean). *Marine Geology*, 138, 237-259. [https://doi.org/10.1016/S0025-](https://doi.org/10.1016/S0025-3227(97)00002-9)
1395 [3227\(97\)00002-9](https://doi.org/10.1016/S0025-3227(97)00002-9)
- 1396 Chen, F., Siebel, W., Satir, M. et al. (2002). Geochronology of the Karadere basement (NW
1397 Turkey) and implications for the geological evolution of the Istanbul zone *Geologische*
1398 *Rundschau = International Journal of Earth Science* [1999], 91, 469–481.
1399 <https://doi.org/10.1007/s00531-001-0239-6>
- 1400 Chousianitis, K., Ganas, A., & Evangelidis, C. P. (2015). Strain and rotation rate patterns of
1401 mainland Greece from continuous GPS data and comparison between seismic and geodetic
1402 moment release. *Journal of Geophysical Research Solid Earth*, 120, 3909– 3931.
1403 <https://doi.org/10.1002/2014JB011762>
- 1404 Chousianitis, K., Ganas, A., & Gianniou, M. (2013). Kinematic interpretation of present-day
1405 crustal deformation in central Greece from continuous GPS measurements. *Journal of*
1406 *Geodynamics*, 71, 1-13. <https://doi.org/10.1016/j.jog.2013.06.004>
- 1407 Cita, M.B., Erba, E., Lucchi, R., Pott, M., van der Meer, R., & Nieto, L. (1996). Stratigraphy and
1408 sedimentation in the Mediterranean Ridge diapiric belt, *Marine Geology*, 132(1–4), 131-150.
1409 [https://doi.org/10.1016/0025-3227\(96\)00157-0](https://doi.org/10.1016/0025-3227(96)00157-0)
- 1410 Clark, S. A., Sobiesiak, M., Zelt, C. A., Magnani, M. B., Miller, M. S., Bezada, M. J., &
1411 Levander, A. (2008). Identification and tectonic implications of a tear in the South American
1412 plate at the southern end of the Lesser Antilles, *Geochemistry, Geophysics, Geosystems*, 9,
1413 Q11004, <https://doi.org/10.1029/2008GC002084>
- 1414 Cocard, M., Kahle, H.-G., Peter, Y., Geiger, A., Veis, G., Felekis, S., Paradissis, D., & Billiris,
1415 H. (1999). New constraints on the rapid crustal motion of the Aegean region: recent results
1416 inferred from GPS measurements (1993-1998). across the West Hellenic Arc, Greece. *Earth*
1417 *and Planetary Science Letters*, 172(1-2), 39-47.
- 1418 Cocchi, L., Passaro, S., Tontini, F.C., & Ventura, G. (2017). Volcanism in slab tear faults is
1419 larger than in island-arcs and back-arcs. *Nature Communications*, 8, 1451.
1420 <https://doi.org/10.1038/s41467-017-01626-w>
- 1421 Coney, P.J., & Harms, T.A. (1984). Cordilleran metamorphic core complexes: Cenozoic
1422 extensional relics of Mesozoic compression. *Geology*, 12(9), 550–554.
1423 [https://doi.org/10.1130/0091-7613\(1984\)12<550:CMCCCE>2.0.CO;2](https://doi.org/10.1130/0091-7613(1984)12<550:CMCCCE>2.0.CO;2)
- 1424 Cornée, J.-J., Quillévéré, F., Moissette, P., Fietzke, J., López-Otálvaro, G.E., Melinte-
1425 Dobrinescu, M., Philippon, M., van Hinsbergen, D.J.J., Agiadi, K., Koskeridou, E., &
1426 Münch, P. (2018). Tectonic motion in oblique subduction forearcs: insights from the
1427 revisited Middle and Upper Pleistocene deposits of Rhodes, Greece. *Journal of the*
1428 *Geological Society*, 176 (1), 78–96. <https://doi.org/10.1144/jgs2018-090>
- 1429 Crameri, F., Magni, V., Domeier, M. et al. (2020). A transdisciplinary and community-driven
1430 database to unravel subduction zone initiation. *Nature Communications*, 11, 3750.
1431 <https://doi.org/10.1038/s41467-020-17522-9>
- 1432 Dannat, C. (1997). *Geochemie, Geochronologie und Nd- und Sr-Isotopie der granitoiden*
1433 *Kerngneise des Menderes Massivs, SW-Türkei*: Ph.D. thesis, Universität Mainz, 120 p.

- 1434 d'Atri, A., Zuffa, G.G., Cavazza, W., Okay, A.I., & Di Vincenzo, G. (2012). Detrital supply from
1435 subduction/accretion complexes to the Eocene–Oligocene post-collisional southern Thrace
1436 Basin (NW Turkey and NE Greece). *Sedimentary Geology*, 243–244, 117-129.
1437 <https://doi.org/10.1016/j.sedgeo.2011.10.008>
- 1438 de Boorder, H., Spakman, W., White, S.H., & Wortel, M.J.R. (1998). Late Cenozoic
1439 mineralization, orogenic collapse and slab detachment in the European Alpine Belt. *Earth
1440 and Planetary Science Letters*, 164(3–4), 569-575. [https://doi.org/10.1016/S0012-
1441 821X\(98\)00247-7](https://doi.org/10.1016/S0012-821X(98)00247-7)
- 1442 de Capitani, C., & Brown, T. H. (1987). The computation of chemical equilibrium in complex
1443 systems containing non-ideal solutions. *Geochimica et Cosmochimica Acta*, 51(10), 2639-
1444 2652.
- 1445 de Capitani, C., & Petrakakis, K. (2010). The computation of equilibrium assemblage diagrams
1446 with Theriak/Domino software. *American Mineralogist*, 95(7), 1006-1016.
- 1447 Delaloye, M., & Bingöl, E. (2000). Granitoids from western and northwestern Anatolia:
1448 geochemistry and modeling of geodynamic evolution. *International Geology Review*, 42,
1449 241–268.
- 1450 Demirbilek, M., Mutlu, H., Fallick, A.E., Sarniz, K., & Kibici, Y. (2018). Petrogenetic evolution
1451 of the Eocene granitoids in eastern part of the Tavşanlı Zone in northwestern Anatolia,
1452 Turkey, *Lithos*, 314–315, 236-259. <https://doi.org/10.1016/j.lithos.2018.06.003>
- 1453 Dewey, J.F., & Şengör, A.M.C. (1979). Aegean and surrounding regions: Complex multiplate
1454 and continuum tectonics in a convergent zone. *Geological Society of America Bulletin*,
1455 90(1), 84–92. [https://doi.org/10.1130/0016-7606\(1979\)90<84:AASRCM>2.0.CO;2](https://doi.org/10.1130/0016-7606(1979)90<84:AASRCM>2.0.CO;2)
- 1456 Di Rosa, M., Farina, F., Marroni, M., Pandolfi, L., Göncüoğlu, M.C., Ellero, A., & Ottria, G.
1457 (2019). U-Pb zircon geochronology of intrusive rocks from an exotic block in the Late
1458 Cretaceous – Paleocene Taraklı Flysch (northern Turkey): Constraints on the tectonics of the
1459 Intrapontide suture zone, *Journal of Asian Earth Sciences*, 171, 277-288.
1460 <https://doi.org/10.1016/j.jseaes.2018.11.017>
- 1461 Dilek, Y., & Altunkaynak, Ş. (2007). Cenozoic Crustal Evolution and Mantle Dynamics of Post-
1462 Collisional Magmatism in Western Anatolia. *International Geology Review*, 49(5), 431-453.
1463 <https://doi.org/10.2747/0020-6814.49.5.431>
- 1464 Dilek, Y., & Sandvol, E. (2009). Seismic structure, crustal architecture and tectonic evolution of
1465 the Anatolian-African Plate Boundary and the Cenozoic Orogenic Belts in the Eastern
1466 Mediterranean Region. *Geological Society, London, Special Publications*, 327, 127-160.
1467 <https://doi.org/10.1144/SP327.8>
- 1468 Doğan, A., & Emre, O. (2006). Ege Graben Sisteminin Kuzey Sınırı: Sındırgı-Sincanlı Fay Zonu
1469 (Northern Boundary of Aegean Graben System: Sındırgı-Sincanlı Fault Zone). 59. Türkiye
1470 Jeoloji Kurultayı, Bildiriler Kitabı.
- 1471 Doğangün, A., Ural, A., Sezen, H., Güney, Y., & Fırat, F.K. (2013). The 2011 Earthquake in
1472 Simav, Turkey and Seismic Damage to Reinforced Concrete Buildings. *Buildings* 3(1), 173-
1473 190. <https://doi.org/10.3390/buildings3010173>
- 1474 Doglioni, C., Agostini, S., Crespi, M., Innocenti, F., Manetti, P., Riguzzi, F., & Savaşçin, Y.
1475 (2002). On the extension in western Anatolia and the Aegean sea. In G. Rosenbaum, G.S.
1476 Lister (Eds.), *Reconstruction of the evolution of the Alpine-Himalayan Orogen*. *Journal of
1477 the Virtual Explorer*, 8, 161-176.
- 1478 Dora, O.O., Candan, O., Durr, S., & Oberhansli, R. (1995) New evidence on the geotectonic
1479 evolution of the Mendere Massif. In O. Piskin, M. Ergun, M.Y. Svascin, G. Tarcan (Eds.),

- 1480 Proceedings of the International Earth Science Colloquium on the Aegean Region. Izmir,
1481 Turkey (Vol. 1, pp. 53-72).
- 1482 Dora, O.Ö, Candan, O., Kaya, O., Koralay, E., & Akal, C. (2005). Menderes Masifi Çine
1483 Asmasifi' ndeki Koçarlı - Bafa - Yatağan - Karacasu arasında uzanan gnays / pist
1484 dokanađynın niteliđi: Jeolojik, tektonik, petrografik ve jeokronolojik bir yaklađım.
1485 YDABÇAG - 101 Y 132 nolu Türkiye Bilimsel ve Teknolojik Arařtırma Kurumu
1486 (TÜBİTAK) projesi, 197p. (unpublished).
- 1487 Dragovic, B., Samanta, L.M., Baxter, E.F., & Selverstone, J. (2012). Using garnet to constrain
1488 the duration and rate of water-releasing metamorphic reactions during subduction: An
1489 example from Sifnos, Greece. *Chemical Geology*, 314–317, 9-22.
1490 <https://doi.org/10.1016/j.chemgeo.2012.04.016>
- 1491 Dürr, S. (1975). Über Alter und geotektonische Stellung des Menderes Kristallins/SW Anatolien
1492 und seine Äquivalente in der Mittleren Aegean. Habilitation Thesis, University of Marburg.
- 1493 Duru, M., Pehlivan, S., Şenturk, Y., Yavaş, F., & Kar, H. (2004). New Results on the
1494 Lithostratigraphy of the Kazdağ Massif in Northwest Turkey. *Turkish Journal of Earth
1495 Sciences*, 13, 177-186.
- 1496 Elburg, M.A., & Smet, I. (2020). Geochemistry of lavas from Aegina and Poros (Aegean Arc,
1497 Greece): Distinguishing upper crustal contamination and source contamination in the Saronic
1498 Gulf area, *Lithos*, 358–359, 105416. <https://doi.org/10.1016/j.lithos.2020.105416>.
- 1499 Elitez, İ, Cenk Yalıtırak, C., & Aktuğ, B. (2016). Extensional and compressional regime driven
1500 left-lateral shear in southwestern Anatolia (eastern Mediterranean): The Burdur-Fethiye
1501 Shear Zone. *Tectonophysics*, 688, 26-35. <https://doi.org/10.1016/j.tecto.2016.09.024>
- 1502 Elmas, A. (2012). Basement types of the Thrace Basin and a new approach to the pre-Eocene
1503 tectonic evolution of the northeastern Aegean and northwestern Anatolia: a review of data
1504 and concepts. *Geologische Rundschau = International Journal of Earth Sciences*, 101, 1895–
1505 1911 (2012). <https://doi.org/10.1007/s00531-012-0756-5>
- 1506 El-Sharkawy, A., Meier, T., Lebedev, S., Behrmann, J. H., Hamada, M., Cristiano, L., et al.
1507 (2020). The slab puzzle of the Alpine-Mediterranean region: Insights from a new, high-
1508 resolution, shear wave velocity model of the upper mantle. *Geochemistry, Geophysics,
1509 Geosystems*, 21, e2020GC008993. <https://doi.org/10.1029/2020GC008993>
- 1510 Emery, K.O., Heezen, B., & Allan, T.D. (1966). Bathymetry of the Eastern Mediterranean sea.
1511 *Deep Sea Research*, 13, 173-192.
- 1512 Emre, Ö, & Duman, T. (2011). 19 May 2011 Simav-Kutahya earthquake (Mw:5.8) in Turkey
1513 pre-assessment, earthquake report. General Directorate of Mineral Research and Exploration
1514 (MTA). Ankara, Turkey: Earth Dynamics Research Center. Turkish.
- 1515 Emre, Ö., Duman, T.Y., & Özalp, S. (2011). 1:250000 scale Active Fault Map Series of Turkey,
1516 Kutahya (NJ 35-4) Quadrangle, Serial Number 10, General Directorate of Mineral Research
1517 and Exploration, Ankara, Turkey.
- 1518 Emre, Ö, Erkal, T., Tchepalyga, A., Kazancı, N., Keçer, M., & Ünay, E. (1998). Neogene
1519 quaternary evolution of the Eastern Marmara Region, Northwest Turkey. *Bulletin of the
1520 Mineral Research Exploration Institute of Turkey*, 120, 119-145.
- 1521 Erdoğan, B., Akay, E., Hasözbeke, A., Satır, M., & Siebel, W. (2013). Stratigraphy and tectonic
1522 evolution of the Kazdağ Massif (NW Anatolia) based on field studies and radiometric ages.
1523 *International Geology Review*, 55(16), 2060- 2082.

- 1524 Ergün, M., Okay, S., Sari, C., Oral, E.Z., Ash, M., Hall, J., & Miller, H. (2005). Gravity
1525 anomalies of the Cyprus Arc and their tectonic implications. *Marine Geology*, 221(1–4), 349-
1526 358. <https://doi.org/10.1016/j.margeo.2005.03.004>
- 1527 Ersoy, E.Y., & Palmer, M.R. (2013). Eocene-Quaternary magmatic activity in the Aegean:
1528 Implications for mantle metasomatism and magma genesis in an evolving orogeny, *Lithos*,
1529 180–181, 5-24. <https://doi.org/10.1016/j.lithos.2013.06.007>
- 1530 Ersoy, E.Y., Çemen, I., Helvacı, C., & Billor, Z., 2014. Tectono-stratigraphy of the Neogene
1531 basins in western Turkey: implications for tectonic evolution of the aegean extended region.
1532 *Tectonophysics*, 635, 33e58. <http://dx.doi.org/10.1016/j.tecto.2014.09.002>
- 1533 Ersoy, E.Y., Helvacı, C., & Sozbilir, H. (2010). Tectono-stratigraphic evolution of the NE-SW-
1534 trending superimposed Selendi basin: implications for late Cenozoic crustal extension in
1535 Western Anatolia, Turkey. *Tectonophysics*, 488, 210–232.
- 1536 Ersoy, E.Y., Palmer, M.R., Genç Ş, C., Prelević, D., Akal, C., & Uysal, I. (2017). Chemo-probe
1537 into the mantle origin of the NW Anatolia Eocene to Miocene volcanic rocks: Implications
1538 for the role of, crustal accretion, subduction, slab roll-back and slab break-off processes in
1539 genesis of post-collisional magmatism, *Lithos*, 288–289, 55-71.
1540 <https://doi.org/10.1016/j.lithos.2017.07.006>
- 1541 Etzel, T.E., Catlos, E.J., Atakturk, K., Kelly, E.D., Lovera, O.M., Çemen, I., Diniz, E., & Stockli,
1542 D. (2019). Implications for thrust-related shortening punctuated by extension from P-T paths
1543 and geochronology of garnet-bearing schists. *Tectonics* 38(6), 1974-1998.
1544 <https://doi.org/10.1029/2018TC005335>
- 1545 Etzel, T.M., Catlos, E.J., Çemen, I., Ozerdem, C., Oyman, T., & Miggins, D. (2020).
1546 Documenting exhumation in the central and northern Menderes Massif (western Turkey):
1547 New insights from garnet-based P-T estimates and K-feldspar ⁴⁰Ar/³⁹Ar geochronology.
1548 *Lithosphere*, 1, 8818289. <https://doi.org/10.2113/2020/8818289>
- 1549 Evangelidis, C.P. (2017). Seismic anisotropy in the Hellenic subduction zone: Effects of slab
1550 segmentation and subslab mantle flow. *Earth and Planetary Science Letters*, 480, 97-106.
1551 <https://doi.org/10.1016/j.epsl.2017.10.003>
- 1552 Eyidoğan, H., & Jackson, J. (1985). A seismological study of normal faulting in the Demirci,
1553 Alaşehir and Gediz earthquakes of 1969–70 in western Turkey: implications for the nature
1554 and geometry of deformation in the continental crust. *Geophysical Journal of the Royal*
1555 *Astronomical Society*, 81, 569-607. <https://doi.org/10.1111/j.1365-246X.1985.tb06423.x>
- 1556 Faccenna, C., Becker, T.W., Auer, L., Billi, A., Boschi, L., Brun, J.-P., Capitanio, F.A.,
1557 Funicello, F., Horvath, F., Jolivet, L., Piromallo, C., Royden, L., Rossetti, F., & Serpelloni,
1558 E. (2014). Mantle dynamics in the Mediterranean, *Review of Geophysics*, 52, 283– 332.
1559 <https://doi.org/10.1002/2013RG000444>
- 1560 Faccenna, C., Bellier, O., Martinod, J., Piromallo, C., & Regard, V. (2006). Slab detachment
1561 beneath eastern Anatolia: A possible cause for the formation of the North Anatolian fault.
1562 *Earth and Planetary Science Letters*, 242(1–2), 85-97.
1563 <https://doi.org/10.1016/j.epsl.2005.11.046>.
- 1564 Faccenna, C., Jolivet, L., Piromallo, C., & Morelli, A. (2003). Subduction and the depth of
1565 convection in the Mediterranean mantle. *Journal of Geophysical Research*, 108(B2).
1566 <https://doi.org/10.1029/2001JB001690>
- 1567 Ferentinos, G., Georgiou, N., Christodoulou, D., Geraga, M., & Papatheodorou, G. (2018).
1568 Propagation and termination of a strike slip fault in an extensional domain: The westward

- 1569 growth of the North Anatolian Fault into the Aegean Sea, *Tectonophysics*, 745, 183-195.
1570 <https://doi.org/10.1016/j.tecto.2018.08.003>
- 1571 Fornash, K.F., & Whitney, D.L. (2020). Lawsonite-rich layers as records of fluid and element
1572 mobility in subducted crust (Sivrihisar Massif, Turkey). *Chemical Geology*, 533, 119356,
1573 <https://doi.org/10.1016/j.chemgeo.2019.119356>
- 1574 Foucher, J.P., Chamot-Rooke, N., Alexandry, S., Augustin, J.M., Monti, S., Pavlakis, P., &
1575 Voisset, M. (1993). Multibeam bathymetry and seabed reflectivity maps of the MEDRIFT
1576 corridor across the eastern Mediterranean Ridge. In: UEG VII., Strasbourg, France. *Terra*
1577 *Cognita*, Abstracts, pp. 278-279.
- 1578 Frassi, C., Marroni, M., Pandolfi, L., Göncüoğlu, M.C., Ellero, A., Ottria, G., Sayit, K.,
1579 McDonald, C.S., Balestrieri, M.L., & Malasoma, A. (2018). Burial and exhumation history
1580 of the Daday Unit (central Pontides, Turkey); implications for the closure of the Intra-Pontide
1581 oceanic basin. In G. Capponi, A. Festa, G. Rebay (Eds.), *Birth and death of oceanic basins;*
1582 *geodynamic processes from rifting to continental collision in Mediterranean and circum-*
1583 *Mediterranean orogeny*. *Geological Magazine*, 155, 356-376.
- 1584 Fytikas, M., Innocenti, F., Manetti, P., Mazzuoli, R., Peccerillo, A., & Villari, L. (1984). Tertiary
1585 to quaternary evolution of volcanism in the Aegean region. In JE Dixon, AHF Robertson
1586 (Eds.), *The Geological Evolution of the Eastern Mediterranean*, Geological Society of
1587 London, Special Publications (Vol. 17, pp. 687–699).
- 1588 Galindo-Zaldívar, J., Nieto, L., & Woodside, J. (1996). Structural features of mud volcanoes and
1589 the fold system of the Mediterranean Ridge, south of Crete. *Marine Geology*, 132(1-4), 95-
1590 112. [https://doi.org/10.1016/0025-3227\(96\)00155-7](https://doi.org/10.1016/0025-3227(96)00155-7)
- 1591 Ganas A., & Parsons T. (2009). Three-dimensional model of Hellenic Arc deformation and
1592 origin of the Cretan uplift. *Journal of Geophysical Research*, 114(B06404), 1–14.
1593 <https://doi.org/10.1029/2008JB005599>
- 1594 Gautier, P., Brun, J-P., Moriceau, R., Sokoutis, D., Martinod, J., & Jolivet, L. (1999). Timing,
1595 kinematics and cause of Aegean extension: a scenario based on a comparison with simple
1596 analogue experiments. *Tectonophysics*, 315(1–4), 31-72. [https://doi.org/10.1016/S0040-](https://doi.org/10.1016/S0040-1951(99)00281-4)
1597 [1951\(99\)00281-4](https://doi.org/10.1016/S0040-1951(99)00281-4)
- 1598 Gautier, Y. (1984). Déformations et métamorphismes associés à la fermeture téthysienne en
1599 Anatolie centrale (région de Sivrihisar, Turquie). PhD thesis, University Paris-Sud, France.
1600 236.
- 1601 Gawthorpe, R.L., & Hurst, M. (1993). Transfer Zones in Extensional Basins: Their Structural
1602 Style and Influence on Drainage Development and Stratigraphy. *Journal of the Geological*
1603 *Society, London*, 150, 1137-1152. <https://doi.org/10.1144/gsjgs.150.6.1137>
- 1604 Genç, SC. (1998). Evolution of the Bayramic, magmatic complex, northwestern Anatolia.
1605 *Journal of Volcanology and Geothermal Research*, 85, 233–249.
- 1606 Gerogiannis, N., Xypolias, P., Chatzaras, V., Aravadinou, E., & Papapavlou, K. (2019).
1607 Deformation within the Cycladic subduction–exhumation channel: new insights from the
1608 enigmatic Makrotantalo nappe (Andros, Aegean). *International Journal of Earth Sciences*,
1609 108, 817–843. <https://doi.org/10.1007/s00531-019-01680-3>
- 1610 Gessner, K., Collins, A.S., Ring, U., & GÜngör, T. (2004). Structural and thermal history of
1611 polyorogenic basement. *Journal of the Geological Society of London*, 161, 93–101.
1612 <http://dx.doi.org/10.1144/0016-764902-166>

- 1613 Gessner, K., Gallardo, L. A., Markwitz, V., Ring, U., & Thomson, S. N. (2013). What caused the
 1614 denudation of the Menderes Massif; review of crustal evolution, lithosphere structure, and
 1615 dynamic topography in southwest Turkey. *Gondwana Research*, 24(1), 243-274.
- 1616 Gessner, K., Markwitz, V., & Güngör, T. (2017). Crustal fluid flow in hot continental extension:
 1617 tectonic framework of geothermal areas and mineral deposits in western Anatolia. *Geological*
 1618 *Society, London, Special Publications*, 453, 289-311. <https://doi.org/10.1144/SP453.7>
- 1619 Gessner, K., Piazzolo, S., Gungor, T., Ring, U., Kroener, A., & Passchier, C. W. (2001). Tectonic
 1620 significance of deformation patterns in granitoid rocks of the Menderes nappes, Anatolide
 1621 Belt, Southwest Turkey. *Geologische Rundschau = International Journal of Earth Sciences*,
 1622 89(4). 766-780.
- 1623 Gessner, K., Ring, U., & Gungor, T. (2011). Field guide to Samos and the Menderes Massif;
 1624 along-strike variations in the Mediterranean Tethyan Orogen. *GSA Field Guide*, 23.
- 1625 Gessner, K., Ring, U., Passchier, C. W., Hetzel, R., & Okay, A. I. (2002). Stratigraphic and
 1626 metamorphic inversions in the central Menderes Massif; a new structural model; discussion
 1627 and reply. *Geologische Rundschau = International Journal of Earth Sciences*, 91(1), 168-178.
- 1628 Gianni, G.M., Navarrete, C. & Spagnotto, S. (2019). Surface and mantle records reveal an
 1629 ancient slab tear beneath Gondwana. *Scientific Reports*, 9, 19774.
 1630 <https://doi.org/10.1038/s41598-019-56335-9>
- 1631 Glodny, J., & Hetzel, R. (2007). Precise U-Pb ages of syn-extensional Miocene intrusions in the
 1632 central Menderes Massif, western Turkey. *Geological Magazine*, 144, 1–12.
- 1633 Göncüoğlu, M.C. (2010). Introduction to the Geology of Turkey: Geodynamic Evolution of the
 1634 Pre-Alpine and Alpine Terranes. General Directorate of Mineral Research and Exploration
 1635 Monography Series, 5, 1-66.
- 1636 Göncüoğlu, M. C., Dirik, K., & Kozlu, H. (1997). General characteristics of pre-alpine and
 1637 Alpine Terranes in Turkey: explanatory notes to the terrane map of Turkey. *Annales*
 1638 *Géologique de Pays Hellenique*, 37, 515–536.
- 1639 Göncüoğlu, M.C., Marroni, M., Pandolfi, L., Ellero, A., Ottria, G., Catanzariti, R., Tekin, U.K.,
 1640 & Sayit, K. (2014). The Arkot Dag Melange in Arac area, central Turkey; evidence of its
 1641 origin within the geodynamic evolution of the Intra-Pontide suture zone. *Journal of Asian*
 1642 *Earth Sciences*, 85, 117-139.
- 1643 Göncüoğlu, M.C., Marroni, M., Sayit, K., Tekin, U.K., Ottria, G., Pandolfi, L., & Ellero, A.
 1644 (2012). The Ayli Dag ophiolite sequence (central-northern Turkey); a fragment of Middle
 1645 Jurassic oceanic lithosphere within the Intra-Pontide suture zone. *Ofioliti*, 37, 77-92.
- 1646 Görgün, E. (2014). Source characteristics and Coulomb stress change of the 19 May 2011 Mw
 1647 6.0 Simav–Kütahya earthquake, Turkey. *Journal of Asian Earth Sciences*, 87, 79-88.
 1648 <https://doi.org/10.1016/j.jseaes.2014.02.016>.
- 1649 Görür, N., Monod, O., Okay, A.I., Sengör, A.M.C., Tüysüz, O., Yigitbas, E., Sakinç, M., &
 1650 Akkök, R. (1997). Palaeogeographic and tectonic position of the Carboniferous rocks of the
 1651 western Pontides (Turkey). in the frame of the Variscan belt. *Bulletin de la Société*
 1652 *Géologique de France*, 168, 197–205.
- 1653 Govers, R., & Wortel, M.J.R. (2005). Lithosphere tearing at STEP faults: response to edges of
 1654 subduction zones. *Earth and Planetary Science Letters*, 236(1–2), 505-523.
 1655 <https://doi.org/10.1016/j.epsl.2005.03.022>.
- 1656 Grasemann, B., Schneider, D.A., Stöckli, D.F., Iglseider, C. (2012). Miocene bivergent crustal
 1657 extension in the Aegean: Evidence from the western Cyclades (Greece). *Lithosphere*, 4 (1),
 1658 23–39. <https://doi.org/10.1130/L164.1>

- 1659 Gürer, Ö, Sangu, E., & Özburan, M. (2006). Neotectonics of the SW Marmara region, NW
1660 Anatolia, Turkey. *Geological Magazine*, 143 (2): 229–241.
1661 <https://doi.org/10.1017/S0016756805001469>
- 1662 Gürsu, S., & Göncüoğlu, M.C. (2006). Petrogenesis and tectonic setting of Cadomian felsic
1663 igneous rocks, Sandıklı area of the western Taurides, Turkey. *Geologische Rundschau =*
1664 *International Journal of Earth Sciences*, 95, 741–757 (2006). [https://doi.org/10.1007/s00531-](https://doi.org/10.1007/s00531-005-0064-4)
1665 [005-0064-4](https://doi.org/10.1007/s00531-005-0064-4)
- 1666 Gürsu, S., Göncüoğlu, M.C., & Bayhan, H. (2004). Geology and geochemistry of the pre-Early
1667 Cambrian rocks in Sandıklı area: implications for the Pan-African evolution in NW
1668 Gondwanaland. *Gondwana Research*, 7(4), 923–935.
- 1669 Gutnic, M., Monod, O., Poisson, A., & Dumont, J.F. (1979). *Geologie des Taurides Occidentales*
1670 (Turquie). *Memoirs of the Geological Society of France*, 58(137), 109pp.
- 1671 Haddad, A., Ganas, A., Kassaras, I., & Lupi, M. (2020). Seismicity and geodynamics of western
1672 Peloponnese and central Ionian Islands: Insights from a local seismic deployment.
1673 *Tectonophysics*, 778, 228353. <https://doi.org/10.1016/j.tecto.2020.228353>.
- 1674 Hall, J., Aksu, A.E., Elitez, I., Yaltırak, C., & Çifçi, G. (2014). The Fethiye–Burdur Fault Zone:
1675 A component of upper plate extension of the subduction transform edge propagator fault
1676 linking Hellenic and Cyprus Arcs, Eastern Mediterranean. *Tectonophysics*, 635, 80–99.
1677 <https://doi.org/10.1016/j.tecto.2014.05.002>
- 1678 Hall, J., Aksu, A.E., Yaltırak, C., & Winsor, J.D. (2009). Structural architecture of the Rhodes
1679 Basin: A deep depocentre that evolved since the Pliocene at the junction of Hellenic and
1680 Cyprus Arcs, eastern Mediterranean. *Marine Geology*, 258(1-4), 1-23.
1681 <https://doi.org/10.1016/j.margeo.2008.02.007>
- 1682 Hall, R., Audley-Charles, M.G., & Carter, D.J. (1984). The significance of Crete for the
1683 evolution of the Eastern Mediterranean. *Geological Society, London, Special Publications*,
1684 17, 499-516. <https://doi.org/10.1144/GSL.SP.1984.017.01.37>
- 1685 Halpaap, F., Rondenay, S., & Ottemöller, L. (2018). Seismicity, deformation, and metamorphism
1686 in the Western Hellenic Subduction Zone: New constraints from tomography. *Journal of*
1687 *Geophysical Research: Solid Earth*, 123, 3000– 3026. <https://doi.org/10.1002/2017JB015154>
- 1688 Hansen, S.E., Evangelidis, C.P., & Papadopoulos, G.A. (2019). Imaging slab detachment within
1689 the Western Hellenic Subduction Zone. *Geochemistry, Geophysics, Geosystems*, 20, 895–
1690 912. <https://doi.org/10.1029/2018GC007810>
- 1691 Harris, N.B.W., Kelly, S., & Okay, A.I. (1994). Postcollision magmatism and tectonics in
1692 northwest Anatolia. *Contributions to Mineralogy and Petrology*, 117, 241–252.
- 1693 Harrison, R.W., Tsiolakis, E., Stone, B.D., Lord, A., McGeehin, J.P., Mahan, S.A., & Chirico, P.
1694 (2012). Late Pleistocene and Holocene uplift history of Cyprus: implications for active
1695 tectonics along the southern margin of the Anatolian microplate. *Geological Society,*
1696 *London, Special Publications*, 372, 561-584. <https://doi.org/10.1144/SP372.3>
- 1697 Hasözbeğ, A., Akay, E., Erdoğan, B., Satır, M., & Siebel, W. (2010). Early Miocene granite
1698 formation by detachment tectonics or not? A case study from the northern Menderes Massif
1699 (Western Turkey). *Journal of Geodynamics*, 50, 67–80.
- 1700 Hatzfeld, D., Pedotti, G., Hatzidimitriou, P., & Makropoulos, K. (1990). The strain pattern in the
1701 western Hellenic arc deduced from a microearthquake survey. *Geophysical Journal*
1702 *International*, 101(1), 181-202.
- 1703 Hayes, G. (2018). Slab2 - A Comprehensive Subduction Zone Geometry Model: U.S. Geological
1704 Survey data release, <https://doi.org/10.5066/F7PV6JNV>

- 1705 Heezen, B.C., & Ewing, M., 1963. The Mid Oceanic Ridge. In M.N. Hill (Ed.), *The Seas* (Vol. 3,
1706 pp. 388-410), Interscience, New York.
- 1707 Henjes-Kunst F., Altherr, R., Kreuzer, H., Hansen, B.T. (1988). Disturbed U-Th-Pb systematics
1708 of young zircons and uranotorites—the case of the Miocene Aegean granitoids (Greece).
1709 *Chemical Geology*, 73(2), 125–145.
- 1710 Hetzel, R., & Reischmann, T. (1996). Intrusion age of Pan-African augen gneisses in the
1711 southern Menderes Massif and the age of cooling after Alpine ductile extensional
1712 metamorphism. *Geological Magazine*, 133(5), 505-572.
- 1713 Hetzel, R., Passchier, C. W., Ring, U., & Dora, O. O. (1995a). Bivergent extension in orogenic
1714 belts; the Menderes Massif (southwestern Turkey). *Geology*, 23(5), 455-458.
- 1715 Hetzel, R., Ring, U., Akal, C., & Troesch, M. (1995b). Miocene NNE-directed extensional
1716 unroofing in the Menderes Massif, southwestern Turkey. *Journal of the Geological Society of*
1717 *London*, 152, 4639654.
- 1718 Holland, T.B., & Powell, R. (1998). An internally consistent thermodynamic data set for phases
1719 of petrological interest. *Journal of Metamorphic Geology*, 16(3), 309-343.
- 1720 Holland, T.B., & Powell, R. (2011). An improved and extended internally consistent
1721 thermodynamic dataset for phases of petrological interest, involving a new equation of state
1722 for solids. *Journal of Metamorphic Geology*, 29(3), 333-383.
- 1723 Hollenstein, C., Müller, M.D., Geiger, A., & Kahle, H.-G. (2008). Crustal motion and
1724 deformation in Greece from a decade of GPS measurements, 1993e2003. *Tectonophysics*,
1725 449, 17e40. <http://dx.doi.org/10.1016/j.tecto.2007.12.006>.
- 1726 Holness, M.B., & Bunbury, J.M. (2006). Insights into continental rift-related magma chambers:
1727 Cognate nodules from the Kula Volcanic Province, Western Turkey, *Journal of Volcanology*
1728 *and Geothermal Research*, 153(3-4), 241-261.
1729 <https://doi.org/10.1016/j.jvolgeores.2005.12.004>
- 1730 Hosseini, K. , Matthews, K. J., Sigloch, K. , Shephard, G. E., Domeier, M. & Tsekhmistrenko,
1731 M. (2018). SubMachine: Web-Based tools for exploring seismic tomography and other
1732 models of Earth's deep interior. *Geochemistry, Geophysics, Geosystems*, 19.
1733 <https://doi.org/10.1029/2018GC007431>
- 1734 Hubert-Ferrari, A., Armijo, R., King, G., Meyer, B., & Barka, A. (2002). Morphology,
1735 displacement, and slip rates along the North Anatolian Fault, Turkey, *Journal of Geophysical*
1736 *Research*, 107(B10), 2235. <https://doi.org/10.1029/2001JB000393>
- 1737 Huchon, P., Lybéris, N., Angelier, J., Le Pichon, X., & Renard, V. (1982). Tectonics of the
1738 hellenic trench: A synthesis of sea-beam and submersible observations, *Tectonophysics*,
1739 86(1-3), 69-112. [https://doi.org/10.1016/0040-1951\(82\)90062-2](https://doi.org/10.1016/0040-1951(82)90062-2)
- 1740 Husson, L., Brun, J-P., Yamato, P., & Faccenna, C. (2009). Episodic slab rollback fosters
1741 exhumation of HP–UHP rocks. *Geophysics Journal International*, 179, 1292–1300
- 1742 Ilhan, E. (1971). Earthquakes in Turkey. In A.S. Campbell (Ed.), *Geology and History of*
1743 *Turkey*, (pp. 431-442). Petroleum Exploration Society of Libya, Tripoli.
- 1744 İnan, S., Pabuçcu, A., Kulak, F., Ergintav, S., Tatar, O., Altunel, E., Akyüz, S., Tan, O., Seyis,
1745 C., Çakmak, R., Saatçılar, R., & Eyidoğan, H. (2012). Microplate boundaries as obstacles to
1746 pre-earthquake strain transfer in Western Turkey: Inferences from continuous geochemical
1747 monitoring. *Journal of Asian Earth Sciences*, 48, 56-71.
1748 <https://doi.org/10.1016/j.jseaes.2011.12.016>.

- 1749 Inel, M., Ozmen, H.B. & Akyol, E. (2013). Observations on the building damages after 19 May
1750 2011 Simav (Turkey) earthquake. *Bulletin of Earthquake Engineering*, 11, 255–283.
1751 <https://doi.org/10.1007/s10518-012-9414-3>
- 1752 Innocenti, F., Agostini, S., Di Vincenzo, G., Doglioni, C., Manetti, P., Savaşçin, M.Y., &
1753 Tonarini, S. (2005). Neogene and Quaternary volcanism in Western Anatolia: Magma
1754 sources and geodynamic evolution, *Marine Geology*, 221(1–4), 397-421.
1755 <https://doi.org/10.1016/j.margeo.2005.03.016>
- 1756 Iredale, L. J., Teyssier, C., & Whitney, D. L. (2013). Cenozoic pure-shear collapse of the
1757 southern Mendere Massif, Turkey. *Special Publication - Geological Society of London*, 372,
1758 323-342. <https://doi.org/10.1144/SP372.15>
- 1759 Işık, V., Seyitoğlu, G., & Çemen, I. (2003). Ductile-brittle transition along the Alasehir
1760 detachment fault and its structural relationship with the Simav detachment fault, Mendere
1761 Massif, western Turkey. *Tectonophysics*, 374, 1–18. [http://dx.doi.org/10.1016/S0040-](http://dx.doi.org/10.1016/S0040-1951(03)00275-0)
1762 [1951\(03\)00275-0](http://dx.doi.org/10.1016/S0040-1951(03)00275-0).
- 1763 Işık, V., & Tekeli, O. (2001). Late orogenic crustal extension in the northern Mendere Massif
1764 (western Turkey); evidence for metamorphic core complex formation. *Geologische*
1765 *Rundschau = International Journal of Earth Sciences*, 89(4). 757-765.
- 1766 Işık, V., Tekeli, O., & Seyitoğlu, G. (2004). The $^{40}\text{Ar}/^{39}\text{Ar}$ age of extensional ductile deformation
1767 and granitoid intrusion in the northern Mendere core complex: implications for the initiation
1768 of extensional tectonics in western Turkey. *Journal of Asian Earth Sciences*, 23, 555–566.
- 1769 Jackson, J. (1994). Active tectonics of the Aegean region. *Annual Reviews of Earth and*
1770 *Planetary Science*, 22, 239-71.
- 1771 Jackson, J., & McKenzie, D. (1984). Active tectonics of the Alpine-Himalayan belt between
1772 western Turkey and Pakistan, *Geophysical Journal of the Royal Astronomical Society*, 77,
1773 185 – 264.
- 1774 John, B.E., & Howard, K.A. (1995). Rapid extension recorded by cooling-age patterns and brittle
1775 deformation, Naxos, Greece. *Journal of Geophysical Research*, 100, 9969–9979.
- 1776 Jolivet, L., & Brun, J.-P. (2010). Cenozoic geodynamic evolution of the Aegean, *International*
1777 *Journal of Earth Sciences*, 99(1), 109-138. <https://doi.org/10.1007/s00531-008-0366-4>
- 1778 Jolivet, L., Brun, J.P., Gautier, P., Lallemand, S., & Patriat, M. (1994). 3D- Kinematics of
1779 extension in the Aegean region from the early Miocene to the present, *Insights from the*
1780 *ductile crust. Bulletin de la Societe Geologique de France*, 165, 195-209.
- 1781 Jolivet, L., & Faccenna, C. (2000). Mediterranean extension and the Africa-Eurasia collision,
1782 *Tectonics*, 19(6), 1095– 106. <https://doi.org/10.1029/2000TC900018>
- 1783 Jolivet, L., Faccenna, C., Huet, B., Labrousse, L., Le Pourhiet, L., et al. (2013). Aegean
1784 tectonics: Strain localisation, slab tearing and trench retreat. *Tectonophysics*, 597-598, 1-33.
- 1785 Jolivet, L., Lecomte, E., Huet, B., Denèle, Y., Lacombe, O., Labrousse, L., Le Pourhiet, L., &
1786 Mehl, C. (2010). The North Cycladic Detachment System. *Earth and Planetary Science*
1787 *Letters*, 289(1–2), 87-104. <https://doi.org/10.1016/j.epsl.2009.10.032>
- 1788 Jolivet, L., Menant, A., Sternai, P., Rabillard, A., Arbaret, L., Augier, R., Laurent, V., Beaudoin,
1789 A., Grasemann, B., Huet, B., Labrousse, L., & Le Pourhiet, L. (2015). The geological
1790 signature of a slab tear below the Aegean, *Tectonophysics*, 659, 166-182.
1791 <https://doi.org/10.1016/j.tecto.2015.08.004>
- 1792 Jolivet, L., & Patriat, M. (1999). Ductile extension and the formation of the Aegean Sea.
1793 *Geological Society, London, Special Publications*, 156, 427-456.
1794 <https://doi.org/10.1144/GSL.SP.1999.156.01.20>

- 1795 Jost, M.L., Knabenbauer, O., Cheng, J., & Harjes, H-P. (2002). Fault plane solutions of
1796 microearthquakes and small events in the Hellenic arc, *Tectonophysics*, 356 (1–3), 87-114.
1797 [https://doi.org/10.1016/S0040-1951\(02\)00378-5](https://doi.org/10.1016/S0040-1951(02)00378-5)
- 1798 Kadir, S., & Kart, F. (2009). The occurrence and origin of the söğüt kaolinite deposits in the
1799 Paleozoic Sarıcakaya granite-granodiorite complexes and overlying Neogene sediments
1800 (Bilecik, northwestern Turkey). *Clays and Clay Minerals*, 57, 311–329.
1801 <https://doi.org/10.1346/CCMN.2009.0570304>
- 1802 Kahle, H.-G., Cocard, M., Peter, Y., Geiger, A., Reilinger, R., Barka, A., & Veis, G. (2000).
1803 GPS-derived strain rate field within the boundary zones of the Eurasian, African, and
1804 Arabian Plates, *Journal of Geophysical Research*, 105(B10), 23353– 23370.
1805 <https://doi.org/10.1029/2000JB900238>
- 1806 Kaldova, J., Leichmann, J., Babek, O., & Melichar, R. (2003). Brunovistulian terrane (Central
1807 Europe) and Istanbul zone (NW Turkey): Late Proterozoic and Paleozoic tectonostratigraphic
1808 development and paleogeography. *Geologica Carpathica*, 54(3), 139-152.
- 1809 Karabulut, H., Paul, A., Özbakır, A.D., Ergün, T., & Şentürk, S. (2019). A new crustal model of
1810 the Anatolia–Aegean domain: evidence for the dominant role of isostasy in the support of the
1811 Anatolian plateau. *Geophysical Journal International*, 218(1), 57–73.
1812 <https://doi.org/10.1093/gji/ggz147>
- 1813 Karacık, Z., & Yılmaz, Y. (1998). Geology of the ignimbrites and the associated volcano-
1814 plutonic complex of the Ezine area, northwestern Anatolia. *Journal of Volcanology and*
1815 *Geothermal Research* 85(1–4), 251–264.
- 1816 Karacık, Z., Yılmaz, Y., Pearce, J.A., & Ece, Ö.I. (2008). Petrochemistry of the south Marmara
1817 granitoids, northwest Anatolia, Turkey. *Geologische Rundschau = International Journal of*
1818 *Earth Sciences* 97, 1181–1200. <https://doi.org/10.1007/s00531-007-0222-y>
- 1819 Karagianni, E.E., Panagiotopoulos, D.G., Panza, G.F., Suhadolc, P., Papazachos, C.B.,
1820 Papazachos, C.B., Kiratzi, A., Hatzfeld, D., Makropoulos, K., Priestley, K., & Vuan, A.
1821 (2002). Rayleigh wave group velocity tomography in the Aegean area. *Tectonophysics*,
1822 358(1–4), 187-209. [https://doi.org/10.1016/S0040-1951\(02\)00424-9](https://doi.org/10.1016/S0040-1951(02)00424-9)
- 1823 Karagianni, E.E., Papazachos, C.B., Panagiotopoulos, D.G., Suhadolc, P., Vuan, A., & Panza,
1824 G.F. (2005). Shear velocity structure in the Aegean area obtained by inversion of Rayleigh
1825 waves. *Geophysical Journal International*, 160(1), 127–143. [https://doi.org/10.1111/j.1365-](https://doi.org/10.1111/j.1365-246X.2005.02354.x)
1826 [246X.2005.02354.x](https://doi.org/10.1111/j.1365-246X.2005.02354.x)
- 1827 Karaoğlu, Ö., & Helvacı, C. (2014). Isotopic evidence for a transition from subduction to slab-
1828 tear related volcanism in western Anatolia, Turkey. *Lithos*, 192–195, 226-239.
1829 <https://doi.org/10.1016/j.lithos.2014.02.006>
- 1830 Karasözen, E., Nissen, E., Bergman, E. A., Johnson, K. L., & Walters, R. J. (2016). Normal
1831 faulting in the Simav graben of western Turkey reassessed with calibrated earthquake
1832 relocations, *Journal of Geophysical Research Solid Earth*, 121, 4553– 4574.
1833 <https://doi.org/10.1002/2016JB012828>
- 1834 Kastens, K.A. (1991). Rate of outward growth of the Mediterranean Ridge accretionary complex,
1835 *Tectonophysics*, 199, 25–50.
- 1836 Kastens, K.A., Nancy, A.B., & Cita, M.B. (1992). Progressive deformation of an evaporites-
1837 bearing accretionary complex: Sea-Marc I, SeaBeam and Piston core observations from the
1838 Mediterranean Ridge. *Marine Geophysical Research*, 14, 249-298.
- 1839 Katzir, Y., Avigad, D., Matthews, A., Garfunkel, Z. & Evans, B.W. (2000). Origin, HP/LT
1840 metamorphism and cooling of ophiolitic mélanges in southern Evia (NW Cyclades), Greece.

- 1841 Journal of Metamorphic Geology, 18, 699-718. <https://doi.org/10.1046/j.1525->
 1842 1314.2000.00281.x
- 1843 Kaya, O. (1981). Miocene reference section for the coastal parts of West Anatolia, Newsletters
 1844 on Stratigraphy, 10, 164-191.
- 1845 Keay, S., Lister, G., & Buick, I. (2001). The timing of partial melting, Barrovian metamorphism
 1846 and granite intrusion in the Naxos metamorphic core complex, Cyclades, Aegean Sea,
 1847 Greece, Tectonophysics, 342, 275-312. [https://doi.org/10.1016/S0040-1951\(01\)00168-8](https://doi.org/10.1016/S0040-1951(01)00168-8).
- 1848 Kempler, D., & Ben-Avraham, Z. (1987). The tectonic evolution of the Cyprean Arc, Annales
 1849 Tectonicae, 1, 58-71.
- 1850 Kendall, J.M., Stuart, G., Ebinger, C. et al. (2005). Magma-assisted rifting in Ethiopia. Nature,
 1851 433, 146–148. <https://doi.org/10.1038/nature03161>
- 1852 Kenyon, N.H., Belderson, R.H., & Stride, A.H. (1982). Detailed tectonic trends on the central
 1853 part of the Hellenic outer ridge and in the Hellenic trench system. Geological Society of
 1854 London, 10, 335-343.
- 1855 Ketin, I. (1948). Über die tektonisch-mechanischen Folgerungen aus den großen anatolischen
 1856 Erdbeben des letzten Dezenniums. Geologische Rundschau = International Journal of Earth
 1857 Sciences, 36, 77–83. <https://doi.org/10.1007/BF01791916>
- 1858 Kind, R., Eken, T., Tilmann, F., Sodoudi, F., Taymaz, T., Bulut, F., Yuan, X., Can, B., &
 1859 Schneider, F. (2015). Thickness of the lithosphere beneath Turkey and surroundings from S-
 1860 receiver functions, Solid Earth, 6, 971–984. <https://doi.org/10.5194/se-6-971-2015>
- 1861 Kinnaird, T., & Robertson, A. (2012). Tectonic and sedimentary response to subduction and
 1862 incipient continental collision in southern Cyprus, easternmost Mediterranean region.
 1863 Geological Society, London, Special Publications, 372, 585-614.
 1864 <https://doi.org/10.1144/SP372.10>
- 1865 Koçyiğit, A., & Deveci, Ş. (2007). A N-S-trending Active Extensional Structure, the Şuhut
 1866 (Afyon). Graben: Commencement Age of the Extensional Neotectonic Period in the Isparta
 1867 Angle, SW Turkey. Turkish Journal of Earth Sciences, 16, 391-416.
- 1868 Kohn, M.J., & Spear, F.S. (1991). Error propagation for barometers: 2. Application to rocks.
 1869 American Mineralogist, 76(1-2), 138–147
- 1870 Kokkalas, S., Paraskevas, X., Koukouvelas, I., & Doutsos, T. (2006). Postcollisional
 1871 contractional and extensional deformation in the Aegean region. Special Paper of the
 1872 Geological Society of America, 409, 97-123. <https://doi.org/10.1130/0-8137-2409-0.97>
- 1873 Komut, T., Gray, R., Pysklywec, R., & Göğüş, O.H. (2012). Mantle flow uplift of western
 1874 Anatolia and the Aegean: Interpretations from geophysical analyses and geodynamic
 1875 modeling. Journal of Geophysical Research, 117(B11412).
 1876 <https://doi.org/10.1029/2012JB009306>
- 1877 Konak, N. (1982). Geology of the Simav region. PhD thesis. Istanbul University, Faculty of
 1878 Earth Sciences, Department of Geological Engineering (in Turkish with English Abstract,
 1879 unpublished).
- 1880 Konak N. (2002). The Geological Map of Turkey, 2002. General Directorate of Mineral
 1881 Research and Exploration Izmir Area Map.
- 1882 Konak, N., Akdeniz, N., Öztürk, E.M. (1987). Geology of the south of Menderes Massif.
 1883 Correlation of Variscan and Pre-Variscan Events of the Alpine Mediterranean Mountain Belt.
 1884 Field Meeting, IGCP Project 5. Publications of the Mineral Research and Exploration
 1885 Institute of Turkey, 42–53.

- 1886 Kopf, A., Mascle, J., & Klaeschen, D. (2003). The Mediterranean Ridge: A mass balance across
1887 the fastest growing accretionary complex on Earth, *Journal of Geophysical Research*,
1888 108(B8), 2372. <https://doi.org/10.1029/2001JB000473>
- 1889 Koralay, O.E. (2015). Late Neoproterozoic granulite facies metamorphism in the Menderes
1890 Massif, Western Anatolia/Turkey: implication for the assembly of Gondwana, *Geodinamica*
1891 *Acta*, 27(4), 244-266. <https://doi.org/10.1080/09853111.2015.1014987>
- 1892 Koralay, O., Chen, F., Oberhansli, R., Wan, Y., & Candan, O. (2006). Age of Granulite Facies
1893 Metamorphism in the Menderes Massif, Western Anatolia / Turkey. 59th Geological Congres
1894 Turkey, Abstracts book, 28-29.
- 1895 Koralay, O., Satir, M., & Dora, O. (2001). Geochemical and geochronological evidence for Early
1896 Triassic calc-alkaline magmatism in the Menderes Massif, western Turkey. *Geologische*
1897 *Rundschau = International Journal of Earth Sciences*, 89, 822–835 (2001).
1898 <https://doi.org/10.1007/s005310000134>
- 1899 Kozur, H. W., & Göncüoğlu, M. C. (2000). Mean features of the pre-Variscan development in
1900 Turkey. *Acta Universitatis Carolinae-Geologica*, 42, 459–464.
- 1901 Kreemer, C., Chamot-Rooke, N., & Le Pichon, X. (2004). Constraints on the evolution and
1902 vertical coherency of deformation in the Northern Aegean from a comparison of geodetic,
1903 geologic and seismologic data, *Earth and Planetary Science Letters*, 225(3–4), 329-346.
1904 <https://doi.org/10.1016/j.epsl.2004.06.018>
- 1905 Kruckenberg, S. C., Vanderhaeghe, O., Ferré, E. C., Teyssier, C., & Whitney, D. L. (2011). Flow
1906 of partially molten crust and the internal dynamics of a migmatite dome, Naxos, Greece.
1907 *Tectonics*, 30, TC3001, <https://doi.org/10.1029/2010TC002751>
- 1908 Kürçer, A., Chatzipetros, A., Tutkun, S. Z., Pavlides, A., Ateş, Ö., & Valkaniotis, S. (2008). The
1909 Yenice–Gönen active fault (NW Turkey): Active tectonics and palaeoseismology,
1910 *Tectonophysics*, 453(1–4), 263-275. <https://doi.org/10.1016/j.tecto.2007.07.010>
- 1911 Lagos, M., Scherer, E.E., Tomaschek, F., Münker, C., Keiter, M., Berndt, J., & Ballhaus, C.
1912 (2007). High precision Lu–Hf geochronology of Eocene eclogite-facies rocks from Syros,
1913 Cyclades, Greece. *Chemical Geology*, 243(1–2), 16-35.
1914 <https://doi.org/10.1016/j.chemgeo.2007.04.008>
- 1915 Lamont, T. N., Searle, M. P., Gopon, P., Roberts, N. M. W., Wade, J., Palin, R. M., & Waters, D.
1916 J. (2020b). The Cycladic Blueschist Unit on Tinos, Greece: Cold NE subduction and SW
1917 directed extrusion of the Cycladic continental margin under the Tsiknias Ophiolite.
1918 *Tectonics*, 39, e2019TC005890. <https://doi.org/10.1029/2019TC005890>
- 1919 Lamont, T.N., Searle, M.P., Waters, D.J., Roberts, N.M.W., Palin, R.M., Smye, A., Dyck, B.,
1920 Gopon, P., Weller, O.M., St-Onge, M.R. (2020a). Compressional origin of the Naxos
1921 metamorphic core complex, Greece: Structure, petrography, and thermobarometry.
1922 *Geological Society of America Bulletin*, 132(1-2), 149–197.
1923 <https://doi.org/10.1130/B31978.1>
- 1924 Lanari, P. & Duesterhoeft, E. (2019). Modeling metamorphic rocks using equilibrium
1925 thermodynamics and internally consistent databases: Past achievements, problems and
1926 perspectives. *Journal of Petrology*, 60, 19–56. <https://doi.org/10.1093/petrology/egy105>
- 1927 Lanari, P., & Engi, M. (2017). Local bulk composition effects on metamorphic mineral
1928 assemblages. *Reviews in Mineralogy and Geochemistry*, 83, 55– 102.
1929 <https://doi.org/10.2138/rmg.2017.83.3>
- 1930 Laurent, V., Lanari, P., Nair, I., Augier, R., Lahfid, A., & Jolivet, L. (2018). Exhumation of
1931 eclogite and blueschist (Cyclades, Greece): Pressure–temperature evolution determined by

- 1932 thermobarometry and garnet equilibrium modelling. *Journal of Metamorphic Geology*, 36,
 1933 769– 798. <https://doi.org/10.1111/jmg.12309>
- 1934 Le Pichon, X., & Angelier, J. (1979). The Hellenic arc and trench system; A key to the
 1935 neotectonic evolution of the eastern Mediterranean area. *Tectonophysics*, 60, 1-42.
- 1936 Le Pichon X., & Angelier J. (1981). The Aegean Sea. *Philosophical Transactions of the Royal*
 1937 *Society of London. Series A., Mathematical and Physical Sciences*, 300, 357-372,
 1938 <http://doi.org/10.1098/rsta.1981.0069>
- 1939 Le Pichon X., Lybéris, N., Angelier, J., & Renard, V. (1982). Strain distribution over the East
 1940 Mediterranean Ridge: a synthesis incorporating new Sea-Beam Data. *Tectonophysics*, 86,
 1941 243-274. [https://doi.org/10.1016/0040-1951\(82\)90069-5](https://doi.org/10.1016/0040-1951(82)90069-5)
- 1942 Le Pichon, X., Chamot-Rooke, N., Lallemand, S., Noomen, R., & Veis, G. (1995). Geodetic
 1943 determination of the kinematics of central Greece with respect to Europe: Implications for
 1944 eastern Mediterranean tectonics. *Journal of Geophysical Research*, 100(B7), 12675– 12690.
 1945 <https://doi.org/10.1029/95JB00317>
- 1946 Le Pichon, X., Lallemand, S.J., Chamot-Rooke, N., Lemeur, D., & Pascal, G. (2002). The
 1947 Mediterranean Ridge backstop and the Hellenic nappes, *Marine Geology*, 186(1-2), 111-
 1948 125. [https://doi.org/10.1016/S0025-3227\(02\)00175-5](https://doi.org/10.1016/S0025-3227(02)00175-5)
- 1949 Le Pichon, X., Şengör, A.M.C., & İmren, C. (2019). A new approach to the opening of the
 1950 eastern Mediterranean Sea and the origin of the Hellenic subduction zone. Part 2: The
 1951 Hellenic subduction zone. *Canadian Journal of Earth Sciences*, 56(11), 1144-1162.
 1952 <https://doi.org/10.1139/cjes-2018-0315>
- 1953 Limonov, A.F., Woodside, J.M., Cita, M.B., & Ivanov, M.K. (1996). The Mediterranean Ridge
 1954 and related mud diapirism: a background. *Marine Geology*, 132(1-4), 7-19.
 1955 [https://doi.org/10.1016/0025-3227\(96\)00150-8](https://doi.org/10.1016/0025-3227(96)00150-8)
- 1956 Lips, A.W., Cassard, D., Sözbilir, H., Yilmaz, H., & Wijbrans, J. R. (2001). Multistage
 1957 exhumation of the Menderes Massif, western Anatolia (Turkey). *Geologische Rundschau =*
 1958 *International Journal of Earth Sciences*, 89(4), 781-792.
- 1959 Lips, A.L.W., Wijbrans, J. R., & White, S.H. (1999). New insights from $^{40}\text{Ar}/^{39}\text{Ar}$ laserprobe
 1960 dating of white mica fabrics from the Pelion Massif, Pelagonian Zone, internal Hellenides,
 1961 Greece; implications for the timing of metamorphic episodes and tectonic events in the
 1962 Aegean region. In B. Durand, L. Jolivet, F. Horvath, M. Seranne (Eds.), *The Mediterranean*
 1963 *basins; Tertiary extension within the Alpine Orogen. Geological Society Special*
 1964 *Publications*, 156, 457-474.
- 1965 Lister, G., Banga, G., & Feenstra, A. (1984). Metamorphic core complexes of Cordilleran type in
 1966 the Cyclades. Aegean Sea, Greece. *Geology*, 12, 221-225.
- 1967 Loos, S., & Reischmann, T. (1999). The evolution of the southern Menderes Massif in SW
 1968 Turkey as revealed by zircon datings. *Journal of the Geological Society of London* 156,
 1969 1021–1030.
- 1970 Lyberis, N. (1984). Tectonic evolution of the North Aegean trough, *Geological Society, London,*
 1971 *Special Publications*, 17, 709-725.
- 1972 Lykousis, V., Alexandri, S., Woodside, J., de Lange, G., Dählmann, A., Perissoratis, C.,
 1973 Heeschen, K., Ioakim, C., Sakellariou, D., Nomikou, P., Rousakis, G., Casas, D., Ballas, D.,
 1974 & Ercilla, G. (2009). Mud volcanoes and gas hydrates in the Anaximander mountains
 1975 (Eastern Mediterranean Sea). *Marine and Petroleum Geology*, 26(6), 854-872.
 1976 <https://doi.org/10.1016/j.marpetgeo.2008.05.002>

- 1977 Maggini, M., & Caputo, R. (2020). Sensitivity analysis for crustal rheological profiles: examples
1978 from the Aegean Region. *Annals of Geophysics*, 63(3), GT334. <http://dx.doi.org/10.4401/ag->
1979 8244
- 1980 Makris, J. (1978). The crust and upper mantle of the Aegean region from deep seismic
1981 soundings, *Tectonophysics*, 46(3–4), 269–284. [https://doi.org/10.1016/0040-1951\(78\)90207-](https://doi.org/10.1016/0040-1951(78)90207-)
1982 X
- 1983 Makris, J., Papoulia, J., & Yegorova T. (2013). A 3-D density model of Greece constrained by
1984 gravity and seismic data. *Geophysics Journal International*, 194, 1–17.
1985 <https://doi.org/10.1093/gji/ggt059>
- 1986 Malandri, C., Soukis, C., Maffione, M., Özkaptan, M., Vassilakis, E., Lozios, S., & van
1987 Hinsbergen, D.J.J. (2017). Vertical-axis rotations accommodated along the Mid-Cycladic
1988 lineament on Paros Island in the extensional heart of the Aegean orocline (Greece).
1989 *Lithosphere*, 9(1), 78–99. <https://doi.org/10.1130/L575>
- 1990 Mantovani, E., Albarello, D., Tamburelli, C., Babbucci, D., & Viti, M. (1997). Plate
1991 convergence, crustal delamination, extrusion tectonics and minimization of shortening work
1992 as main controlling factors of the recent Mediterranean deformation pattern. In E. Mantovani
1993 (Ed.), *Geodynamics of the Mediterranean region and its implications for seismic and*
1994 *volcanic risk. Annali di Geofisica (Vol. 40, pp. 611-643).*
- 1995 Marroni, M., Frassi, C., Göncüoğlu, M.C., Di Vincenzo, G., Pandolfi, L., Rebay, G., Ellero, A.,
1996 & Ottria, G. (2014). Late Jurassic amphibolite-facies metamorphism in the Intra-Pontide
1997 Suture Zone (Turkey): an eastward extension of the Vardar Ocean from the Balkans into
1998 Anatolia? *Journal of the Geological Society*, 171(5), 605–608.
1999 <https://doi.org/10.1144/jgs2013-104>
- 2000 Marsellos, A.E., Kidd, W.S.F., & Garver, J.I. (2010). Extension and exhumation of the HP/LT
2001 rocks in the Hellenic forearc ridge. *American Journal of Science* 310(1), 1-36.
2002 <https://doi.org/10.2475/01.2010.01>
- 2003 Matsuda, J., Senoh, K., Maruoka, T., Sato, H., & Mitropoulos P. (1999). K-Ar ages of the
2004 Aegean volcanic rocks and their implication for the arc-trench system. *Geochemical Journal*,
2005 33, 369-377. <https://doi.org/10.2343/geochemj.33.369>
- 2006 McClusky S. et al., (2000). Global positioning system constraints on plate kinematics and
2007 dynamics in the eastern Mediterranean and Caucasus. *Journal of Geophysical Research*,
2008 105(B3), 5695–5719. <https://doi.org/10.1029/1999JB900351>
- 2009 McKenzie, D. (1972). Active Tectonics of the Mediterranean Region. *Geophysical Journal of the*
2010 *Royal Astronomical Society*, 30, 109-185. <https://doi.org/10.1111/j.1365->
2011 246X.1972.tb02351.x
- 2012 McKenzie, D. (1978). Active tectonics of the Alpine-Himalayan belt: the Aegean Sea and
2013 surrounding regions. *Geophysics Journal of the Royal Astronomical Society*, 55, 217-254.
- 2014 McKenzie, D., & Bickle, M.J. (1988). The volume and composition of melt generated by
2015 extension of the lithosphere, *Journal of Petrology*, 29(3), 625-679.
2016 <https://doi.org/10.1093/petrology/29.3.625>
- 2017 Meier, T., Becker, D., Endrun, B., Rische, M., Bohnhoff, M., Stöckhert, B., & Harjes, H.-P.
2018 (2007). A model for the Hellenic subduction zone in the area of Crete based on seismological
2019 investigations. *Geological Society, London, Special Publications*, 291, 183-199.
2020 <https://doi.org/10.1144/SP291.9>
- 2021 Meighan, H. E., ten Brink, U., & Pulliam, J. (2013), Slab tears and intermediate-depth
2022 seismicity, *Geophysical Research Letters*, 40, 4244– 4248. <https://doi.org/10.1002/grl.50830>

- 2023 Menant, A., Jolivet, L., Tuduri, J., Loiselet, C., Bertrand, G., & Guillou-Frottier, L. (2018). 3D
 2024 subduction dynamics: A first-order parameter of the transition from copper- to gold-rich
 2025 deposits in the eastern Mediterranean region, *Ore Geology Reviews*, 94, 118-135.
 2026 <https://doi.org/10.1016/j.oregeorev.2018.01.023>
- 2027 Menant, A., Jolivet, L., & Vrielynck, B. (2016). Kinematic reconstructions and magmatic
 2028 evolution illuminating crustal and mantle dynamics of the eastern Mediterranean region since
 2029 the late Cretaceous. *Tectonophysics*, 675, 103-140.
 2030 <https://doi.org/10.1016/j.tecto.2016.03.007>
- 2031 Meng, J., Sinoplu, O., Zhou, Z., Tokay, B., Kusky, T., Bozkurt, E., Wang, L. (2021). Greece and
 2032 Turkey Shaken by African tectonic retreat. *Scientific Reports*, 11, 6486.
 2033 <https://doi.org/10.1038/s41598-021-86063-y>
- 2034 Mercier, J.L. (1981). Extensional-compressional tectonics associated with the Aegean Arc:
 2035 comparison with the Andean Cordillera of south Peru-north Bolivia. *Philosophical*
 2036 *Transactions of the Royal Society of London A (Mathematical and Physical Sciences)*,
 2037 300(1454), 337-355.
- 2038 Meulenkaamp, J.E., Wortel, M.J.R., van Wamel, W.A., Spakman, W., & Hoogerduyn, S.E.
 2039 (1988). On the Hellenic subduction zone and the geodynamic evolution of Crete since the
 2040 late middle Miocene. *Tectonophysics*, 146, 203-215.
- 2041 Moix, P., Beccalotto, L., Kozur, H.W., Hochard, C., Rosselet, F., & Stampfli, G.M. (2008). A
 2042 new classification of the Turkish terranes and sutures and its implication for the paleotectonic
 2043 history of the region. *Tectonophysics*, 451(1–4), 7-39.
 2044 <https://doi.org/10.1016/j.tecto.2007.11.044>
- 2045 Morris, A., & Anderson, M. (1996). First palaeomagnetic results from the Cycladic Massif,
 2046 Greece, and their implications for Miocene extension directions and tectonic models in the
 2047 Aegean, *Earth and Planetary Science Letters*, 142(3–4), 397-408.
 2048 [https://doi.org/10.1016/0012-821X\(96\)00114-8](https://doi.org/10.1016/0012-821X(96)00114-8)
- 2049 Morris, A., & Robertson, A.H.F. (1993). Miocene remagnetisation of carbonate platform and
 2050 Antalya Complex units within the Isparta angle, SW Turkey, *Tectonophysics*, 220(1–4), 243-
 2051 266. [https://doi.org/10.1016/0040-1951\(93\)90234-B](https://doi.org/10.1016/0040-1951(93)90234-B)
- 2052 Mouslopoulou, V., Nicol, A., Begg, J., Oncken, O., & Moreno, M. (2015). Clusters of
 2053 megathrust earthquakes on upper plate faults control the Eastern Mediterranean hazard.
 2054 *Geophysical Research Letters*, 42, 10,282–10,289. <https://doi.org/10.1002/2015GL066371>
- 2055 Moynihan, D.P., & Pattison, D.M. (2013). An automated method for the calculation of P-T paths
 2056 from garnet zoning, with application to metapelitic schist from the Kootenay Arc, British
 2057 Columbia, Canada. *Journal of Metamorphic Geology*, 31(5). 525-548.
- 2058 Müller, P., Kreuzer, H., Lenz, H., & Harre, W. (1979). Radiometric dating of two extrusives
 2059 from a Lower Pliocene Marine Section on Aegina Island, Greece. *Newsletters on*
 2060 *Stratigraphy*, 8(1), 70 – 78. <https://doi.org/10.1127/nos/8/1979/70>
- 2061 Mutlu, A.K., (2020). Seismicity, focal mechanism, and stress tensor analysis of the Simav
 2062 region, western Turkey. *Open Geosciences*, 12(1), 479-490. <https://doi.org/10.1515/geo-2020-0010>
- 2063
- 2064 Neubauer, F. (2002). Evolution of late Neoproterozoic to early Paleozoic tectonic elements in
 2065 Central and Southeast European Alpine mountain belts: review and synthesis,
 2066 *Tectonophysics*, 352(1-2), 87-103. [https://doi.org/10.1016/S0040-1951\(02\)00190-7](https://doi.org/10.1016/S0040-1951(02)00190-7)

- 2067 Nyst, M., & Thatcher, W. (2004). New constraints on the active tectonic deformation of the
 2068 Aegean. *Journal of Geophysical Research*, 109(11), 23.
 2069 <https://doi.org/10.1029/2003JB002830>
- 2070 Oberhänsli, R., Candan, O. Dora, O.O., & Dürr, H.S. (1997). Eclogites within the Menderes
 2071 crystalline complex, western Turkey, Anatolia. *Lithos*, 41, 135–150.
- 2072 Oberhänsli, R., Candan, O., & Wilke, F. (2010). Geochronological Evidence of Pan-African
 2073 Eclogites from the Central Menderes Massif, Turkey. *Turkish Journal of Earth Science*,
 2074 19(4), 431-447.
- 2075 Oelsner, F., Candan, O., & Oberhänsli, R. (1997). New evidence for the time of the high-grade
 2076 metamorphism in the Menderes Massif, SW-Turkey. *Terra Nostra*, 87. Jahrestagung der
 2077 Geologischen Vereinigung Fundamental geologic processes, 15
- 2078 Okal, E.A., Synolakis, C.E., Uslu, B., Kalligeris, N., & Voukouvalas, E. (2009). The 1956
 2079 earthquake and tsunami in Amorgos, Greece, *Geophysical Journal International*, 178(3),
 2080 1533–1554. <https://doi.org/10.1111/j.1365-246X.2009.04237.x>
- 2081 Okay, A.I. (1980a). Mineralogy, petrology and phase relations of glaucophane–lawsonite zone
 2082 blueschists from the Tavşanlı region, northwest Turkey. *Contributions to Mineralogy and
 2083 Petrology*, 72, 243–255.
- 2084 Okay, A.I. (1980b). Lawsonite zone blueschists and a sodic amphibole producing reaction in the
 2085 Tavşanlı region, northwest Turkey. *Contributions to Mineralogy and Petrology*, 75, 179–186.
- 2086 Okay, A.I. (1982). Incipient blueschist metamorphism and metasomatism in the Tavşanlı region,
 2087 northwest Turkey. *Contributions to Mineralogy and Petrology*, 79, 361–367.
- 2088 Okay, A.I. (1984). Distribution and characteristics of the north-west Turkish blueschists. In J.E.
 2089 Dixon, A.H.F. Robertson (Eds.), *The Geological Evolution of the Eastern Mediterranean*.
 2090 Geological Society of London Special Publications, 17, 455–466.
- 2091 Okay, A.I. (1986). High-pressure/low-temperature metamorphic rocks of Turkey. In B.W. Evans,
 2092 E.H. Brown (Eds.), *Blueschists and eclogites*. *Memoir-Geological Society of America*, 164,
 2093 333–347.
- 2094 Okay, A.I. (2001). Stratigraphic and metamorphic inversions in the central Menderes Massif; a
 2095 new structural model. *Geologische Rundschau = International Journal of Earth Sciences*,
 2096 89(4), 709727.
- 2097 Okay, A.I. (2008). *Geology of Turkey: A synopsis*. *Anschnitt*, 21, 19–42.
- 2098 Okay, A.I., Bozkurt, E., Satır, M., Yiğitbaş, E., Crowley, Q.G., Shang, C.K. (2008). Defining the
 2099 southern margin of Avalonia in the Pontides: Geochronological data from the Late
 2100 Proterozoic and Ordovician granitoids from NW Turkey, *Tectonophysics*, 461(1-4), 252-264.
 2101 <https://doi.org/10.1016/j.tecto.2008.02.004>
- 2102 Okay, A.I., & Kelley, S.P. (1994). Tectonic setting, petrology and geochronology of jadeite+
 2103 glaucophane and chloritoid+glaucophane schists from north-west Turkey. *Journal of
 2104 Metamorphic Geology*, 12, 455–466.
- 2105 Okay, A.I., Monod, O., & Monié, P. (2002). Triassic blueschists and eclogites from northwest
 2106 Turkey: vestiges of the Paleo-Tethyan subduction. *Lithos*, 64(3), 155-178.
 2107 [https://doi.org/10.1016/S0024-4937\(02\)00200-1](https://doi.org/10.1016/S0024-4937(02)00200-1)
- 2108 Okay, A.I., Ozcan, E., Cavazza, M., Okay, N., & Less, G. (2010). Basement types, Lower
 2109 Eocene Series, Upper Eocene olistostromes and the initiation of the Southern Thrace Basin,
 2110 NW Turkey. *Turkish Journal of Earth Sciences*, 19, 1–25. [https://doi.org/10.3906/yer-0902-](https://doi.org/10.3906/yer-0902-10)
 2111 10

- 2112 Okay A.I., & Satir, M. (2000). Coeval plutonism and metamorphism in a latest Oligocene
2113 metamorphic core complex in northwest Turkey. *Geological Magazine*, 137, 495-516.
- 2114 Okay, A.I., & Satir, M. (2006). Geochronology of Eocene plutonism and metamorphism in
2115 northwest Turkey: evidence for a possible magmatic arc. *Geodinamica Acta* 19, 251–265.
- 2116 Okay, A.I., Satir, M., Maluski, H., Siyako, M., Monie, P., Metzger, R., & Akyüz, S. (1996).
2117 Paleo- and Neo-Tethyan events in northwestern Turkey: geologic and geochronologic
2118 constraints. In T.M. Harrison (Ed.), *The Tectonic Evolution of Asia*. Cambridge University
2119 Press, Cambridge, pp. 420–441.
- 2120 Okay, A.I., Satir, M., & Siebel, W. (2006). Pre-Alpide orogenic events in the Eastern
2121 Mediterranean region. In D.G. Gee, R.A. Stephenson (Eds.), *European Lithosphere*
2122 *Dynamics*. Geological Society, London, *Memoirs*, 32, 389–405.
- 2123 Okay, A.I., Satir, M., Tuysuz, O., Akyuzm S., & Chen, F. (2001). The tectonics of Strandja
2124 Massif: late-Variscan and mid-Mesozoic deformation and metamorphism in the northern
2125 Aegean. *Geologische Rundschau = International Journal of Earth Sciences*, 90, 217–233.
- 2126 Okay, A.I., Siyako, M., & Burkan, K.A. (1991). Geology and tectonic evolution of the Biga
2127 Peninsula, northwest Turkey. *Bulletin of Technical University Istanbul*, 44, 191–256.
- 2128 Okay, A.I., Sunal, G., Sherlock, S., Altner, D., Tuysuz, O., Kylander-Clark, A.R.C., & Aygul,
2129 M. (2013). Early Cretaceous sedimentation and orogeny on the active margin of Eurasia;
2130 southern-central Pontides, Turkey. *Tectonics*, 32, 1247-1271.
- 2131 Okay, A.I., Sunal, G., Sherlock, S., Kylander-Clark, A. R. C., & Özcan, E. (2020). İzmir-Ankara
2132 suture as a Triassic to Cretaceous plate boundary—Data from central Anatolia. *Tectonics*, 39,
2133 e2019TC005849. <https://doi.org/10.1029/2019TC005849>
- 2134 Okay A.I., & Tüysüz, O. (1999). Tethyan sutures of northern Turkey. In B. Durand, L. Jolivet, F.
2135 Horváth, M. Séranne (Eds.), *The Mediterranean Basins: Tertiary Extension with the Alpine*
2136 *Orogen*. Geological Society, London, *Special Publications* (Vol. 156, pp. 475–515).
2137 <https://doi.org/10.1144/GSL.SP.1999.156.01.22>
- 2138 Okay, A.I., & Whitney, D.L. (2010). Blueschists, eclogites, ophiolites and suture zones in
2139 northwest Turkey: A review and a field excursion guide. *Ofioliti*, 35(2), 131-172.
- 2140 Okrusch, M., & Bröcker, M. (1990). Eclogites associated with high-grade blueschists in the
2141 Cyclades archipelago, Greece: a review. *European Journal of Mineralogy*, 2, 451–478.
- 2142 Oner, Z., Dilek, Y., & Kadioglu, Y.K. (2010). Geology and geochemistry of the synextensional
2143 Salihli granitoid in the Menderes core complex, western Anatolia, Turkey. *International*
2144 *Geology Review*, 52(2-3), 336-368. <https://doi.org/10.1080/00206810902815871>
- 2145 Oral B., Reilinger R.E., Nafi Toksöz M., King R.W., Aykut Barka A., Kinik I., & Lenk O.
2146 (1995). Global Positioning System offers evidence of plate motions in eastern Mediterranean.
2147 *EOS*, *Transactions American Geophysical Union*, 76, 9–11.
- 2148 Oygür, V., & Erler, A. (2000). Metalogeny of Simav graben [in Turkish]. *Geological Bulletin of*
2149 *Turkey*, 43(1), 7-19.
- 2150 Özbakır, A.D., Govers, R., & Fichtner, A. (2020). The Kefalonia Transform Fault: A STEP fault
2151 in the making. *Tectonophysics*, 787, 228471. <https://doi.org/10.1016/j.tecto.2020.228471>.
- 2152 Özbakır, A.D., Şengör, A.M.C., Wortel, M.J.R., & Govers, R. (2013). The Pliny–Strabo trench
2153 region: A large shear zone resulting from slab tearing. *Earth and Planetary Science Letters*,
2154 375, 188-195. <https://doi.org/10.1016/j.epsl.2013.05.025>
- 2155 Özcan, A., Göncüoğlu, M.C., Turhan, N., Uysal, S., Şentürk, K., & Işık, A. (1988). Late
2156 Paleozoic evolution of the Kütahya–Bolkardağ Belt. *METU Journal of Pure and Applied*
2157 *Science* 21 (1/3), 211–220.

- 2158 Özdamar, S., Billor, M.Z., Sunal, G., Esenli, F., & Roden, N.F. (2013). First U–Pb SHRIMP
2159 zircon and $^{40}\text{Ar}/^{39}\text{Ar}$ ages of metarhyolites from the Afyon–Bolkardag Zone, SW Turkey:
2160 Implications for the rifting and closure of the Neo-Tethys, *Gondwana Research*, 24(1), 377-
2161 391. <https://doi.org/10.1016/j.gr.2012.10.006>
- 2162 Ozgenc I., & Ilbeyli, N. (2008). Petrogenesis of the Late Cenozoic Egrigöz pluton in western
2163 Anatolia, Turkey: Implications for magma genesis and crustal processes, *International*
2164 *Geology Review*, 50(4), 375-391. <https://doi.org/10.2747/0020-6814.50.4.375>
- 2165 Özgül N. (1997). Stratigraphy of the tectono-stratigraphic units in the region Bozkır–Hadım–
2166 Taşkent (northern central Taurides). *Maden Tetkik ve Arama Dergisi*, 119, 113-174.
- 2167 Özkaymak, C., Sözbilir, H., & Uzel, B. (2013). Neogene-Quaternary evolution of the Manisa
2168 Basin: evidence for variation in the stress pattern of the Izmir-Balikesir Transfer Zone,
2169 western Anatolia. *Journal of Geodynamics*, 65, 117-35.
- 2170 Özsayin, E., & Dirik, K. (2007). Quaternary activity of the Cihanbeyli and Yeniceoba fault
2171 zones: İnönü-Eskiflehir fault system, central Anatolia. *Turkish Journal of Earth Sciences*, 16,
2172 471–492.
- 2173 Palin, R.M., Weller, O.M., Waters, D.J., & Dyck, B. (2016). Quantifying geological uncertainty
2174 in metamorphic phase equilibria modelling; a Monte Carlo assessment and implications for
2175 tectonic interpretations. *Geoscience Frontiers*, 7(4), 591-607.
2176 <https://doi.org/10.1016/j.gsf.2015.08.005>.
- 2177 Papadopoulos, G.A. (1997). On the interpretation of large-scale seismic tomography images in
2178 the Aegean sea area. *Annals of Geophysics*, 40(1), 37-42. <https://doi.org/10.4401/ag-3933>
- 2179 Papadopoulos, T., Wyss, M., & Schmerge, D.L. (1988). Earthquake locations in the western
2180 Hellenic arc relative to the plate boundary. *Bulletin of the Seismological Society of America*,
2181 78(3), 1222-1231.
- 2182 Papanikolaou, D. (1987). Tectonic evolution of the Cycladic blueschist belt (Aegean Sea,
2183 Greece). In: *Chemical Transport in Metasomatic Processes*, Helgeson, H. C., (Ed.), pp. 429–
2184 450. NATO ASI Series, Reidel, Dordrecht
- 2185 Papanikolaou, D.J., & Royden, L.H. (2007). Disruption of the Hellenic arc: Late Miocene
2186 extensional detachment faults and steep Pliocene-Quaternary normal faults—Or what
2187 happened at Corinth? *Tectonics*, 26, TC5003. <https://doi.org/10.1029/2006TC002007>
- 2188 Papazachos B.C., & Comninakis P.E. (1971). Geophysical and tectonic features of the Aegean
2189 Arc. *Journal of Geophysical Research*, 76(8517).
- 2190 Papazachos B.C., & Delibasis N.D. (1969). Tectonic stress field and seismic faulting in the area
2191 of Greece. *Tectonophysics*, 7, 231–255. [https://doi.org/10.1016/0040-1951\(69\)90069-9](https://doi.org/10.1016/0040-1951(69)90069-9)
- 2192 Papazachos B.C., Karakostas, V.G., Papazachos, C.B., & Scordilis, E.M. (2000). The geometry
2193 of the Wadati–Benioff zone and lithospheric kinematics in the Hellenic arc. *Tectonophysics*,
2194 319(4), 275-300. [https://doi.org/10.1016/S0040-1951\(99\)00299-1](https://doi.org/10.1016/S0040-1951(99)00299-1)
- 2195 Papazachos, C.B. (1999). Seismological and GPS evidence for the Aegean-Anatolia interaction.
2196 *Geophysical Research Letters*, 26(17), 2653-2656.
- 2197 Papazachos, C.B. (2019). Deep Structure and Active Tectonics of the South Aegean Volcanic
2198 Arc. *Elements*, 15(3), 153–158. <https://doi.org/10.2138/gselements.15.3.153>
- 2199 Parra, T., Vidal, O., & Jolivet, L. (2002). Relation between the intensity of deformation and
2200 retrogression in blueschist metapelites of Tinos Island (Greece) evidenced by chlorite–mica
2201 local equilibria. *Lithos*, 63(1–2), 41-66. [https://doi.org/10.1016/S0024-4937\(02\)00115-9](https://doi.org/10.1016/S0024-4937(02)00115-9)
- 2202 Pearce, F.D., Rondenay, S., Sachpazi, M., Charalampakis, M., & Royden, L. H. (2012). Seismic
2203 investigation of the transition from continental to oceanic subduction along the western

- 2204 Hellenic Subduction Zone. *Journal of Geophysical Research*, 117, B07306,
2205 <https://doi.org/10.1029/2011JB009023>
- 2206 Pe-Piper, G. (2000). Origin of S-type granites coeval with I-type granites in the Hellenic
2207 subduction system, Miocene of Naxos, Greece. *European Journal of Mineralogy*, 12(4), 859–
2208 875. <https://doi.org/10.1127/0935-1221/2000/0012-0859>
- 2209 Pe-Piper, G., & Piper, D.J.W. (2001). Late Cenozoic, post-collisional Aegean igneous rocks: Nd,
2210 Pb and Sr isotopic constraints on petrogenetic and tectonic models. *Geological Magazine*,
2211 138, 653–668.
- 2212 Pe-Piper, G., & Piper, D.J.W. (2005). The South Aegean active volcanic arc: relationships
2213 between magmatism and tectonics. In: Michael Fytikas, M., & Vougioukalakis, G.E. (Eds).
2214 *Developments in Volcanology*, 7, 113-133. [https://doi.org/10.1016/S1871-644X\(05\)80034-8](https://doi.org/10.1016/S1871-644X(05)80034-8)
- 2215 Pe-Piper, G., Piper, D.J.W., & Matarangas, S. (2002). Regional implications of geochemistry and
2216 style of emplacement of Miocene I-type diorite and granite, Delos, Cyclades, Greece. *Lithos*,
2217 60(1–2), 47-66. [https://doi.org/10.1016/S0024-4937\(01\)00068-8](https://doi.org/10.1016/S0024-4937(01)00068-8)
- 2218 Perkins, R.J., Cooper, F.J., Condon, D.J., Tattitch, B., & Naden, J. (2018). Post-collisional
2219 Cenozoic extension in the northern Aegean: The high-K to shoshonitic intrusive rocks of the
2220 Maronia Magmatic Corridor, northeastern Greece. *Lithosphere*, 10(5), 582–601.
2221 <https://doi.org/10.1130/L730.1>
- 2222 Peterek, A., & Schwarze, J. (2004). Architecture and Late Pliocene to recent evolution of outer-
2223 arc basins of the Hellenic subduction zone (south-central Crete, Greece). *Journal of*
2224 *Geodynamics*, 38(1), 19-55. <https://doi.org/10.1016/j.jog.2004.03.002>
- 2225 Philippon, M., Brun, J.-P., Gueydan, F., & Sokoutis, D. (2014). The interaction between Aegean
2226 back-arc extension and Anatolia escape since Middle Miocene, *Tectonophysics*, 631, 176-
2227 188. <https://doi.org/10.1016/j.tecto.2014.04.039>
- 2228 Piper, J.D.A., Gürsoy, H., Tatar, O., Beck, M.E., Rao, A., Koçbulut, F., & Mesci, B.L. (2010).
2229 Distributed neotectonic deformation in the Anatolides of Turkey: A paleomagnetic analysis.
2230 *Tectonophysics*, 488(1–4), 31–50. <https://doi.org/10.1016/j.tecto.2009.05.026>
- 2231 Platt, J.D., Brantut, N., & Rice, J.R. (2015). Strain localization driven by thermal decomposition
2232 during seismic shear. *Journal of Geophysical Research Solid Earth*, 120, 4405– 4433.
2233 <https://doi.org/10.1002/2014JB011493>
- 2234 Plunder, A., Agard, P., Chopin, C., & Okay, A.I. (2013). Geodynamics of the Tavşanlı zone,
2235 western Turkey: Insights into subduction/obduction processes, *Tectonophysics*, 608, 884-
2236 903. <https://doi.org/10.1016/j.tecto.2013.07.028>
- 2237 Portner, D.E., Delph, J.R., Biryol, C.B., Beck, S.L., Zandt, G., Özacar, A.A., Sandvol, E., &
2238 Türkelli, N. (2018). Subduction termination through progressive slab deformation across
2239 Eastern Mediterranean subduction zones from updated P-wave tomography beneath Anatolia.
2240 *Geosphere*, 14(3), 907–925. <https://doi.org/10.1130/GES01617.1>
- 2241 Pourteau, A., Candan, O., & Oberhänsli, R. (2010). High-pressure metasediments in central
2242 Turkey: Constraints on the Neotethyan closure history. *Tectonics*, 29, 1–18.
- 2243 Pourteau, A., Oberhänsli, R., Candan, O., Barrier, E., & Vrielynck, B. (2016). Neotethyan
2244 closure history of western Anatolia: a geodynamic discussion. *Geologische Rundschau =*
2245 *International Journal of Earth Sciences*, 105, 203–224. [https://doi.org/10.1007/s00531-015-](https://doi.org/10.1007/s00531-015-1226-7)
2246 [1226-7](https://doi.org/10.1007/s00531-015-1226-7)
- 2247 Pourteau, A., Sudo, M., Candan, O., Lanari, P., Vidal, O., & Oberhänsli, R. (2013). Neotethys
2248 closure history of Anatolia; insights from ⁴⁰Ar-³⁹Ar geochronology and P-T estimation in
2249 highpressure metasedimentary rocks. *Journal of Metamorphic Geology*, 31(6), 585-606.

- 2250 Rabayrol, F., & Hart, C.J.R. (2021). Petrogenetic and tectonic controls on magma fertility and
2251 the formation of post-subduction porphyry and epithermal mineralization along the late
2252 Cenozoic Anatolian Metallogenic Trend, Turkey. *Mineralium Deposita*, 56, 279–306.
2253 <https://doi.org/10.1007/s00126-020-00967-9>
- 2254 Rabayrol, F., Hart, C.J.R., & Creaser, R.A. (2019). Tectonic Triggers for Postsubduction
2255 Magmatic-Hydrothermal Gold Metallogeny in the Late Cenozoic Anatolian Metallogenic
2256 Trend, Turkey. *Economic Geology*, 114 (7), 1339–1363.
2257 <https://doi.org/10.5382/econgeo.4682>
- 2258 Rabillard, A., Jolivet, L., Arbaret, L., Bessière, E., Laurent, V., Menant, A., et al. (2018).
2259 Synextensional granitoids and detachment systems within Cycladic metamorphic core
2260 complexes (Aegean Sea, Greece): Toward a regional tectonomagmatic model. *Tectonics*, 37,
2261 2328– 2362. <https://doi.org/10.1029/2017TC004697>
- 2262 Ramseyer, K., Aldahan, A.A., Collini, B., & Landström, O. (1992). Petrological modifications in
2263 granitic rocks from the siljan impact structure: evidence from cathodoluminescence,
2264 *Tectonophysics*, 216(1–2), 195-204. [https://doi.org/10.1016/0040-1951\(92\)90166-4](https://doi.org/10.1016/0040-1951(92)90166-4)
- 2265 Régnier, J. L., Mezger, J. E., & Passchier, C. W. (2007). Metamorphism of Precambrian-
2266 Palaeozoic schists of the Menderes core series and contact relationships with Proterozoic
2267 orthogneisses of the western Cine Massif, Anatolide belt, western Turkey. *Geological*
2268 *Magazine*, 144(1), 67-104.
- 2269 Régnier, J. L., Ring, U., Passchier, C. W., Gessner, K., & Gungor, T. (2003). Contrasting
2270 metamorphic evolution of metasedimentary rocks from the Cine and Selimiye nappes in the
2271 Anatolide Belt, western Turkey. *Journal of Metamorphic Geology*, 21(7). 699-721
- 2272 Reilinger, R., et al. (2006). GPS constraints on continental deformation in the Africa-Arabia-
2273 Eurasia continental collision zone and implications for the dynamics of plate interactions,
2274 *Journal of Geophysical Research*, 111, B05411. <https://doi.org/10.1029/2005JB004051>
- 2275 Reilinger, R.E., McClusky, S.C., Oral, M. B., King, R. W., Toksoz, M. N., Barka, A. A., Kinik,
2276 I., Lenk, O., & Sanli, I. (1997). Global Positioning System measurements of present-day
2277 crustal movements in the Arabia-Africa-Eurasia plate collision zone. *Journal of Geophysical*
2278 *Research*, 102(B5), 9983– 9999. <https://doi.org/10.1029/96JB03736>
- 2279 Reilinger, R., McClusky, S., Paradissis, D., Ergintav, S., & Vernant, P. (2010). Geodetic
2280 constraints on the tectonic evolution of the Aegean region and strain accumulation along the
2281 Hellenic subduction zone. *Tectonophysics*, 488(1-4), 22-30.
2282 <https://doi.org/10.1016/j.tecto.2009.05.027>
- 2283 Rimmelé, G., Parra, T., Goffé, B., Oberhansli, R., Jolivet, L., & Candan, O. (2005). Exhumation
2284 paths of high-pressure–low-temperature metamorphic rocks from the Lycian Nappes and the
2285 Menderes Massif (SW Turkey): A multi-equilibrium approach. *Journal of Petrology*, 46,
2286 641– 669.
- 2287 Ring, U., Buchwaldt, R., & Gessner, K. (2004). Pb/Pb dating of garnet from the Anatolide belt in
2288 western Turkey: Regional implications and speculations on the role Anatolia played during
2289 the amalgamation of Gondwana. *Zeitschrift der Deutschen Geologischen Gesellschaft*,
2290 154(4), 537-555. <https://doi.org/10.1127/zdgg/154/2004/537>
- 2291 Ring, U., & Collins, A.S. (2005). U-Pb SIMS dating of synkinematic granites: timing of core-
2292 complex formation in the northern Anatolide belt of western Turkey. *Journal of the*
2293 *Geological Society, London*, 162, 289–298.

- 2294 Ring, U., Gessner, K., Gungor, T., & Passchier, C.W. (1999). The Menderes Massif of western
 2295 Turkey and the Cycladic Massif in the Aegean; do they really correlate? *Journal of the*
 2296 *Geological Society of London*, 156(1), 3-6.
- 2297 Ring, U., Johnson, C., Hetzel, R., & Gessner, K. (2003). Tectonic denudation of a Late
 2298 Cretaceous-Tertiary collisional belt; regionally symmetric cooling patterns and their relation
 2299 to extensional faults in the Anatolide Belt of western Turkey. *Geological Magazine*, 140(4),
 2300 421-441.
- 2301 Ring, U., Willner, A.P., & Lackmann, W. (2001). Stacking of nappes with different pressure-
 2302 temperature paths; an example from the Menderes Nappes of western Turkey. *American*
 2303 *Journal of Science*, 301(10), 912-944.
- 2304 Robertson, A.H.F., & Dixon, J.E. (1984). Introduction: aspects of the geological evolution of the
 2305 Eastern Mediterranean. Geological Society, London, Special Publications, 17, 1-74.
 2306 <https://doi.org/10.1144/GSL.SP.1984.017.01.02>
- 2307 Robertson, A.H.F., & Ustaömer, T. (2004). Tectonic evolution of the Intra-Pontide suture zone
 2308 in the Armutlu Peninsula, NW Turkey. *Tectonophysics*, 381(1–4), 175-209.
 2309 <https://doi.org/10.1016/j.tecto.2002.06.002>
- 2310 Robertson, A.H.F., & Ustaömer, T. (2009a). Formation of the Late Palaeozoic Konya Complex
 2311 and comparable units in southern Turkey by subduction–accretion processes: Implications for
 2312 the tectonic development of Tethys in the Eastern Mediterranean region. *Tectonophysics*,
 2313 473(1–2), 113-148. <https://doi.org/10.1016/j.tecto.2008.10.027>
- 2314 Robertson, A.H.F., & Ustaömer, T. (2009b). Upper Palaeozoic subduction/accretion processes in
 2315 the closure of Palaeotethys: Evidence from the Chios Melange (E Greece), the Karaburun
 2316 Melange (W Turkey), and the Teke Dere Unit (SW Turkey). *Sedimentary Geology*, 220(1-2),
 2317 29-59. <https://doi.org/10.1016/j.sedgeo.2009.06.005>
- 2318 Robertson, A.H.F., Clift, P.D., Degnan, P.J., & Jones, G. (1991). Paleogeographic and
 2319 paleotectonic evolution of eastern Mediterranean Neotethys. *Palaeogeography,*
 2320 *Palaeoclimatology, Palaeoecology*, 87, 289–343.
- 2321 Roche, V., Jolivet, L., Papanikolaou, D., Bozkurt, E., Menant, A., & Rimmelé, G. (2019). Slab
 2322 fragmentation beneath the Aegean/Anatolia transition zone: Insights from the tectonic and
 2323 metamorphic evolution of the Eastern Aegean region, *Tectonophysics*, 754, 101-129.
 2324 <https://doi.org/10.1016/j.tecto.2019.01.016>
- 2325 Roche, V., Conand, C., Jolivet, L., & Augier, R. (2018). Tectonic evolution of Leros Island
 2326 (Dodecanese, Greece) and correlations between the Aegean Domain and the Menderes
 2327 Massif. *Journal of the Geological Society, Geological Society of London*, 1, 836-849.
 2328 [ff10.1144/jgs2018-028ff.ffinsu-01795049](https://doi.org/10.1144/jgs2018-028ff.ffinsu-01795049)
- 2329 Roche, V., Sternai, P., Guillou-Frottier, L., Menant, A., Jolivet, L., Bouchot, V., & Gerya, T.
 2330 (2018). Emplacement of metamorphic core complexes and associated geothermal systems
 2331 controlled by slab dynamics. *Earth and Planetary Science Letters*, 498, 322-333.
 2332 <https://doi.org/10.1016/j.epsl.2018.06.043>
- 2333 Rosenbaum, G., Avigad, D., Sánchez-Gómez, M (2002). Coaxial flattening at deep levels of
 2334 orogenic belts: evidence from blueschists and eclogites on Syros and Sifnos (Cyclades,
 2335 Greece). *Journal of Structural Geology*, 24(9), 1451-1462. [https://doi.org/10.1016/S0191-](https://doi.org/10.1016/S0191-8141(01)00143-2)
 2336 [8141\(01\)00143-2](https://doi.org/10.1016/S0191-8141(01)00143-2).
- 2337 Rossetti, F., Riccardo Asti, R., Faccenna, C., Gerdes, A., Lucci, F., & Theyed, T. (2017).
 2338 Magmatism and crustal extension: Constraining activation of the ductile shearing along the
 2339 Gediz detachment, Menderes Massif (western Turkey). *Lithos*, 282–283, 145–162.

- 2340 Royden, L.H. (1993). The tectonic expression slab pull at continental convergent boundaries,
2341 *Tectonics*, 12(2), 303– 325. <https://doi.org/10.1029/92TC02248>
- 2342 Royden L.H., & Husson L. (2009). Subduction with Variations in Slab Buoyancy: Models and
2343 Application to the Banda and Apennine Systems. In S. Lallemand, F. Funiciello (Eds.),
2344 *Subduction Zone Geodynamics*. *Frontiers in Earth Sciences*. Springer, Berlin, Heidelberg.
2345 https://doi.org/10.1007/978-3-540-87974-9_2
- 2346 Royden, L.H., & Papanikolaou, D.J. (2011). Slab segmentation and late Cenozoic disruption of
2347 the Hellenic arc. *Geochemistry, Geophysics, Geosystems*, AGU and the Geochemical
2348 Society, 12(3), <https://doi.org/10.1029/2010GC003280>
- 2349 Sachpazi, M., Laigle, M., Charalampakis, M., Diaz, J., Kissling, E., Gesret, A., Becel, A., Flueh,
2350 E., Miles, P., & Hirn, A. (2016). Segmented Hellenic slab rollback driving Aegean
2351 deformation and seismicity, *Geophysical Research Letters*, 43, 65-658.
2352 <https://doi.org/10.1002/2015GL066818>
- 2353 Şahin, S.Y., Aysal, N., Güngör, Y., Peytcheva, I., & Neubauer, F. (2014). Geochemistry and U–
2354 Pb zircon geochronology of metagranites in Istranca (Strandja). Zone, NW Pontides, Turkey:
2355 Implications for the geodynamic evolution of Cadomian orogeny, *Gondwana Research*,
2356 26(2), 755-771. <https://doi.org/10.1016/j.gr.2013.07.011>
- 2357 Şahin, S.Y., Örgün, Y., & Güngör, Y. (2010). Mineral and whole-rock geochemistry of the
2358 Kestanol Granitoid (Ezine-Çanakale). and its mafic microgranular enclaves in
2359 Northwestern Anatolia: Evidence of felsic and mafic magma Interaction. *Turkish Journal of*
2360 *Earth Sciences*, 19(1), 101-122.
- 2361 Sakellariou, D., Mascle, J., & Lykousis, V. (2013). Strike slip tectonics and transtensional
2362 deformation in the Aegean region and the Hellenic arc: Preliminary results. *Bulletin of the*
2363 *Geological Society of Greece*, 47(2), 647-656. <https://doi.org/10.12681/bgsg.11098>
- 2364 Salaün, G., Pedersen, H.A., Paul, A., Farra, V., Karabulut, H., Hatzfeld, D., Papazachos, C.,
2365 Childs, D.M., Pequegnat, C., & SIMBAAD Team (2012). High-resolution surface wave
2366 tomography beneath the Aegean-Anatolia region: constraints on upper-mantle structure.
2367 *Geophysical Journal International*, 190(1), 406–420. [https://doi.org/10.1111/j.1365-](https://doi.org/10.1111/j.1365-246X.2012.05483.x)
2368 [246X.2012.05483.x](https://doi.org/10.1111/j.1365-246X.2012.05483.x)
- 2369 Saltogianni, V., Mouslopoulou, V., Oncken, O., Nicol, A., Gianniou, M., & Mertikas, S. (2020).
2370 Elastic fault interactions and earthquake rupture along the southern Hellenic subduction plate
2371 interface zone in Greece. *Geophysical Research Letters*, 47, e2019GL086604.
2372 <https://doi.org/10.1029/2019GL086604>
- 2373 Şaroğlu, F., Emre, Ö., & Kuşçu, İ. (1992). Active Fault Map of Turkey, General Directorate of
2374 Mineral Research and Exploration, Ankara, Turkey.
- 2375 Satir, M., & Friedrichsen, H. (1986). The origin and evolution of the Menderes Massif, W-
2376 Turkey; a rubidium/strontium and oxygen isotope study. *Geologische Rundschau =*
2377 *International Journal of Earth Sciences*, 75(3), 703-714.
- 2378 Satir, M., & Taubald, H. (2001). Hydrogen and oxygen isotope evidence for fluid-rock
2379 interactions in the Menderes Massif, western Turkey. *Geologische Rundschau = International*
2380 *Journal of Earth Sciences*, 89(4), 812-821.
- 2381 Saunders, A.D., & Tarney, J. (1984). Geochemical characteristics of basaltic volcanism within
2382 back-arc basins. *Geological Society, London, Special Publications*, 16, 59-76.
2383 <https://doi.org/10.1144/GSL.SP.1984.016.01.05>

- 2384 Saunders, P., Priestley, K., & Taymaz, T. (1998). Variations in the crustal structure beneath
2385 western Turkey. *Geophysical Journal International*, 134(2), 373–389.
2386 <https://doi.org/10.1046/j.1365-246x.1998.00571.x>
- 2387 Savostin, L.A., Sibuet, J.-C., Zonenshain, L.P., Le Pichon, X., & Roulet, M.-J. (1986). Kinematic
2388 evolution of the Tethys belt from the Atlantic ocean to the Pamirs since the Triassic,
2389 *Tectonophysics*, 123(1-4), 1-35. [https://doi.org/10.1016/0040-1951\(86\)90192-7](https://doi.org/10.1016/0040-1951(86)90192-7)
- 2390 Sayit, K., Marroni, M., Göncüoğlu, M.C., Pandolfi, L., Ellero, A., Ottria, G., & Frassi, C. (2016).
2391 Geological setting and geochemical signatures of the mafic rocks from the Intra-Pontide
2392 Suture Zone: implications for the geodynamic reconstruction of the Mesozoic Neotethys.
2393 *Geologische Rundschau = International Journal of Earth Sciences*, 105(1), 39-64.
- 2394 Schaarschmidt, A., Haase, K. M., Voudouris, P. C., Melfos, V., & Klemd, R. (2021). Migration
2395 of arc magmatism above mantle wedge diapirs with variable sediment contribution in the
2396 Aegean. *Geochemistry, Geophysics, Geosystems*, 22, e2020GC009565.
2397 <https://doi.org/10.1029/2020GC009565>
- 2398 Schellart, W., Freeman, J., Stegman, D. et al. (2007). Evolution and diversity of subduction
2399 zones controlled by slab width. *Nature*, 446, 308–311. <https://doi.org/10.1038/nature05615>
- 2400 Schildgen, T.F., Yıldırım, C., Cosentino, D., & Strecker, M.R. (2014). Linking slab break-off,
2401 Hellenic trench retreat, and uplift of the Central and Eastern Anatolian plateaus. *Earth-*
2402 *Science Reviews*, 128, 147-168. <https://doi.org/10.1016/j.earscirev.2013.11.006>.
- 2403 Schuiling, R.D. (1962). On petrology, age and structure of the Menderes migmatite complex
2404 (SW-Turkey). *Bulletin of the Mineral Research Exploration Institute of Turkey*, 58, 71-84.
- 2405 Searle, M., & Lamont, T. (2020a). Compressional origin of the Aegean Orogeny, Greece.
2406 *Geoscience Frontiers*, <https://doi.org/10.1016/j.gsf.2020.07.008>.
- 2407 Searle, M., & Lamont, T. (2020b). Compressional metamorphic core complexes, low-angle
2408 normal faults and extensional fabrics in compressional tectonic settings. *Geological*
2409 *Magazine*, 157(1), 101-118. doi:10.1017/S0016756819000207
- 2410 Seaton, N.C.A., Whitney, D.L., Teyssier, C., Toraman, E., & Heizler, M.T. (2009).
2411 Recrystallization of high-pressure marble (Sivrihisar, Turkey). *Tectonophysics*, 479(3–4),
2412 241–253. <https://doi.org/10.1016/j.tecto.2009.08.015>
- 2413 Seghedi I., Helvacı, C., & Pécskay, Z. (2015). Composite volcanoes in the south-eastern part of
2414 İzmir–Balıkesir Transfer Zone, Western Anatolia, Turkey. *Journal of Volcanology and*
2415 *Geothermal Research*, 291, 72-85. <https://doi.org/10.1016/j.jvolgeores.2014.12.019>
- 2416 Senel, M., & Aydal, N. (2002). Geological Map of Turkey (Izmir and Istanbul sheets): Maden
2417 Tetkik ve Arama Genel Mudurlugu, Eskisehir Yolu, Turkey, scale 1:500,000.
- 2418 Seman, S., Stockli, D.F., & Soukis, K. (2017). The provenance and internal structure of the
2419 Cycladic Blueschist Unit revealed by detrital zircon geochronology, Western Cyclades,
2420 Greece. *Tectonics*, 36, 1407–1429. <https://doi.org/10.1002/2016TC004378>.
- 2421 Şengör, A.M.C., Görür, N., & Şaroğlu, F. (1985). Strike-slip faulting and related basin formation
2422 in zones of tectonic escape: Turkey as a case study. In K.T. Biddle, N. Christie-Blick (Eds.),
2423 *Strike-slip Faulting and Basin Formation*, Society for Economic Paleontology Mineralogy
2424 *Special Publications*, 37, 227-264.
- 2425 Şengör, A.M.C., Satır, M., & Akkök, R. (1984). Timing of tectonic events in the Menderes
2426 Massif, Western Turkey. Implications for tectonic evolution and evidence for Pan-African
2427 basement in Turkey. *Tectonics*, 3, 693 -707.
- 2428 Şengör, A.M.C., & Yılmaz, Y. (1981). Tethyan evolution of Turkey: A plate tectonic approach.
2429 *Tectonophysics*, 75, 181–241.

- 2430 Şengör, A.M.C., & Zabcı, C. (2019). The North Anatolian Fault and the North Anatolian Shear
2431 Zone. In: Landscapes and Landforms of Turkey, Kuzucuoğlu, C., Çiner, A., Kazancı, N.
2432 (Eds.), Springer International Publishing, World Geomorphological Landscapes.
2433 https://doi.org/10.1007/978-3-030-03515-0_27
- 2434 Şengün, F., Yiğitbaş, E., & Tunç, E. (2011). Geology and tectonic emplacement of eclogite and
2435 blueschists, Biga Peninsula, northwest Turkey. *Turkish Journal of Earth Sciences*, 20(3),
2436 273-285.
- 2437 Seyitoğlu, G. (1997). Late Cenozoic tectono-sedimentary development of the Selendi and Usak-
2438 Gu're basins: a contribution to the discussion on the development of east-west and north
2439 trending basins in western Turkey. *Geological Magazine*, 134, 163–175.
- 2440 Seyitoğlu, G., & Scott, B.C. (1996). The cause of north-south extensional tectonics in western
2441 Turkey: Tectonic escape vs. back-arc spreading vs. orogenic collapse. *Journal of*
2442 *Geodynamics*, 22, 145 -153.
- 2443 Seyitoğlu, G., Işık, V., & Çemen, I. (2004). Complete Tertiary exhumation history of the
2444 Menderes Massif, western Turkey: an alternative working hypothesis. *Terra Nova*, 16, 358–
2445 363.
- 2446 Shaw, B., & Jackson, J. (2010). Earthquake mechanisms and active tectonics of the Hellenic
2447 subduction zone. *Geophysical Journal International*, 181, 966-984.
2448 <https://doi.org/10.1111/j.1365-246X.2010.04551.x>
- 2449 Sherlock, S., Kelley, S., Inger, S., Harris, N., & Okay, A. (1999). ^{40}Ar - ^{39}Ar and Rb-Sr
2450 geochronology of high-pressure metamorphism and exhumation history of the Tavşanlı
2451 Zone, NW Turkey. *Contributions to Mineralogy and Petrology*, 137, 46–58.
- 2452 Shin, T.A., Catlos, E.J., Jacob, L., & Black, K. (2013). Relationships between very high pressure
2453 subduction complex assemblages and intrusive granitoids in the Tavşanlı Zone, Sivrihisar
2454 Massif, central Anatolia. *Tectonophysics*, 595–596, 183–197.
- 2455 Snopek, K., Meier, T., Endrun, B., Bohnhoff, M., & Casten, U. (2007). Comparison of
2456 gravimetric and seismic constraints on the structure of the Aegean lithosphere in the forearc
2457 of the Hellenic subduction zone in the area of Crete. *Journal of Geodynamics*, 44(3–5), 173-
2458 185. <https://doi.org/10.1016/j.jog.2007.03.005>.
- 2459 Sodoudi, F., Kind, R., Hatzfeld, D., Priestley, K., Hanka, W., Wylegalla, K., Stavrakakis, G.,
2460 Vafidis, A., Harjes, H.-P., & Bohnhoff, M. (2006). Lithospheric structure of the Aegean
2461 obtained from P and S receiver functions, *Journal of Geophysical Research*, 111, B12307.
2462 <https://doi.org/10.1029/2005JB003932>
- 2463 Sokoutis, D., Brun, J.P., Van den Driessche, J., & Pavlides, S. (1993). A major Oligo-Miocene
2464 detachment in southern Rhodope controlling north Aegean extension. *Journal of the*
2465 *Geological Society*, 150, 243-246. <https://doi.org/10.1144/gsjgs.150.2.0243>
- 2466 Sözbilir, H., Sari, Uzel, B., Ökmen, S., & Akkiraz, S. (2011). Tectonic implications of
2467 transtensional supradetachment basin development in an extension-parallel transfer zone: the
2468 Kocacay Basin, western Anatolia, Turkey. *Basin Research*, 23, 423–448.
2469 <https://doi.org/10.1111/j.1365-2117.2010.00496.x>
- 2470 Spakman, W. (1990). Tomographic images of the upper mantle below central Europe and the
2471 Mediterranean. *Terra Nova*, 2, 542-553. <https://doi.org/10.1111/j.1365-3121.1990.tb00119.x>
- 2472 Spakman, W. (1991). Delay-time tomography of the upper mantle below Europe, the
2473 Mediterranean, and Asia Minor, *Geophysical Journal International*, 107(2), 309–332.
2474 <https://doi.org/10.1111/j.1365-246X.1991.tb00828.x>

- 2475 Spakman, W., Wortel, M.J.R., & Vlaar, N.J. (1988). The Hellenic subduction zone: A
2476 tomographic image and its geodynamic implications. *Geophysical Research Letters*, 15, 60–
2477 63.
- 2478 Spear, F. S., & Peacock, S. M. (1989). Metamorphic pressure-temperature-time paths. *American*
2479 *Geophysical Union Short Course in Geology*, 7, 102.
- 2480 Speciale, P.A., Catlos, E.J., Yıldız, G.O., Shin, T.A., & Black, K.N. (2012). Zircon ages from the
2481 Beypazarı granitoid pluton (north central Turkey): tectonic implications. *Geodinamica Acta*,
2482 25(3-4), 162-182. <https://doi.org/10.1080/09853111.2013.858955>.
- 2483 Stampfli, G.M. (2000). Tethyan oceans. In E. Bozkurt, J.A. Winchester, J.D.A. Piper (Eds.),
2484 *Tectonics and magmatism in Turkey and surrounding area*. Geological Society of London,
2485 *Special Publication*, London (Vol. 173, pp. 1-23).
- 2486 Stamfli, G.M., & Kozur, H.W. (2006). Europe from the Variscan to the Alpine cycles.
2487 *Geological Society, London, Memoirs*, 32, 57-82.
2488 <https://doi.org/10.1144/GSL.MEM.2006.032.01.04>
- 2489 Stanley, D., Knight, R., Stuckenrath, R., & Catani, G. (1978). High sedimentation rates and
2490 variable dispersal patterns in the western Hellenic Trench. *Nature*, 273, 110–113.
2491 <https://doi.org/10.1038/273110a0>
- 2492 Stouraiti, C., Baziotis, I., Asimow, P.D., & Downes, H. (2018). Geochemistry of the Serifos
2493 calc-alkaline granodiorite pluton, Greece: constraining the crust and mantle contributions to
2494 I-type granitoids. *Geologische Rundschau = International Journal of Earth Science* [1999],
2495 107, 1657–1688. <https://doi.org/10.1007/s00531-017-1565-7>
- 2496 Stouraiti, C., Mitropoulos, P., Tarney, J., Barreiro, B., McGrath, A.M., & Baltatzis, E. (2010).
2497 Geochemistry and petrogenesis of late Miocene granitoids, Cyclades, southern Aegean:
2498 Nature of source components. *Lithos*, 114(3–4), 337-352.
2499 <https://doi.org/10.1016/j.lithos.2009.09.010>.
- 2500 Suckale, J., Rondenay, S., Sachpazi, M., Charalampakis, M., Hosa, A., Royden, L.H. (2009).
2501 High-resolution seismic imaging of the western Hellenic subduction zone using teleseismic
2502 scattered waves, *Geophysical Journal International*, 178(2), 775–791.
2503 <https://doi.org/10.1111/j.1365-246X.2009.04170.x>
- 2504 Sümer, Ö, Uzel, B., Özkaymak, C., & Sözbilir, H. (2018). Kinematics of the Havran-Balıkesir
2505 Fault Zone and its implication on geodynamic evolution of the Southern Marmara Region,
2506 NW Anatolia, *Geodinamica Acta*, 30(1), 306-323.
2507 <https://doi.org/10.1080/09853111.2018.1540145>
- 2508 Sunal, G. (2012). Devonian magmatism in the western Sakarya Zone, Karacabey region, NW
2509 Turkey, *Geodinamica Acta*, 25(3-4), 183-201.
2510 <https://doi.org/10.1080/09853111.2013.858947>
- 2511 Symeou, V., Homberg, C., Nader, F. H., Darnault, R., Lecomte, J.-C., & Papadimitriou, N.
2512 (2018). Longitudinal and temporal evolution of the tectonic style along the Cyprus Arc
2513 system, assessed through 2-D reflection seismic interpretation. *Tectonics*, 37, 30– 47.
2514 <https://doi.org/10.1002/2017TC004667>
- 2515 Tan, O. (2013). The dense micro-earthquake activity at the boundary between the Anatolian and
2516 South Aegean microplates. *Journal of Geodynamics*, 65, 199-217.
- 2517 Tatar, O., Akpınar, Z., Gürsoy, H., Piper, J.D.A., Koçbulut, F., Mesci, B.L., Polat, A., & Roberts,
2518 A.P. (2013). Palaeomagnetic evidence for the neotectonic evolution of the Erzincan Basin,
2519 North Anatolian Fault Zone, Turkey, *Journal of Geodynamics*, 65, 244-258.
2520 <https://doi.org/10.1016/j.jog.2012.03.009>

- 2521 Taymaz, T., Jackson, J., & McKenzie, D. (1991). Active tectonics of the north and central
2522 Aegean Sea. *Geophysical Journal International*, 106(2), 433–490.
2523 <https://doi.org/10.1111/j.1365-246X.1991.tb03906.x>
- 2524 Tekin, U.K., Göncüoğlu, M.C., & Turhan, N. (2002). First evidence of Late Carnian radiolarians
2525 from the Izmir–Ankara suture complex, central Sakarya, Turkey: implications for the
2526 opening age of the Izmir–Ankara branch of Neo-Tethys. *Geobios*, 35(1), 127–135.
2527 [https://doi.org/10.1016/S0016-6995\(02\)00015-3](https://doi.org/10.1016/S0016-6995(02)00015-3)
- 2528 ten Veen, J. H., & Kleinspehn, K. L. (2002). Geodynamics along an increasingly curved
2529 convergent plate margin: Late Miocene-Pleistocene Rhodes, Greece, *Tectonics*, 21(3),
2530 <https://doi.org/10.1029/2001TC001287>
- 2531 Teyssier, C., & Whitney, D.L. (2002). Gneiss domes and orogeny. *Geology*, 30(12), 1139–1142.
2532 [https://doi.org/10.1130/0091-7613\(2002\)030<1139:GDAO>2.0.CO;2](https://doi.org/10.1130/0091-7613(2002)030<1139:GDAO>2.0.CO;2)
- 2533 Thomson, S.N., & Ring, U. (2006). Thermochronologic evaluation of post collision extension in
2534 the Anatolide orogen, western Turkey. *Tectonics* 25: TC3005.
- 2535 Tirel, C., Brun, J.-P., & Burov, E. (2008). Dynamics and structural development of metamorphic
2536 core complexes. *Journal of Geophysical Research*, 113, B04403.
2537 <http://dx.doi.org/10.1029/2005JB003694.fayon>
- 2538 Tirel, C., Gueydan, F., Tiberi, C., & Brun, J-P. (2004). Aegean crustal thickness inferred from
2539 gravity inversion. Geodynamical implications. *Earth and Planetary Science Letters*, 228(3–
2540 4), 267–280. <https://doi.org/10.1016/j.epsl.2004.10.023>.
- 2541 Tiryakioğlu, İ. (2015). Geodetic aspects of the 19 May 2011 Simav earthquake in Turkey.
2542 *Geomatics, Natural Hazards and Risk*, 6(1), 76–89.
2543 <https://doi.org/10.1080/19475705.2013.831379>
- 2544 Toker, C.E., Ulugergerli, E.U., Kilic, A.R. (2018). The Naşa intrusion (Western Anatolia) and its
2545 tectonic implication: A joint analyses of gravity and earthquake catalog data. *Bulletin of*
2546 *Mineral and Resource Exploration*, 156, 247–258.
- 2547 Toker, C.E., Ulugergerli, E.U., Kilic, A.R. (2019). Using non-derivative filters for the tectonic
2548 implications: A case study in Simav graben, western Turkey. *Symposium on the Application*
2549 *of Geophysics to Engineering and Environmental Problems 2019*. May 2019, 304–307.
- 2550 Tomaschek, F., Kennedy, A.K., Villa, I.M., Lagos, M., & Ballhaus, C. (2003). Zircons from
2551 Syros, Cyclades, Greece—Recrystallization and mobilization of zircon during high-pressure
2552 metamorphism. *Journal of Petrology*, 44(11), 1977–2002.
2553 <https://doi.org/10.1093/petrology/egg067>
- 2554 Topuz, G., Candan, O., Okay, A.I., von Quadt, A., Othman, M., Zack, T., & Wang, J. (2020).
2555 Silurian anorogenic basic and acidic magmatism in Northwest Turkey: Implications for the
2556 opening of the Paleo-Tethys, *Lithos*, 356–357, 105302.
2557 <https://doi.org/10.1016/j.lithos.2019.105302>
- 2558 Topuz, G., & Okay, A.I. (2017). Late Eocene–Early Oligocene two-mica granites in NW Turkey
2559 (the Uludağ Massif): Water-fluxed melting products of a mafic metagreywacke, *Lithos*, 268–
2560 271, 334–350. <https://doi.org/10.1016/j.lithos.2016.11.010>
- 2561 Ünay, E., Emre, Ö, Erkal, T., & Keçer, M. (2001). The rodent fauna from the Adapazarı pull-
2562 apart basin (NW Anatolia): its bearings on the age of the North Anatolian fault, *Geodinamica*
2563 *Acta*, 14(1-3), 169–175. <https://doi.org/10.1080/09853111.2001.11432442>
- 2564 Ustaömer, A.P., Mundil, R., & Renne, P.R. (2005). U/Pb and Pb/Pb zircon ages for arc-related
2565 intrusions of the Bolu Massif (W Pontides, NW Turkey): Evidence for Late Precambrian
2566 (Cadomian) age. *Terra Nova*, 17, 215–223. <https://doi.org/10.1111/j.1365-3121.2005.00594.x>

- 2567 Ustaömer, P.A., Ustaömer, T., Collins, A.S., & Robertson, A.H.F. (2009). Cadomian
2568 (Ediacaran–Cambrian). arc magmatism in the Bitlis Massif, SE Turkey: Magmatism along
2569 the developing northern margin of Gondwana, *Tectonophysics*, 473(1-2), 99-112.
2570 <https://doi.org/10.1016/j.tecto.2008.06.010>
- 2571 Ustaömer, P.A., Ustaömer, T., Gerdes, A., & Zulauf, G. (2011). Detrital zircon ages from a
2572 Lower Ordovician quartzite of the İstanbul exotic terrane (NW Turkey): evidence for
2573 Amazonian affinity. *Geologische Rundschau = International Journal of Earth Sciences*, 100,
2574 23–41 (2011). <https://doi.org/10.1007/s00531-009-0498-1>
- 2575 Ustaömer, P.A., Ustaömer, T., & Robertson, A.H.F. (2012). Ion probe U-Pb dating of the central
2576 Sakarya basement: A peri-Gondwana terrane intruded by Late Lower Carboniferous
2577 subduction/collision-related granitic rocks. *Turkish Journal of Earth Sciences*, 21, 905–932.
- 2578 Ustaömer, T., Ustaömer, P.A., Robertson, A.H.F., & Gerdes, A. (2016). Implications of U–Pb
2579 and Lu–Hf isotopic analysis of detrital zircons for the depositional age, provenance and
2580 tectonic setting of the Permian–Triassic Palaeotethyan Karakaya Complex, NW Turkey.
2581 *Geologische Rundschau = International Journal of Earth Sciences*, 105, 7–38.
2582 <https://doi.org/10.1007/s00531-015-1225-8>
- 2583 Ustaömer, T., Ustaömer, P.A., Robertson, A.H.F., & Gerdes, A. (2020). U-Pb-Hf isotopic data
2584 from detrital zircons in late Carboniferous and Mid-Late Triassic sandstones, and also
2585 Carboniferous granites from the Tauride and Anatolide continental units in S Turkey:
2586 implications for Tethyan palaeogeography. *International Geology Review*, 62(9), 1159-1186.
2587 <https://doi.org/10.1080/00206814.2019.1636415>
- 2588 Uzel, B., Kuiper, K., Sözbilir, H., Kaymakci, N., Langereis, C.G., & Boehm, K. (2020). Miocene
2589 geochronology and stratigraphy of western Anatolia: Insights from new Ar/Ar dataset.
2590 *Lithos*, 352–353, 105305. <https://doi.org/10.1016/j.lithos.2019.105305>
- 2591 Uzel, B., Sözbilir, H., C, Özkaymaka, Ç, Kaymakçı, N., & Langereis, C.G. (2013). Structural
2592 evidence for strike-slip deformation in the Izmir–Balıkesir transfer zone and consequences
2593 for late Cenozoic evolution of western Anatolia (Turkey). *Journal of Geodynamics*, 65, 94–
2594 116.
- 2595 Vanderhaeghe, O. (2004). Structural development of the Naxos migmatite dome. In: Whitney,
2596 D.L, Teyssier, C., & Siddoway, C.S. (Eds.), *Gneiss domes in orogeny*. Geological Society of
2597 America Special Paper, 380, 211–228.
- 2598 van der Meer, D.G., van Hinsbergen, D.J.J., & Spakman, W. (2018). Atlas of the underworld:
2599 Slab remnants in the mantle, their sinking history, and a new outlook on lower mantle
2600 viscosity. *Tectonophysics*, 723, 309-448. <https://doi.org/10.1016/j.tecto.2017.10.004>.
- 2601 van Hinsbergen, D.J.J., & Schmid, S.M. (2012). Map view restoration of Aegean–West
2602 Anatolian accretion and extension since the Eocene, *Tectonics*, 31, TC5005.
2603 <https://doi.org/10.1029/2012TC003132>
- 2604 van Hinsbergen, D.J.J., Hafkenscheid, E., Spakman, W., Meulenkaamp, J.E., & Wortel, R. (2005).
2605 Nappe stacking resulting from subduction of oceanic and continental lithosphere below
2606 Greece. *Geology*, 33 (4), 325–328. <https://doi.org/10.1130/G20878.1>
- 2607 van Hinsbergen, D.J.J., Kaymakçı, N., Spakman, W., & Torsvik, T.H. (2010). Reconciling the
2608 geological history of western Turkey with plate circuits and mantle tomography, *Earth and
2609 Planetary Science Letters*, 297(3–4), 674-686.
- 2610 Ventouzi, C., Papazachos, C., Hatzidimitriou, P., Papaioannou, C., & EGELADOS Working
2611 Group, (2018). Anelastic P- and S- upper mantle attenuation tomography of the southern

- 2612 Aegean Sea subduction area (Hellenic Arc) using intermediate-depth earthquake data.
 2613 *Geophysical Journal International*, 215(1), 635–658. <https://doi.org/10.1093/gji/ggy292>
 2614 von Blanckenburg, F., & Davies, J.H. (1995). Slab breakoff: A model for syncollisional
 2615 magmatism and tectonics in the Alps, *Tectonics*, 14(1), 120–131.
 2616 <https://doi.org/10.1029/94TC02051>
 2617 von Raumer, J.F., Stampfli, G.M., Arenas, R., & Martínez, S.S. (2015). Ediacaran to Cambrian
 2618 oceanic rocks of the Gondwana margin and their tectonic interpretation. *Geologische*
 2619 *Rundschau = International Journal of Earth Sciences*, 104, 1107–1121 (2015).
 2620 <https://doi.org/10.1007/s00531-015-1142-x>
 2621 Walcott, C.R.L., & White, S.H. (1998). Constraints on the kinematics of post-orogenic extension
 2622 imposed by stretching lineations in the Aegean region. *Tectonophysics*, 298, 155e175.
 2623 Wallace, L.M., Ellis, S., & Mann, P. (2008). Tectonic block rotation, arc curvature, and back-arc
 2624 rifting: insights into these processes in the Mediterranean and the western Pacific. *IOP*
 2625 *Conference Series: Earth and Environmental Sciences*, 2, 012010.
 2626 <https://doi.org/10.1088/1755-1307/2/1/012010>
 2627 Wallace, L.M., McCaffrey, R., Beavan, J., & Ellis, S. (2005). Rapid microplate rotations and
 2628 backarc rifting at the transition between collision and subduction. *Geology*, 33, 857–860.
 2629 <https://doi.org/10.1130/G21834.1>
 2630 Wei, W., Zhao, D., Wei, F., Bai, X., & Xu, J. (2019). Mantle dynamics of the Eastern
 2631 Mediterranean and Middle East: Constraints from P-wave anisotropic tomography.
 2632 *Geochemistry, Geophysics, Geosystems*, 20, 4505–4530.
 2633 <https://doi.org/10.1029/2019GC008512>
 2634 Westaway, R. (1994). Present-day kinematics of the Middle East and eastern Mediterranean,
 2635 *Journal of Geophysical Research*, 99(B6), 12071–12090. <https://doi.org/10.1029/94JB00335>
 2636 Westbrook, G.K., & Reston, T.J. (2002). The accretionary complex of the Mediterranean Ridge:
 2637 tectonics, fluid flow and the formation of brine lakes -an introduction to the special issue of
 2638 *Marine Geology*. *Marine Geology*, 186, 1-8.
 2639 Westerweel, J., Uzel, B., Langereis, C.G., Kaymakci, N., & Sözbilir, H. (2020). Paleomagnetism
 2640 of the Miocene Soma basin and its structural implications on the central sector of a crustal-
 2641 scale transfer zone in western Anatolia (Turkey). *Journal of Asian Earth Sciences*, 193,
 2642 <https://doi.org/10.1016/j.jseaes.2020.104305>
 2643 White, R.W., Powell, R., Holland, T.J.B., Johnson, T.E., & Green, E.C.R. (2014). New mineral
 2644 activity-composition relations for thermodynamic calculations in metapelitic systems.
 2645 *Journal of Metamorphic Geology*, 32, 261–286.
 2646 Whitney, D.L., & Bozkurt, E. (2002). Metamorphic history of the southern Menderes Massif,
 2647 western Turkey. *Geological Society of America Bulletin*, 114(7), 829-838.
 2648 Whitney, D.L., Teyssier, C., Rey, P., & Buck, W.R. (2013). Continental and oceanic core
 2649 complexes. *Geological Society of America Bulletin*, 125(3-4), 273–298.
 2650 <https://doi.org/10.1130/B30754.1>
 2651 Whitney, D.L., Teyssier, C., Toraman, E., Seaton, N.C.A., & Fayon, A.K. (2011). Metamorphic
 2652 and tectonic evolution of a structurally continuous blueschist-to-Barrovian terrane, Sivrihisar
 2653 Massif, Turkey. *Journal of Metamorphic Geology*, 29, 193–212.
 2654 Woodside, J.M., Mascle, J., Huguen, C., & Volkonskaia, A. (2000). The Rhodes Basin, a post-
 2655 Miocene tectonic trough. *Marine Geology*, 165, 1–12.

- 2656 Woodside, J.M., Mascle, J., Zitter, T.A.C., Limonov, A.F., Ergün, M., & Volkonskaia, A.
 2657 (2002). The Florence Rise, the Western Bend of the Cyprus Arc. *Marine Geology*, 185(3–4),
 2658 177-194. [https://doi.org/10.1016/S0025-3227\(02\)00194-9](https://doi.org/10.1016/S0025-3227(02)00194-9)
- 2659 Wortel, M.J.R., & Spakman, W. (1992). Structure and dynamics of subducted lithosphere in the
 2660 Mediterranean region. *Proceedings of the Koninklijke Nederlandse Akademie van*
 2661 *Wetenschappen*, 95(3), 325-347.
- 2662 Wortel, M.J.R., & Spakman, W. (2000). Subduction and slab detachment in the Mediterranean-
 2663 Carpathian region. *Science*, 290, 1910-1917. <https://doi.org/10.1126/science.290.5498.1910>
- 2664 Xypolias, P., & Alsop, G.I. (2014). Regional flow perturbation folding within an exhumation
 2665 channel: A case study from the Cycladic Blueschists. *Journal of Structural Geology*, 62, 141-
 2666 155, <https://doi.org/10.1016/j.jsg.2014.02.001>.
- 2667 Xypolias, P., Iliopoulos, I., Chatzaras, V., & Kokkalas, S. (2012). Subduction- and exhumation-
 2668 related structures in the Cycladic Blueschists: Insights from south Evia Island (Aegean
 2669 region, Greece), *Tectonics*, 31, TC2001, doi:10.1029/2011TC002946.
- 2670 Yiğitbaş, E., Kerrich, R., Yılmaz, Y., Elmas, A., & Xie, Q. (2004). Characteristics and
 2671 geochemistry of Precambrian ophiolites and related volcanics from the Istanbul–Zonguldak
 2672 Unit, Northwestern Anatolia, Turkey: following the missing chain of the Precambrian South
 2673 European suture zone to the east, *Precambrian Research*, 132(1-2), 179-206.
 2674 <https://doi.org/10.1016/j.precamres.2004.03.003>
- 2675 Yılmaz, Y., Genc, C., Karacik, Z., & Altunkaynak, S. (2001). Two contrasting magmatic
 2676 associations of NW Anatolia and their tectonic significance. *Journal of Geodynamics*, 31(3),
 2677 243-271.
- 2678 Yılmaz, Y., Tüysüz, O., Yiğitbas, E., Genç, C., & Şengör, A.M.C. (1997). Geology and tectonic
 2679 evolution of the Pontides. In A.G. Robinson (Ed.), *Regional and petroleum geology of the*
 2680 *Black Sea and surrounding region. American Association of Petroleum Geology Memiors*
 2681 (Vol. 68, pp. 183-226), Tulsa, Oklahoma.
- 2682 Yolsal-Çevikbilen, S., Taymaz, T., & Helvacı, C. (2014). Earthquake mechanisms in the Gulfs of
 2683 Gökova, Sığacık, Kuşadası, and the Simav Region (western Turkey): Neotectonics,
 2684 seismotectonics and geodynamic implications. *Tectonophysics*, 635, 100-124.
 2685 <https://doi.org/10.1016/j.tecto.2014.05.001>
- 2686 Yoshioka, T. (1996). Evolution of fault geometry and development of strike-slip basins:
 2687 Comparative studies on the transform zones in Turkey and Japan. *Island Arc*, 5, 407-419.
 2688 <https://doi.org/10.1111/j.1440-1738.1996.tb00162.x>
- 2689 Zhu, L., Mitchell, B. J., Akyol, N., Çemen, I., & Kekoali, K. (2006). Crustal thickness
 2690 variations in the Aegean region and implications for the extension of continental crust,
 2691 *Journal of Geophysical Research*, 111, B01301. <https://doi.org/10.1029/2005JB003770>
- 2692 Zitter, T.A.C., Woodside, J.M., & Mascle, J. (2003). The Anaximander Mountains: a clue to the
 2693 tectonics of southwest Anatolia. *Geological Journal*, 38, 375-394.
 2694 <https://doi.org/10.1002/gj.961>
- 2695 Zlatkin, O., Avigad, D., & Gerdes, A. (2013). Evolution and provenance of Neoproterozoic
 2696 basement and Lower Paleozoic siliciclastic cover of the Menderes Massif (western Taurides):
 2697 Coupled U–Pb–Hf zircon isotope geochemistry, *Gondwana Research*, 23(2), 682-700.
 2698 <https://doi.org/10.1016/j.gr.2012.05.006>
- 2699
 2700
 2701

2702 **Tables**
 2703 **Table 1.** Brief summary of some available ages from granitic assemblages that intrude the
 2704 Istanbul-Zonguldak Zone.

Granite	Location ^a	Approach	Age	Reference
Late Pan-African Granitoids or Cadomian Granitoids				
Karadere (Karabuk metagranite)	1	U-Pb zrn	924±4 620±2	Chen et al. (2002)
Karadere (Karabuk metatonalite)	1	U-Pb zrn	668±7 589±4	Chen et al. (2002)
Bolu (Tüllükiris)	2	U-Pb zrn	576±6	Ustaömer et al. (2005)
Bolu (Kapıkaya)	2	U-Pb zrn	565.3±1.9	Ustaömer et al. (2005)
Karadere (Karabuk)	1	Sm-Nd grt + wr	559±8	Chen et al. (2002)
Devonian				
Bolu	2		389, 200 273-255 229.6±4.2/2.3	Ustaömer et al. (2012)
Bolu	2	⁴⁰ Ar/ ³⁹ Ar or + hbl	381.1±7.1 93.3±2.0	Delaloye and Bingöl (2000)
Permo-Triassic				
Bolu (Sünnice Group)	2	²⁰⁷ Pb/ ²⁰⁶ Pb zrn	262±19	Ustaömer et al. (2005)
Sancaktepe	3	U-Pb zrn	257.3±1.5 253.7±1.8	Aysal et al. (2018)
Akyazi	4	⁴⁰ Ar/ ³⁹ Ar or + chl	240.4±4.9 86.1±2.0	Delaloye and Bingöl (2000)

2705 ^a See Figure 4 for locations of these granite bodies.

2706 ^b Abbreviations after Whitney and Evans (2010), wr= whole rock.

2707
 2708
 2709
 2710
 2711
 2712
 2713
 2714
 2715
 2716
 2717

2718 **Table 2.** Brief summary of some available ages from granitic assemblages that intrude the
 2719 Tavşanlı Zone.

Granite	Location	Approach	Age	Reference
Western Tavşanlı Zone: Suture Zone Granitoids				
Topuk	5	$^{40}\text{Ar}/^{39}\text{Ar}$ bt+kfs	63.5±2.8 43.0±2.7	Delaloye and Bingöl (2000)
Orhaneli	6	$^{40}\text{Ar}/^{39}\text{Ar}$ bt+hbl	57.9±1.2 31.4±0.6	Delaloye and Bingöl (2000)
Orhaneli	6	$^{40}\text{Ar}/^{39}\text{Ar}$ bt+hbl	52.6±0.4 52.4±1.4	Harris et al. (1994)
Topuk	5	$^{40}\text{Ar}/^{39}\text{Ar}$ bt+hbl	47.8±0.4	Harris et al. (1994)
Tepeldag (Gürgenyayla)	7	U-Pb zrn	44.9±0.2	Okay and Satir (2006)
Tepeldag (Gürgenyayla)	7	Rb-Sr bt	44.7±0.4	Okay and Satir (2006)
Eastern Tavşanlı Granitoids				
Kaymaz	9	U-Pb zrn	84.98±6.27	Gautier (1984)
Sivrihisar	10	U-Pb zrn	79.9±8.6 42.4±2.4	Shin et al. (2013)
Sarıkavak (Topkaya)	11	U-Pb zrn	65.9±3.8	Gautier (1984)
Sivrihisar	10	$^{40}\text{Ar}/^{39}\text{Ar}$ bt+hbl	62.9±1.3 56.8±0.2	Delaloye and Bingöl (2000)
Karacaören (Günyüzü)	10	$^{40}\text{Ar}/^{39}\text{Ar}$ hbl+bt	59.3±3.0 46.7±2.3	Demirbilek et al. (2018)
Tekoren granodiorite (Günyüzü)	10	$^{40}\text{Ar}/^{39}\text{Ar}$ hbl+bt	57.8±2.3 23.4±1.1	Demirbilek et al. (2018)
Dinek granodiorite (Günyüzü)	10	$^{40}\text{Ar}/^{39}\text{Ar}$ hbl+kfs	55.9±2.7 45.3±1.8	Demirbilek et al. (2018)
Kaymaz	9	$^{40}\text{Ar}/^{39}\text{Ar}$ kfs	54.0±2.1 52.1±2.0	Demirbilek et al. (2018)
Sivrihisar	10	$^{40}\text{Ar}/^{39}\text{Ar}$ hbl	53.2±2.1 44.7±1.7	Demirbilek et al. (2018)
Kadinicik (Günyüzü)	10	$^{40}\text{Ar}/^{39}\text{Ar}$ hbl+wr	52.8±2.4 45.7±1.7	Demirbilek et al. (2018)
Kaymaz	9	U-Pb zrn	44.3±4.9 19.4±4.5	Shin et al. (2013)
Sivrihisar (Kadnicik/Günyüzü)	10	Rb-Sr kfs+bt	47.0±1.6	Bağcı et al. (2012)
Sivrihisar	10	$^{40}\text{Ar}/^{39}\text{Ar}$ kfs	46.02±0.21	This study
Sivrihisar (Karacaören /Günyüzü)	10	Rb-Sr kfs+bt	40.8±3.0	Bağcı et al. (2012)

2720 ^a See Figure 4 for locations of these granite bodies.

2721 ^b Abbreviations after Whitney and Evans (2010), wr= whole rock.

2722

2723 **Table 3.** Brief summary of some available ages from granitic assemblages associated with
 2724 rocks between the Sakarya and Istanbul Zones.

Granite	Location	Approach	Age	Reference
Middle Eocene Magmatic Rocks (South Marmara Granitoids)				
Şevketiye	12	⁴⁰ Ar/ ³⁹ Ar ms	71.9±1.8	Delaloye and Bingöl (2000)
İlyasdağ tonalite (Marmara Island)	13	U-Pb zrn	56.7±0.8 46.1±0.7	Ustaömer et al. (2009)
Karabiga (Lapeski)	14	U-Pb xtm	52.7±1.9	Beccaletto et al. (2007)
Fistikli (Armutlu–Yalova)	15	⁴⁰ Ar/ ³⁹ Ar bt+ms	48.2±1.0 34.3±0.9	Delaloye and Bingöl (2000)
Karabiga (Lapeski)	14	⁴⁰ Ar/ ³⁹ Ar bt	45.3±0.9	Delaloye and Bingöl (2000)
Kapıdağ	16	⁴⁰ Ar/ ³⁹ Ar hbl+bt	42.2±1.0 38.2±0.8	Delaloye and Bingöl (2000)
Avsa Island	17	K-Ar bt	40.9±1.1	Karacık et al. (2008)

2725 ^a See Figure 4 for locations of these granite bodies.

2726 ^b Abbreviations after Whitney and Evans (2010), wr= whole rock.

2727

2728

2729

2730

2731

2732

2733

2734

2735

2736

2737

2738

2739

2740

2741

2742

2743

2744

2745

2746

2747

2748

2749

2750

2751

2752 **Table 4.** Brief summary of some available ages from granitic assemblages that intrude the
 2753 Central Sakarya Zone.

Granite	Location	Approach	Age	Reference
Late Pan-African Grantoids or Cadomian Granitoids				
Pamukova	18	U-Pb zrn	582.0±9.1 446.0±3.8	Okay et al. (2008)
Gemlik	15	U-Pb zrn	575.5±3.6 438.9±4.5	Okay et al. (2008)
Silurian-Devonian				
Saricakaya	19	U-Pb zrn	419±6 434±7 319±5 Ma	Topuz et al. (2020)
Carboniferous				
Inhisar	18	⁴⁰ Ar/ ³⁹ Ar ms+chl	348.5±6.6 213.5±4.4	Delaloye and Bingöl (2000)
Gevyke	20	U-Pb zrn	327±12	Ustaömer et al. (2016)
Söğüt granite (Saricakaya, Çaltı)	19	U-Pb zrn	327.2±1.9	Ustaömer et al. (2012)
Söğüt granite (Saricakaya, Küplü)	19	U-Pb zrn	324.3±1.3	Ustaömer et al. (2012)
Söğüt granite (Saricakaya, Borçak)	19	U-Pb zrn	319.5±1.1	Ustaömer et al. (2012)
Bilecik	21	⁴⁰ Ar/ ³⁹ Ar bt+or	312.1±6.0 233.5±4.8	Delaloye and Bingöl (2000)
Permian				
Söğüt granite	19	⁴⁰ Ar/ ³⁹ Ar bt	290±4.8	Okay et al. (2002)
Jurassic to Late Cretaceous				
Pamukova	18	⁴⁰ Ar/ ³⁹ Ar or +chl	168.2±3.5 123.0±2.8	Delaloye and Bingöl (2000)
Bey pazari	22	U-Pb zrn	95.4±4.2 70.5±3.4	Speciale et al. (2012)
Bey pazari	22	⁴⁰ Ar/ ³⁹ Ar bt	80.1±1.4 79.2±0.9	Okay et al. (2020)
Bey pazari	22	U-Pb zrn	74.8±0.4 73.2±1.4	Okay et al. (2020)
Bey pazari	22	⁴⁰ Ar/ ³⁹ Ar hbl	82.9±1.8 77.7±4.5	Delaloye and Bingöl (2000)

2754 ^a See Figure 4 for locations of these granite bodies.

2755 ^b Abbreviations after Whitney and Evans (2010), wr= whole rock.

2756
2757
2758
2759

2760 **Table 5.** Brief summary of some available ages from granitic assemblages that intrude the
 2761 Western Pontides Zone.

Granite	Location	Approach	Age	Reference
Proterozoic				
Karacabey (Tamsali)	23	U-Pb zrn (inherited cores)	1961.9±16.4 804±10.5	Aysal et al. (2012)
Evciler (Kazdağ)	24	U-Pb zrn	805, 286	Ustaomer et al. (2012)
Karaburun	25	U-Pb zrn	1800, 960, 380, 297	Ustaomer et al. (2012)
Devonian				
Güveylərbası (Çamlık-related)	26	U-Pb zrn	401.5±4.8	Aysal et al. (2012)
Karacabey (Tamsali)	23	U-Pb zrn	400.3±1.4	Aysal et al. (2012)
Eybek (Çamlık)	27	U-Pb zrn	397.5±1.4	Okay et al. (2006)
Karacabey (Tamsali)	23	Pb-Pb zrn	395.9±4.1 393.8±2.7	Sunal (2012)
Güveylərbası	26	U-Pb zrn	371.2 ± 2.3	Ustaömer et al. (2016)
Permo-Triassic				
Karacabey (Tamsali)	23	⁴⁰ Ar/ ³⁹ Ar bt	298.3±5.8 199.4±4.0	Delaloye and Bingöl (2000)
Karacabey (Tamsali)	23	⁴⁰ Ar/ ³⁹ Ar bt	304.5±3.7 223.0±7.5	Sunal (2012)
Kozak	28	U-Pb zrn	280.2±18.2 259.1±13.8	Black et al. (2013)
Karaburun	25	U-Pb zrn	244.4±1.5	Ustaomer et al. (2012)
Evciler	24	U-Pb zrn	229.6±0.60	Ustaomer et al. (2012)
Karacabey (Tamsali)	23	(U/Th)-He zrn	93.0±6.9	Sunal (2012)
Late Eocene-Oligocene-Miocene				
Kozak	28	⁴⁰ Ar/ ³⁹ Ar or +bt	37.6±3.3 19.5±0.4	Delaloye and Bingöl (2000)
Kozak	28	U-Pb zrn	36.5±6.6 17.1±0.7	Black et al. (2013)
Evciler (Kazdağ)	24	⁴⁰ Ar/ ³⁹ Ar chl+bt	36.0±1.4 26.4±0.6	Delaloye and Bingöl (2000)
Evciler (Kazdağ)	24	U-Pb zrn	24.8±4.6	Erdoğan et al. (2013)
Evciler (Kazdağ)	24	²⁰⁷ Pb- ²⁰⁶ Pb zrn	28.2±4.1 26.0±5.6	Erdoğan et al. (2013)
Uludağ	29	U-Pb zrn	34.71±0.34 28.24±0.39	Topuz and Okay (2017)
Eybek	27	U-Pb zrn	32.5±3.0 21.0±1.2	Black et al. (2013)
Katrandag	30	⁴⁰ Ar/ ³⁹ Ar hbl+chl	27.6±0.6 24.7±0.6	Delaloye and Bingöl (2000)

Uludağ	29	$^{40}\text{Ar}/^{39}\text{Ar}$ bt	26.8±0.8 24.7±0.7	Delaloye and Bingöl (2000)
Eybek	27	$^{40}\text{Ar}/^{39}\text{Ar}$ bt	26.6±0.8 21.1±0.4	Delaloye and Bingöl (2000)
Cataldag (Bozenkoy)	31	K-Ar bt+hbl	25.9±0.5 21.27±0.44	Boztuğ et al. (2009)
Evciler (Kazdağ)	24	Rb-Sr	25.0± 0.3	Birkle (1992) Genc (1998)
Kozak	28	K-Ar bt+hbl	23.0±3.8 14.6±1.0	Boztuğ et al. (2009)
Cataldag (Cataltepe)	31	K-Ar bt	22.0±0.3 21.7±0.1	Boztuğ et al. (2009)
Cataldag (Turfaldag)	31	K-Ar bt	21.9±0.6 21.2±0.6	Boztuğ et al. (2009)
Cataldag (Balicikhisar)	31	$^{40}\text{Ar}/^{39}\text{Ar}$ bt	20.8±0.4	Delaloye and Bingöl (2000)
Evciler (Kazdağ)	24	Rb-Sr	20.7±0.2 20.5±0.2	Okay and Satir (2000)

Younger South Marmara Granitoid Bodies

Yenice	32	$^{40}\text{Ar}/^{39}\text{Ar}$ hbl	47.6±1.4 20.1±1.1	Delaloye and Bingöl (2000)
Ilica	33	K-Ar hbl	37.9±0.1 25.6±1.9	Boztuğ et al. (2009)
Kizildam	34	K-Ar wr+bt	23.9±0.6 20.7±0.8	Karacık et al. (2008)
Danishment	35	K-Ar wr+bt	23.2±1.1 22.1±0.6	Karacık et al. (2008)
Ilica	33	K-Ar wr+bt	22.8±0.5 18.4±2.2	Karacık et al. (2008)
Sarioluk	36	K-Ar hbl	22.6±0.8	Karacık et al. (2008)
Yenice	32	K-Ar wr+bt	21.9±1.1 18.8±1.3	Karacık et al. (2008)
Davutlar	37	K-Ar wr+bt	21.6±0.6 18.4±1.1	Karacık et al. (2008)
Yeniköy	36	K-Ar wr	20.1±1.0	Karacık et al. (2008)

2762 ^a See Figure 4 for locations of these granite bodies.

2763 ^b Abbreviations after Whitney and Evans (2010), wr= whole rock.

2764
2765
2766
2767
2768
2769
2770
2771
2772

2773 **Table 6.** Brief summary of some available ages from granitic assemblages that intrude the
 2774 Rhodope-Strandja Zone (Biga Peninsula only).

Granite	Location	Approach	Age	Reference
Kuscayir	38	$^{40}\text{Ar}/^{39}\text{Ar}$ hbl	39.4±0.8 35.7±0.8	Delaloye and Bingöl (2000)
Kestanbol (Ezine)	39	U-Pb zrn	26.2±2.0	Black et al. (2013)
Kestanbol (Ezine)	39	$^{40}\text{Ar}/^{39}\text{Ar}$	18.8±1.0 22.21±0.07 21.22±0.09	Akal (2013)
Kestanbol (Ezine)	39	$^{40}\text{Ar}/^{39}\text{Ar}$ hbl	20.5±0.6	Delaloye and Bingöl (2000)

2775 ^a See Figure 4 for locations of these granite bodies.

2776 ^b Abbreviations after Whitney and Evans (2010), wr= whole rock.

2777
 2778
 2779
 2780
 2781
 2782
 2783
 2784
 2785
 2786
 2787
 2788
 2789
 2790
 2791
 2792
 2793
 2794
 2795
 2796
 2797
 2798
 2799
 2800
 2801
 2802
 2803
 2804
 2805
 2806
 2807
 2808
 2809

2810 **Table 7.** Brief summary of some available ages from granitic assemblages that intrude the
 2811 Afyon Zone.

Granite	Location	Approach	Age	Reference
Paleozoic Granitoids				
Sandıklı	39	U-Pb zrn	541±9	Gürsu et al. (2004)
Alaçam	41	U-Pb zrn	331.3±1.7	Candan et al. (2016)
(basement)			314.3±4.8	
Alaçam	41	U-Pb zrn	314.9±2.7	Hasözbek et al. (2010)
(basement)				
Late Eocene-Oligocene-Miocene				
Balkan (Muratdag)	40	⁴⁰ Ar/ ³⁹ Ar or	35.5±3.0	Delaloye and Bingöl (2000)
Koyunoba	42	U-Pb zrn	30.0±3.9	Catlos et al. (2012)
			14.7±2.6	
Alaçam	41	⁴⁰ Ar/ ³⁹ Ar or	27.1±1.0	Delaloye and Bingöl (2000)
			18.5±1.8	
Alaçam	41	U-Pb zrn	25.3±1.5	Catlos et al. (2012)
			17.5±0.9	
Egrigöz	43	⁴⁰ Ar/ ³⁹ Ar bt+or	24.6±1.4	Delaloye and Bingöl (2000)
			20.0±0.7	
Egrigöz	43	U-Pb zrn	24.1±1.3	Catlos et al. (2012)
			5.7±0.6	
Egrigöz	43	U-Pb zrn	20.7±0.6	Ring and Collins (2005)
Koyunoba	42	⁴⁰ Ar/ ³⁹ Ar kfs	20.37±0.03	Etzel et al. (2020)
Alaçam	41	Rb-Sr bt	20.17±0.20	Hasözbek et al. (2010)
			20.01±0.20	
Egrigöz	43	⁴⁰ Ar/ ³⁹ Ar ms	20.2±0.3	Işık et al. (2004)
Egrigöz	43	⁴⁰ Ar/ ³⁹ Ar kfs	20.02±0.03	Etzel et al. (2020)
Alaçam	41	U-Pb zrn	20.0±1.4	Hasözbek et al. (2010)
			20.3±3.3	
Baklan	40	⁴⁰ Ar/ ³⁹ Ar wr	19.3±0.9	Aydoğan et al. (2008)
			17.8±0.7	

2812 ^a See Figure 4 for locations of these granite bodies.

2813 ^b Abbreviations after Whitney and Evans (2010), wr= whole rock.

2814

2815

2816

2817

2818

2819

2820

2821

2822

2823

2824

2825 **Table 8.** Brief summary of some available ages from granitic assemblages that intrude the
 2826 Menderes Massif.

Granite	Location	Approach	Age	Reference
Late Pan-African Granitoids or Cadomian Granitoids				
Çine Massif metagranites	north of Milas	U-Pb zrn	662±3	Loos and Reichmann (1999)
			517±6	
Demirci–Gördes		²⁰⁷ Pb/ ²⁰⁶ Pb zrn	537.2 ±2.4 544.1 ± 4.3	Dannat (1997)
Ödemiş–Kiraz		²⁰⁷ Pb/ ²⁰⁶ Pb zrn	528.0 ±4.3	Dannat (1997)
			570 ± 5	
Çine Massif		²⁰⁷ Pb/ ²⁰⁶ Pb zrn	546.0±1.6 546.4± 0.8	Hetzl and Reischmann (1996)
			521±5	
Bafa Lake-Çine Massif		U-Pb zrn	572±7	Loos and Reischmann (1999)
			541±14	
Yatağan		²⁰⁷ Pb/ ²⁰⁶ Pb zrn	566±9	Gessner et al. (2004)
North of Yatağan		²⁰⁷ Pb/ ²⁰⁶ Pb zrn	555.5±6.2	Dora et al. (2005)
		U/Pb zrn	549±26	Dora et al. (2005)
Triassic				
Alasehir	44	U-Pb zrn	222.9±1.1	Ustaömer et al. (2016)
Late Eocene-Oligocene-Miocene				
Alasehir	44	⁴⁰ Ar/ ³⁹ Ar bt	36.4±2.2 16.6±0.3	Delaloye and Bingöl (2000)
Gordes	45	⁴⁰ Ar/ ³⁹ Ar ms	28.8±0.6	
Salihli	46	Th-Pb mnz	19.4±0.7 21.7±4.5	Catlos et al. (2010)
			9.6±1.6	
Turgutlu	47	Th-Pb mnz	19.2±5.1 11.5±0.8	Catlos et al. (2010)
Salihli	46	U-Pb ttn	17.07±0.2	
			14.36±0.3	Rossetti et al. (2017)
Turgutlu	47	U-Pb mnz	16.1±0.2	
Salihli	46	U-Pb aln	15.0±0.3	Glony and Hetzel (2007)
Turgutlu	47	⁴⁰ Ar/ ³⁹ Ar kfs	14.06±0.03	Glony and Hetzel (2007)
Salihli	46	⁴⁰ Ar/ ³⁹ Ar kfs	5.05±0.02	Etzel et al. (2020)
				Etzel et al. (2020)

2827 ^a See Figure 4 for locations of these granite bodies.

2828 ^b Abbreviations after Whitney and Evans (2010), wr= whole rock.

2829
2830
2831
2832
2833
2834

2835 **Table 9.** List of selected earthquake events along the Simav Fault and associated fault systems.

No. ^a	Event-ID ^b	Time (UTC)	Latitude	Longitude	Depth (km)	Rms ^c	Mag ^d
1	465625	2/18/2020 16:09	39.1015	27.8453	14.68	0.45	5.2
2	150860	12/10/2011 5:15	38.8625	30.1883	13.44	0.96	4.2
3	319040	12/2/2015 15:52	39.1495	28.154	10.85	0.4	4.0
4	132605	6/10/2011 22:47	39.0975	28.3405	34.38	0.85	4.7
5	160143	3/29/2012 10:13	38.6035	30.004	12.77	0.73	4.2
6	367059	3/29/2017 18:10	38.2003	31.0575	14.87	0.36	4.0
7	495401	2/9/2021 15:51	38.5965	31.6318	7.01	0.49	4.7
8	495403	2/9/2021 15:53	38.59	31.6495	4.61	0.41	4.1
9	367501	4/3/2017 9:05	38.4801	31.7975	13.84	0.25	4.0
10	136512	7/27/2011 9:58	38.3278	31.8802	17.79	0.33	4.8
11	128573	5/19/2011 20:15	39.1328	29.082	24.46	0.49	5.7
12	128577	5/19/2011 20:25	39.1442	29.1078	7.00	0.44	4.6
13	128603	5/19/2011 21:12	39.113	29.0377	7.74	0.57	4.8
14	128672	5/20/2011 0:13	39.1413	29.1065	16.92	0.62	4.1
15	128701	5/20/2011 0:58	39.1147	29.0837	17.38	0.78	4.3
16	129252	5/21/2011 21:43	39.1037	29.0513	7.00	0.11	4.0
17	129791	5/24/2011 2:55	39.1013	29.0217	16.80	0.45	4.2
18	131192	5/30/2011 22:03	39.1567	29.0112	15.29	0.85	4.0
19	132022	6/5/2011 21:29	39.143	29.095	6.98	0.55	4.0
20	134386	6/29/2011 11:40	39.1232	29.0032	9.28	0.75	4.0
21	135896	7/19/2011 21:16	39.1048	29.093	17.66	0.67	4.1
22	138300	8/25/2011 4:19	39.139	29.0957	22.54	0.77	4.3
23	161414	4/16/2012 10:10	39.1227	29.1222	6.90	0.5	4.7
24	161595	4/17/2012 20:45	39.1468	29.1142	6.99	0.58	4.5
25	161902	4/20/2012 16:39	39.1525	29.0975	20.59	0.81	4.4
26	177315	10/30/2012 0:12	39.1385	29.1787	21.35	0.76	4.1
27	188611	3/12/2013 20:47	39.1203	29.0583	12.81	0.52	4.1
28	197002	6/9/2013 14:18	39.1392	29.022	15.61	0.68	4.1
29	234353	7/15/2014 12:25	39.13	29.0041	9.92	0.32	4.1
30	309933	9/3/2015 8:23	39.1226	29.1225	10.24	0.49	4.1

2836 a. See Figure 7A for events 1-10 and Figure 7B for events 11-30.

2837 b. Parameters were extracted from <https://depem.afad.gov.tr/depemkatalogu> 1900-20XX
2838 Earthquake Catalog ($M \geq 4.0$), Turkish Ministry of the Interior, Disaster and Emergency
2839 Management Presidency, Earthquake Department (AFAD).

2840 c. Rms= root-mean-square (RMS) travel time residual in seconds.

2841 d. All magnitudes are ML (original magnitude relationship defined for local earthquakes),
2842 except events 1, 3, 6, 7, 9, 29, and 30, which are moment magnitudes (M_w).

2843

2844

2845

2846

2847 **Table 10.** List of selected earthquake events along the Aegean-Anatolian plate boundary.

No. ^a	Event-ID ^b	Time (UTC)	Latitude	Longitude	Depth (km)	Rms ^c	Mag ^d
1	199626	7/12/2013 0:36	40.3738	25.946	27.85	0.45	4.3
2	201060	7/30/2013 5:33	40.3028	25.7902	20.01	0.52	5.3
3	184151	1/19/2013 19:26	39.6382	25.6795	20.91	0.5	4.2
4	360268	2/6/2017 10:58	39.5275	26.1373	9.83	0.21	5.3
5	183497	1/12/2013 13:47	39.6447	25.6733	6.89	0.8	4.0
6	155511	1/29/2012 21:03	38.7387	26.0447	32.39	0.68	4.2
7	101387	3/26/2010 18:35	38.1457	26.177	24.26	0.2	4.7
8	426091	11/27/2018 23:16	36.7565	25.877	16.15	0.62	4.4
9	426096	11/27/2018 23:46	36.6493	25.4535	5.95	0.75	4.1
10	418888	8/19/2018 5:46	35.8861	26.0695	28.49	0.77	4.9
11	309516	8/27/2015 0:25	34.7751	25.8068	7.06	0.52	4.5
12	472843	5/2/2020 16:44	34.5521	25.8181	6.76	0.56	5.1
13	472824	5/2/2020 13:45	34.2973	25.7371	9.63	0.98	5.2
14	472819	5/2/2020 12:51	34.2226	25.8253	6.65	0.98	6.4
15	472825	5/2/2020 13:33	33.9548	26.0141	6.5	0.96	4.6
16	472827	5/2/2020 14:21	34.2123	26.232	5.86	0.93	4.8
17	294406	4/16/2015 18:07	34.8643	26.7275	12.34	0.62	5.9
18	169403	7/4/2012 23:46	35.1613	26.9993	34.09	0.35	5.0
19	293183	3/27/2015 23:34	35.7295	26.576	56.13	0.47	5.0
20	507881	8/1/2021 4:31	36.3843	27.0805	10.86	0.17	5.5
21	187555	2/27/2013 22:05	36.7298	26.5115	140.27	0.43	4.1
22	417483	7/26/2018 8:17	37.6546	26.6698	4.5	0.52	4.5
23	483762	10/30/2020 11:51	37.879	26.703	14.9	1	6.6
24	375576	6/12/2017 12:28	38.8486	26.313	15.96	0.28	6.2
25	431610	2/20/2019 18:23	39.6011	26.4261	5.8	0.37	5.0
26	411695	5/3/2018 2:04	39.967	26.8993	10.39	0.35	4.3
27	284923	12/16/2014 9:02	40.1298	27.0845	17.35	0.29	4.3
28	115792	11/3/2010 2:51	40.3997	26.3147	28.9	0.59	5.1
29	199626	7/12/2013 0:36	40.3738	25.946	27.85	0.45	4.3

2848 a. See Figure 11 for events.

2849 b. Parameters were extracted from <https://depem.afad.gov.tr/depemkatalogu> 1900-20XX
2850 Earthquake Catalog ($M \geq 4.0$), Turkish Ministry of the Interior, Disaster and Emergency
2851 Management Presidency, Earthquake Department (AFAD).

2852 c. Rms= root-mean-square (RMS) travel time residual in seconds.

2853 d. All magnitudes are ML (original magnitude relationship defined for local earthquakes),
2854 except events 4, 8-14, 16, 17, 19, 20, 23-28, which are moment magnitudes (M_w).

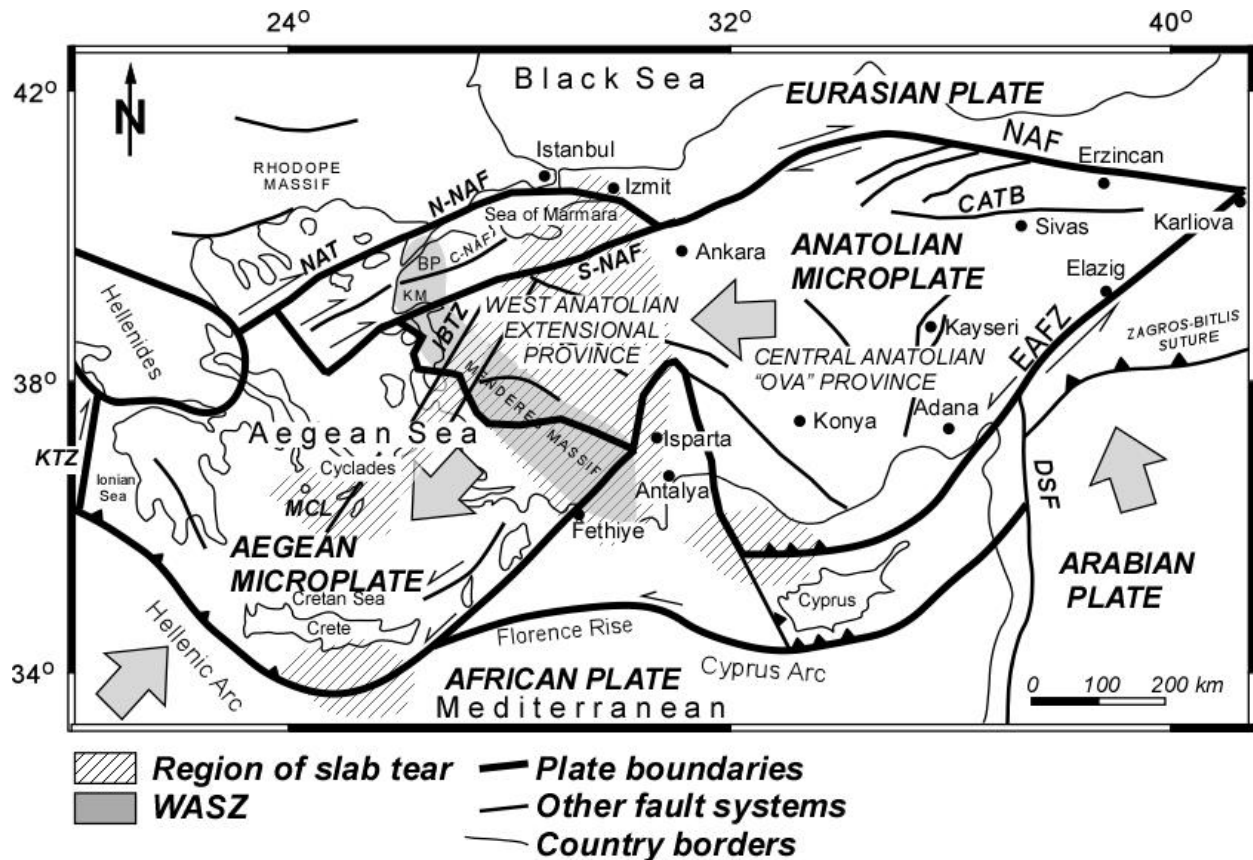


Figure 1. Tectonic map of the Aegean and Anatolian microplates. Plate boundaries after McClusky et al. (2000), Nyst & Thatcher (2004), Piper et al. (2010), Harrison et al. (2012), and Tan (2013). Only some major fault systems are labeled. NAF= North Anatolian Fault, EAFZ= East Anatolian Fault Zone, CATB = Central Anatolian Thrust Belt, DSF = Dead Sea Fault; KTZ = Kephallonia Transform Zone; MCL= Mid-Cycladic lineament; İBTZ= Izmir-Balıkesir transfer zone; NAT= North Aegean Trough; NAF = North Anatolian Fault (N-, northern, C- central, and S- southern segments); KM= Kazdağ Massif. Region of slab tear in western Turkey and the Aegean after Jolivet et al. (2015), near Crete (Özbakır et al., 2013), Cyprus (Woodside et al., 2002), and between the Aegean domain and the Menderes Massif (Roche et al., 2019). Boundaries between Central and Western Anatolia after Şengör et al. (1985).

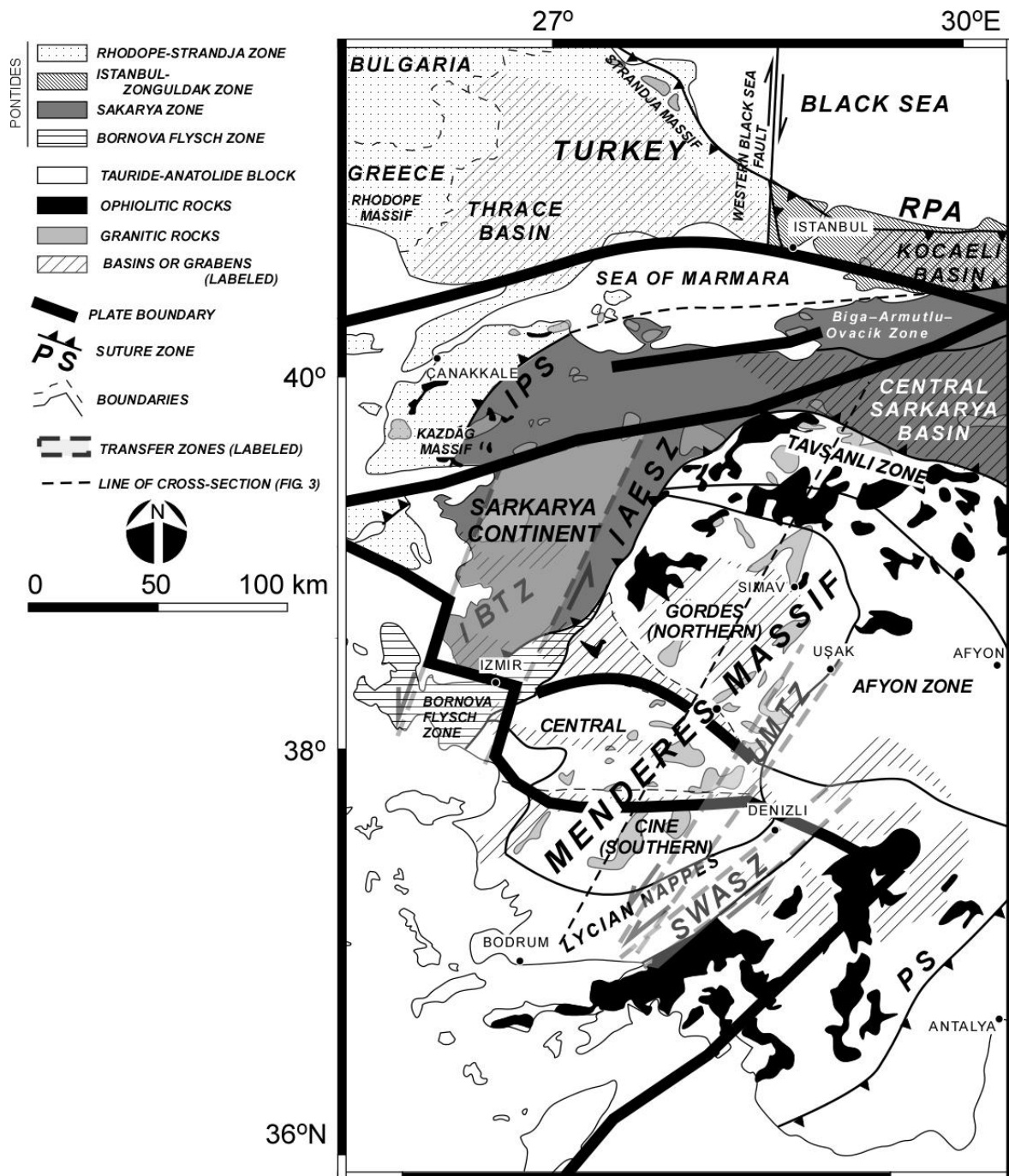


Figure 2. Geological map of Western Anatolia focusing on the ophiolite and granite assemblages along the boundary between the Aegean and Anatolia microplates. Plate boundary after Nyst & Thatcher (2004). Terrane boundaries, major fault systems, and transfer zones after Okay (2008), Akbayram et al. (2016), Oner et al. (2010), and Karaoğlu & Helvacı (2014). Abbreviations: RPA= Rhodope-Pontide Arc; İBTZ = Izmir–Balıkesir Transfer Zone (also sometimes referred to as the Western Anatolia Transfer Zone, Gessner et al., 2013; 2017); SWASZ= South West Anatolian Shear Zone; IPS= Intra-Pontide suture zone; IAESZ = Izmir-Ankara-Erzincan suture zone; PS = Pamphylian suture zone; UMTZ= Uşak-Muğla Transfer Zone.

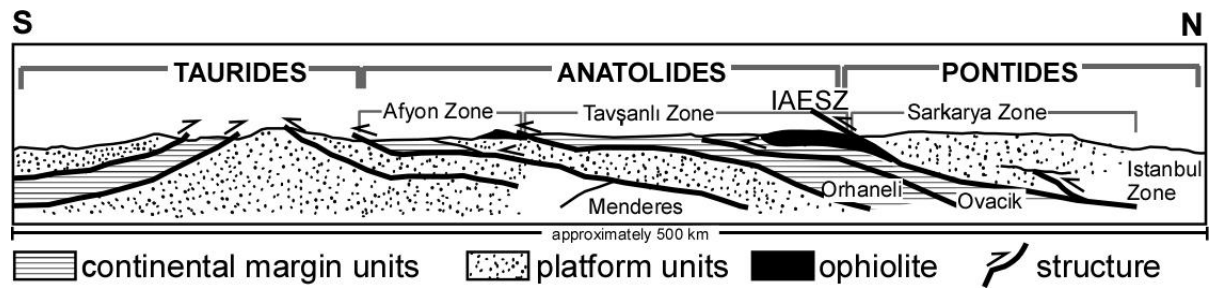


Figure 3. North-south generalized cross-section across western Turkey after Okay (1986) and Shin et al. (2013). IAESZ=İzmir-Ankara-Erzincan Suture Zone. See Figure 2 for the approximate line of section on the geological map.

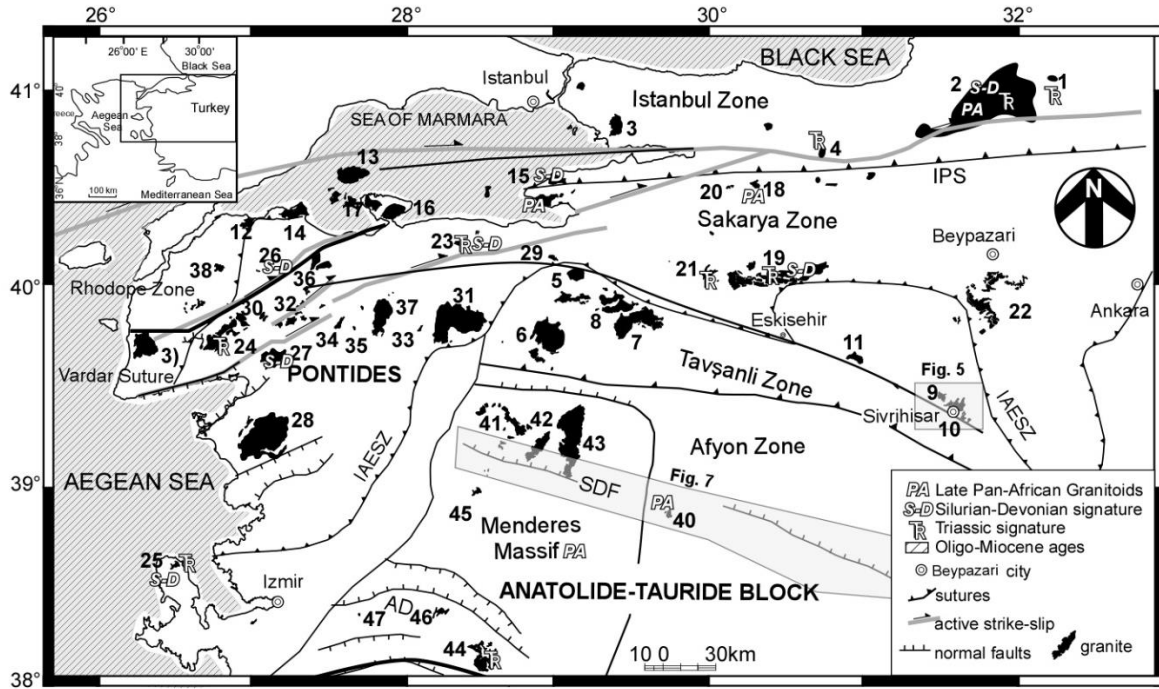


Figure 4. Geological map showing structures and locations of Western Anatolia granite bodies. Base map after Delaloye & Bingöl (2000), Senel & Aydal (2002), and Okay (2008). See Tables 1-7 for the granite names that correspond to the numbers in this figure. Abbreviations: IPS = Intrapontide Suture Zone, IAESZ = Izmir-Ankara-Erzincan Suture Zone, SDF= Simav Detachment Fault, AD= Alasehir Detachment. Locations of Figures 5 and 7 are indicated.

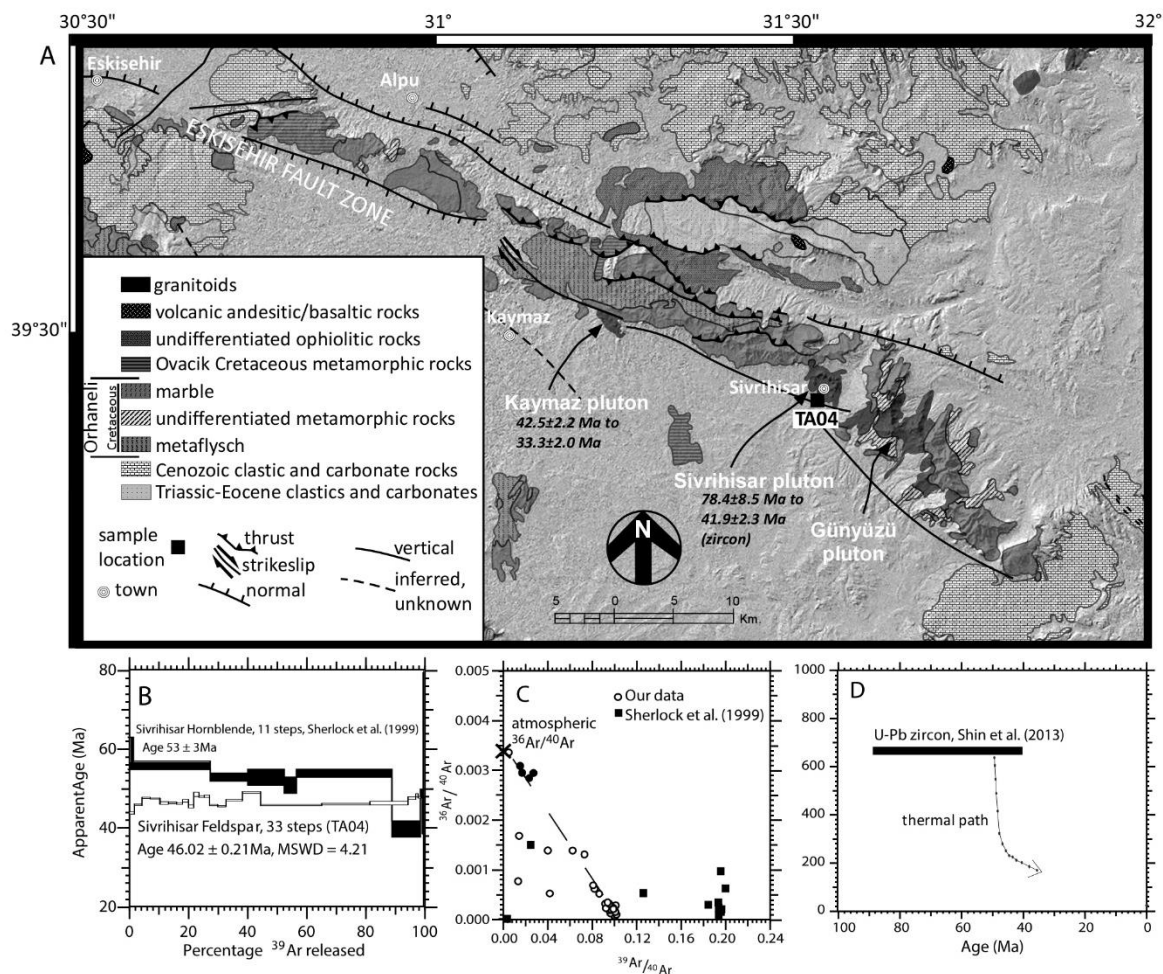


Figure 5. (A) Simplified geologic map of the Sivrihisar Massif (eastern Tavşanlı Zone) overlain on a hillshade raster. Map after Senel & Aydal (2002), Özsayın & Dirik (2007), and Shin et al. (2013). See the data repository for the color figure. (B) Sivrihisar granite K-feldspar age spectra for sample TA04. The upper profile by Sherlock et al. (1999) and the lower are our results. (C) $^{36}\text{Ar}/^{40}\text{Ar}$ vs. $^{39}\text{Ar}/^{40}\text{Ar}$ plot comparing our data to Sherlock et al. (1999). Our results show mixing between a radiogenic and atmospheric component of argon with four lower points from initial isothermal steps. Sherlock et al. (1999) data is affected by excess argon (ArE). (D) One possible thermal history path for the Sivrihisar granite based on the rapidly cooled K-feldspar ages, zircon ages, and zircon saturation temperature from Shin et al (2013).

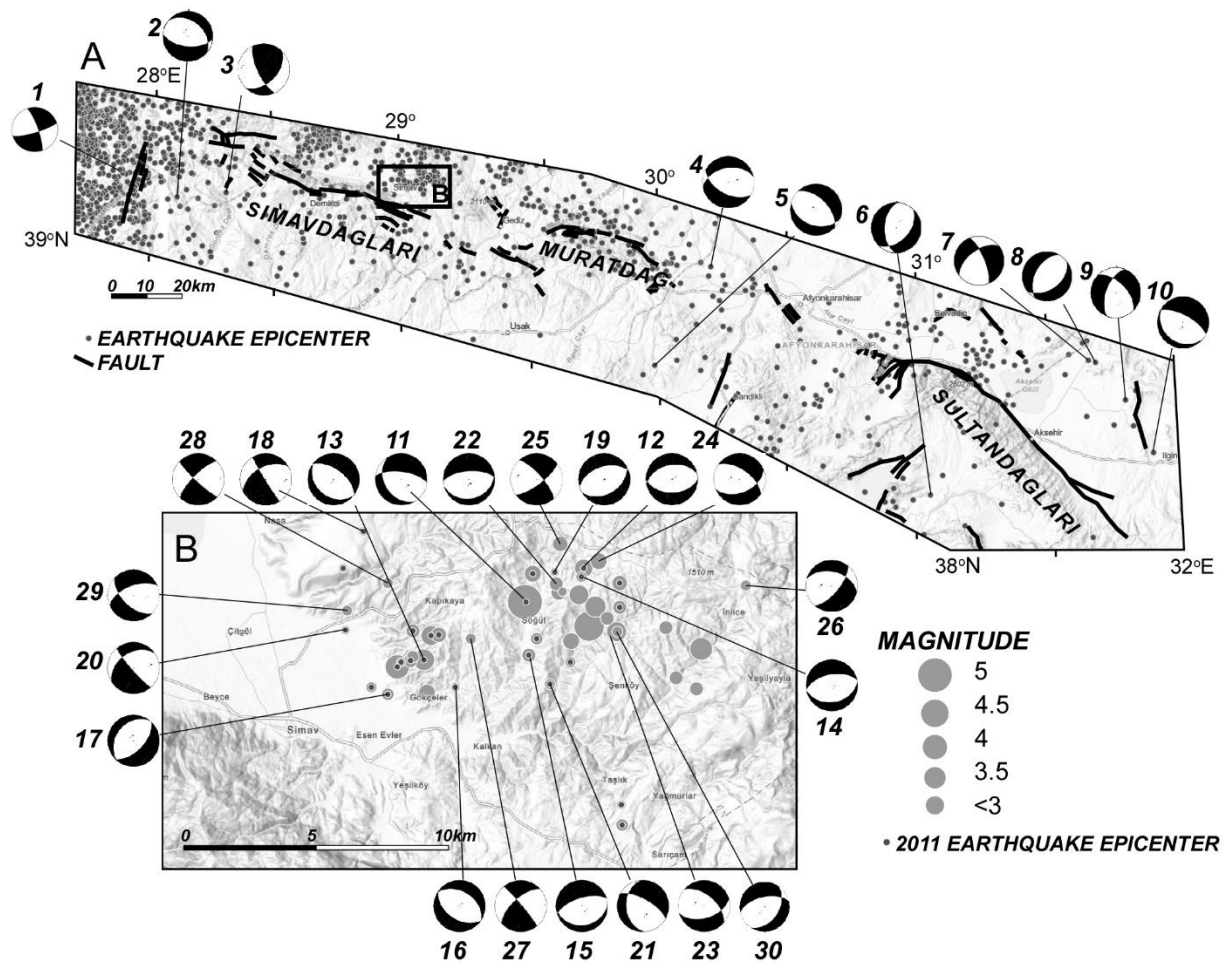


Figure 7. (A) Map of the Simav Fault and associated structures. Small dots are extracted from the USGS Earthquake Catalog magnitude 2.5+ (<http://earthquake.usgs.gov/earthquakes/search>) of events from 1952-2021. Location of fault strands after Konak (2002). Inset shows the location near the town on Simav in panel (B). (B) Map of the surrounding area of Simav with earthquakes plotted. In this map, events were extracted from the Turkish Ministry of the Interior, Disaster and Emergency Management Presidency, Earthquake Department Earthquake Catalog ($M \geq 4.0$), 1900-20XX (<https://depem.afad.gov.tr/depemkatalogu>). The size of the circle represents magnitude. The figure highlights 2011 earthquakes by additional solid dots. Base maps in both panels are from ESRI. Focal mechanism solutions in both panels were extracted from the Turkish catalog. See Table 9 for details of the events. For locations of faults in panel (B), see Mutlu (2020).

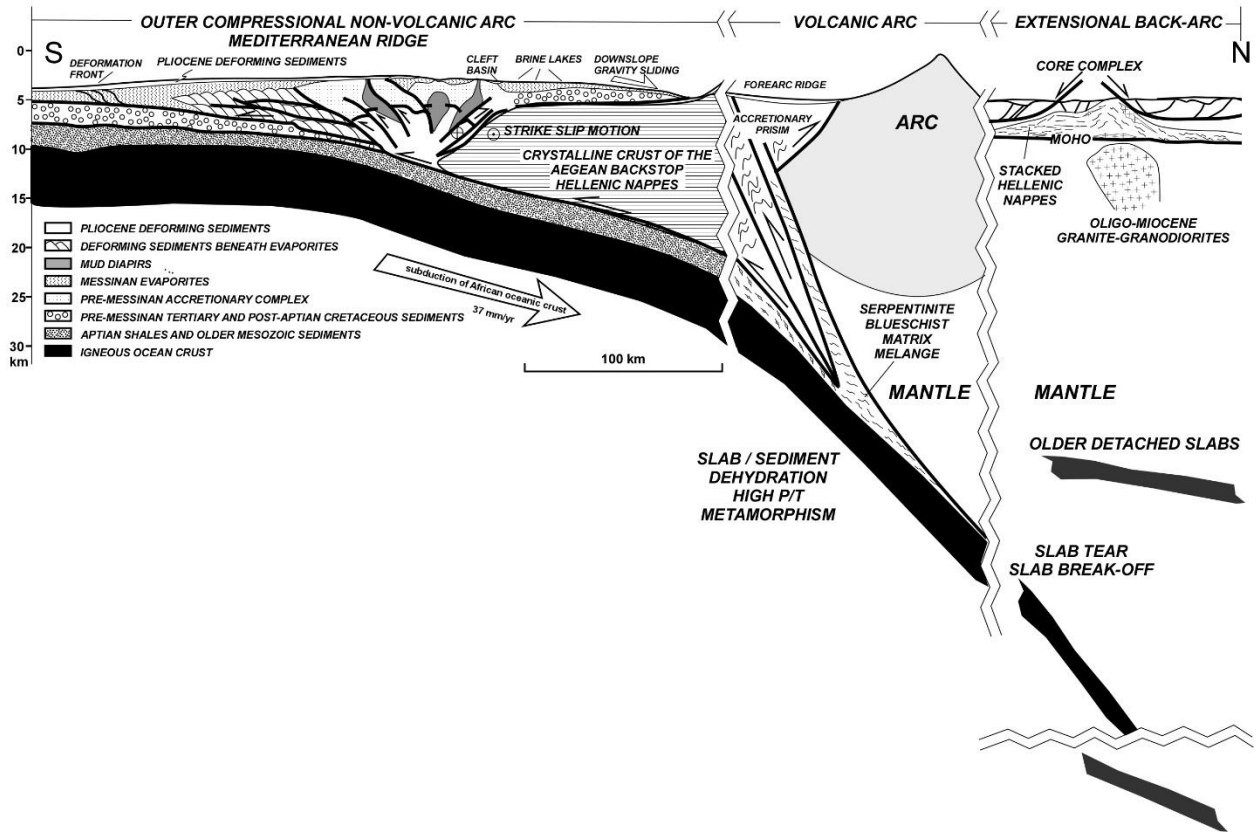


Figure 8. North-south generalized cross-section through the Hellenic arc system showing the key structural elements. Map of the Mediterranean Ridge after Westbrook & Reston (2002).

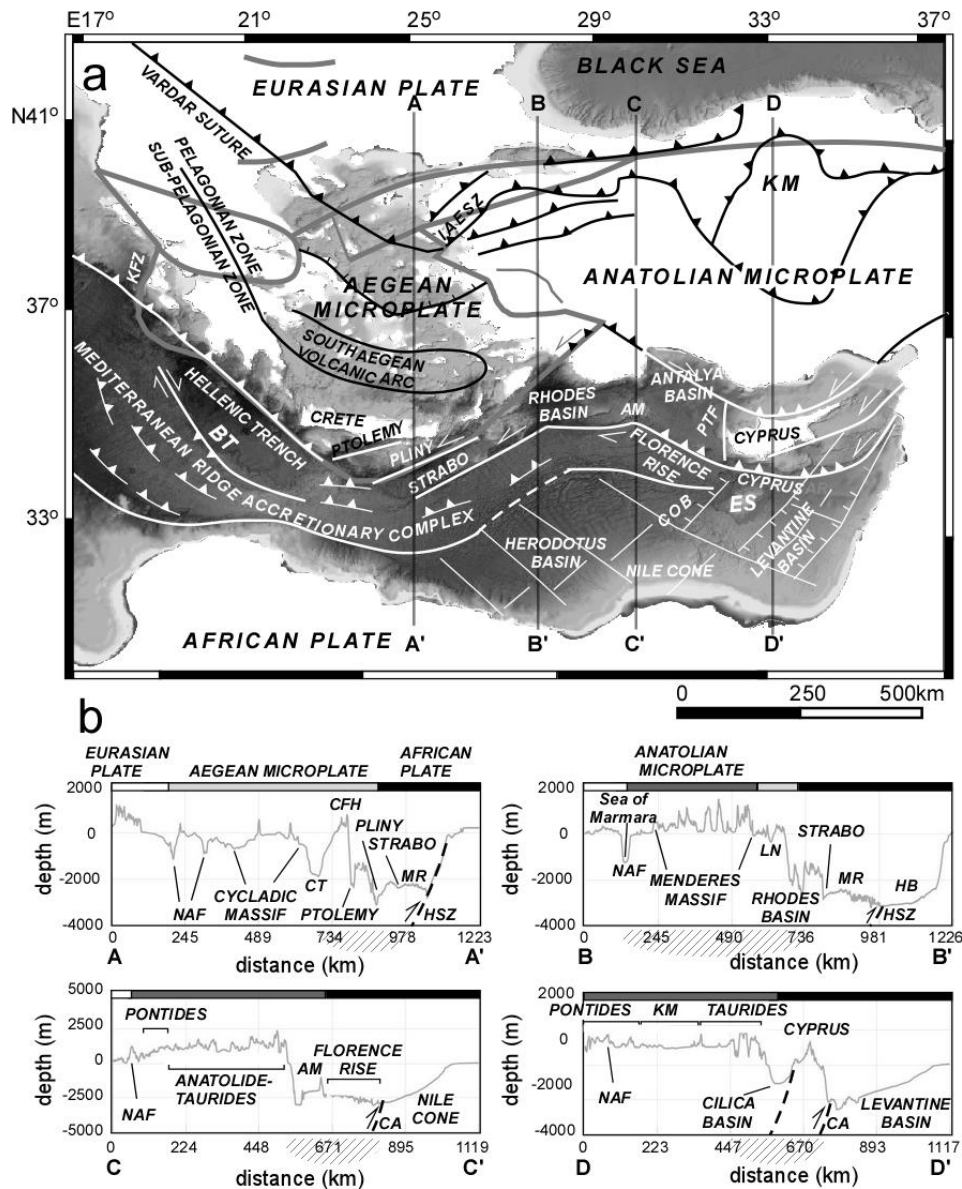


Figure 9. (A) EMODnet Digital Bathymetry map with some structures overlain. The Aegean and Anatolian microplate boundaries are shown in grey after Nyst and Thatcher (2004). Other structures after Hall et al. (1984) and (2009), Woodside et al. (2002), Peterek & Schwarze (2004), Meier et al. (2007); Kinnaird & Robertson (2012), and Symeou et al. (2018). Abbreviations: BT= Backthrust; KFZ = Kephallonia Fault Zone; IAESZ = Izmir-Ankara-Erzincan Suture Zone; KM= Kirşehir Massif, AM= Anaximander Mountains; PTF = Paphos Transform Fault, ES = Eratosthenes Seamount. (B) Profiles along the lines of section shown in panel (A). Abbreviations: CT= CFH = LN= Lycian Nappes, MR= Mediterranean Ridge Accretionary Complex, HB = Herodotus Basin, HSZ= Hellenic Shear Zone, NAF= North Anatolian Fault; AM = Anaximander Mountains; CA= Cyprus Arc. Hashed regions in panel (B) indicate area speculated to be affected by slab tear (e.g., Woodside et al., 2002; Özbakır et al., 2013; Jolivet et al., 2015). See supplementary files for the color figure.

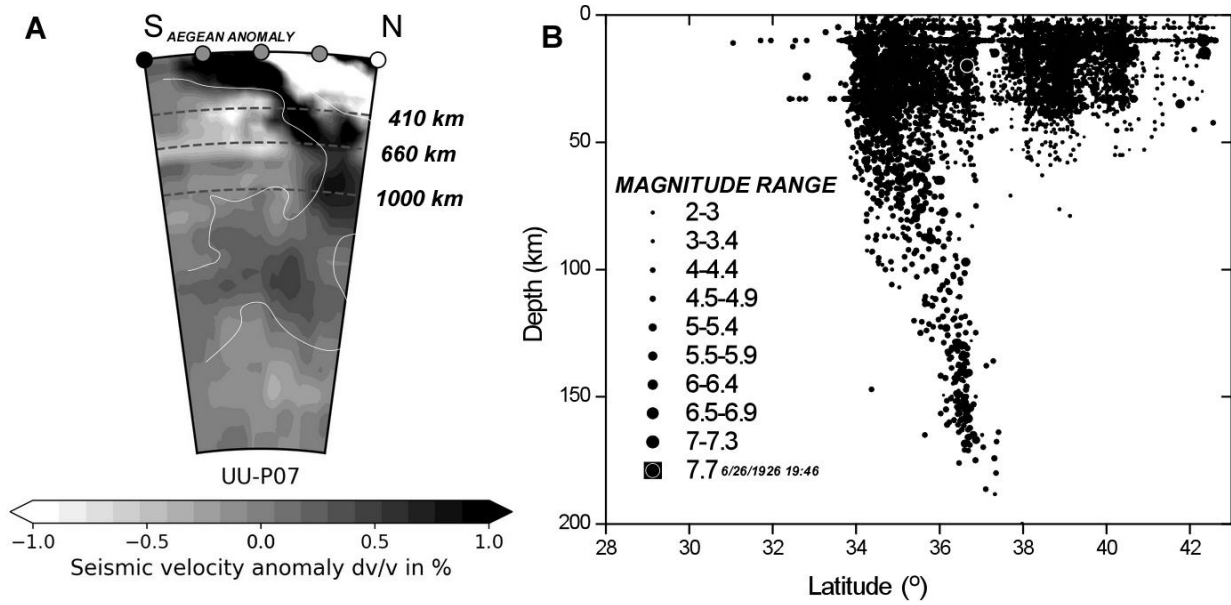


Figure 10. (A) Cross-section of the Aegean anomaly interpreted as the African slab using the UUP07 P-wave model (Amaru, 2007). The line of section used latitude of 28° - 43° and longitude of 24° - 28° . For more detailed views of the anomaly, see van der Meer et al. (2018), Wei et al. (2019), Blom et al. (2020), and El-Sharkawy et al. (2021). The depths of the dashed lines are 410, 660, 1000 km from the surface. Interpretations of the geology below 1000 are debated and discussed in the text. Image created using Hosseini et al. (2018). (B) Depth vs. estimated earthquake depth for the same latitude and longitude as seen in panel (A). In this map, events were extracted from the Turkish Ministry of the Interior, Disaster and Emergency Management Presidency, Earthquake Department Earthquake Catalog ($M \geq 4.0$), 1900-20XX (<https://depem.afad.gov.tr/depemkatalogu>). Events are from 01/24/1900 to 6/17/2021. We indicate the largest event (6/26/1926, 19:46).

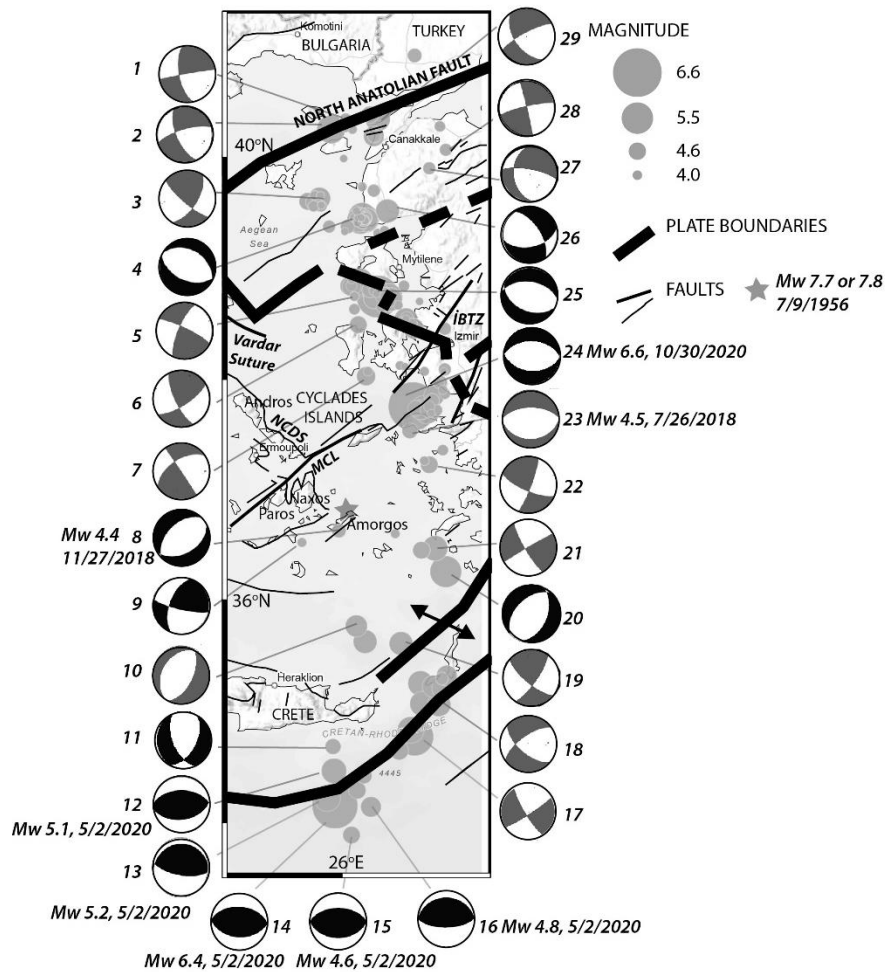


Figure 11. Map of plate boundaries between the Aegean and Anatolian microplates with some faults indicated (after Nyst & Thatcher, 2004; Uzel et al., 2013; Pe-Piper et al., 2002; Menant et al., 2016). Focal mechanisms are from the Turkish Ministry of the Interior, Disaster and Emergency Management Presidency, Earthquake Department Earthquake Catalog ($M \geq 4.0$), 1900-20XX (<https://depem.afad.gov.tr/depemkatalogu>). Events are only from 2010-2020 and details are presented in Table 10. The size of the circle represents magnitude. The 9 July 1956 Amorgos earthquake epicenter is also indicated after Alatza et al. (2020). See Okal et al. (2009) for discussions regarding the focal mechanism of this event. The base map is from ESRI. The abbreviations İBTZ = Izmir–Balıkesir transfer zone; NCSD= North Cyclades Detachment System; MCL= Mid-Cycladic Lineament.

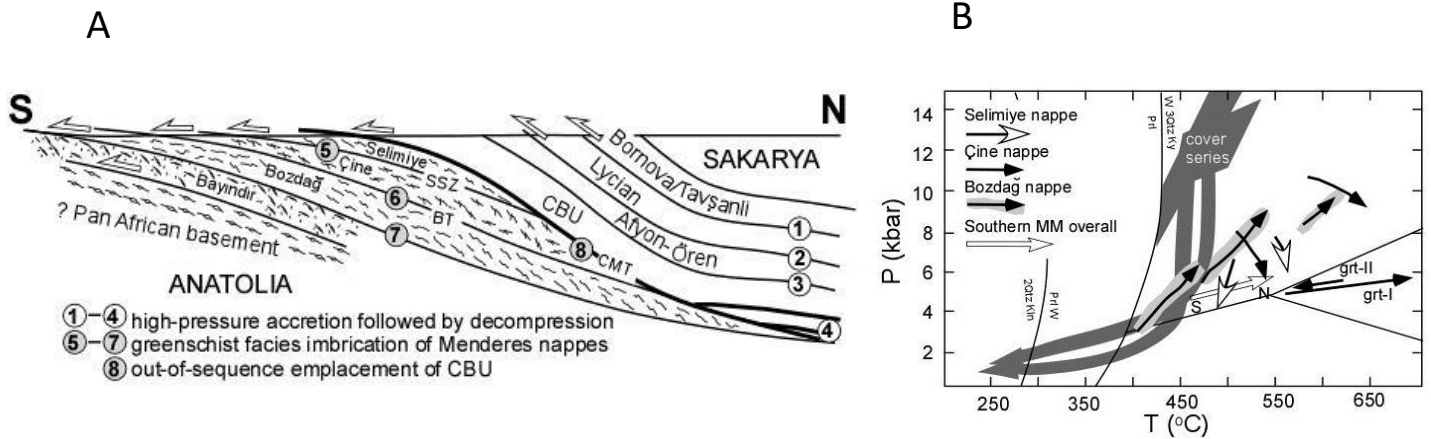


Figure 12. (A) Interpretative thrust sequence during the formation of Anatolide belt after Gessner et al. (2013). CBU= Cyclades Blueschist Unit; CMT= Cyclades Menderes Thrust; SSZ= Selimiye Shear Zone, BT= Bozdağ Thrust. (B) P-T paths from Menderes Massif nappes (Ring et al., 2001; Whitney & Bozkurt, 2002; Rimmelé et al., 2005; Régnier et al., 2007).

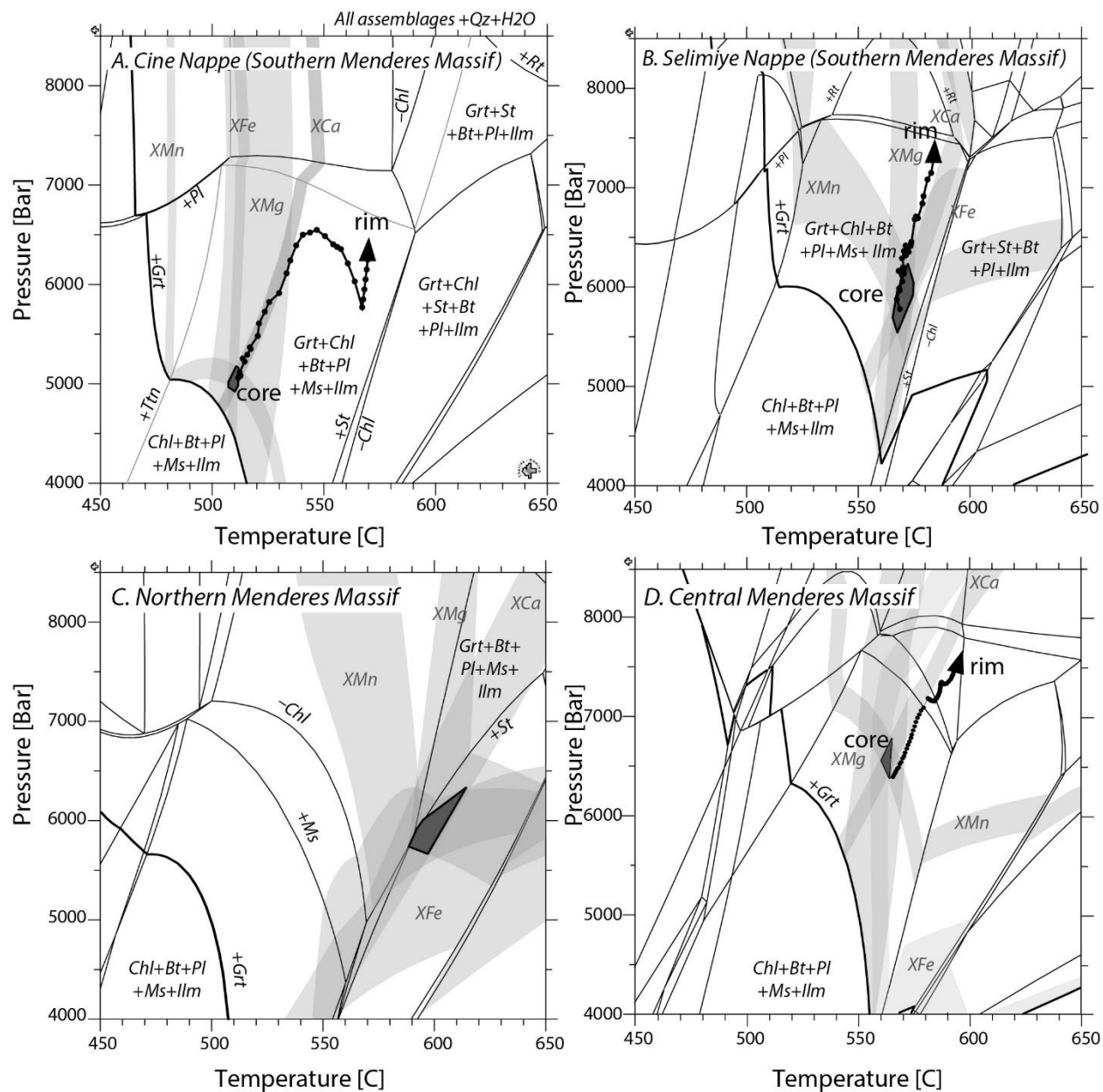


Figure 13. Isochemical phase diagrams with overlapping garnet core compositional isopleths for garnet-bearing samples from the (A) Çine nappe, (B) Selimiye nappe after Etzel et al. (2019), (C) Northern Menderes Massif using data from Cenki-Tok et al. (2016), and (D) the Central Menderes Massif (Etzel et al., 2020). Mineral abbreviations after de Capitani and Brown (1987) and de Capitani and Petrakakis (2010). Labeled stripes are compositional isopleths of ± 0.1 mole fraction for endmember garnet core compositional contents, except for panel (D), which overlies ± 0.2 mole fraction and is for the reported representative composition for that garnet by Cenki-Tok et al. (2016). The grey polygon in each diagram represents the conditions estimated for garnet growth in the samples. High-resolution P-T paths for the samples are shown in panels (A), (B), and (D). See supplementary figures for this figure in color.

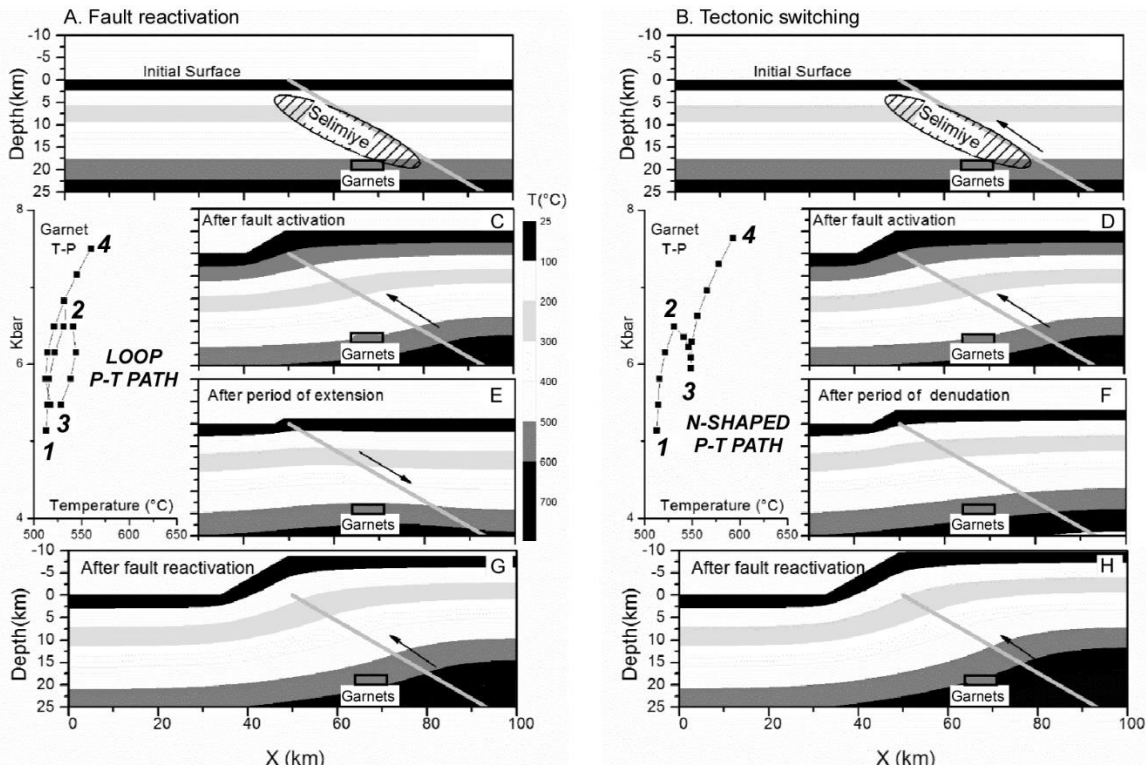


Figure 14. Snapshots of thermal models of the Çine nappe for the (left) fault reactivation and (right) tectonic switching model after Etzel et al. (2019). (A) and (B) are the upper equilibrium thermal grid (depth vs. horizontal distance) before faulting with the position of fault (grey line) arbitrarily selected at 30°. Fault displacement varies linearly. The grid includes reflecting side boundaries and top and bottom maintained at 25°C and 700°C and an initial geothermal gradient at 25°C/km indicated by shaded bars. The position of the Selimiye samples is inferred by a hatch area, and the grey bar represents the approximate initial location of the Çine nappe garnet with the N-shaped P-T path. This is also represented by point 1 in P-T path insets. In panels (C) and (D), the fault is activated and a finite-difference solution to the diffusion-advection equation is used to examine the P-T variations in the hanging wall and footwall as a result of motion. The rock sample experiences the path from 1 to 2 on the P-T path insets. In panels (E) and (F), motion stops. In panel (E), extension occurs, whereas denudation occurs in panel (F). This is modeled based on the mid-rim lower pressure portion of the garnet P-T path and is represented by points 2 to 3 on the P-T path insets. In panels (G) and (H), the fault is reactivated, represented by points 3 to 4 on the P-T path insets.